ACROSS THE IMMUNE SYSTEM: FROM PATHOGENESIS TO THERAPEUTIC DEVELOPMENT FOR HIGH-RISK PATHOGENS

by

IAN ANDREW DURIE

(Under the Direction of Scott Pegan)

ABSTRACT

Viral infections cause significant mortality every year. WHO has listed *BetaCoronaviruses* and Crimean-Congo Hemorrhagic Fever (CCHFV), a top priority for therapeutic research and development because of their high-level risk to national security and public health. Coronaviruses universally encode Papain-Like proteases (PLP) which assist in its replication process while also antagonizing the innate immune system. We investigated the closely related *Alphacoronavirus* genra PEDV to reveal whether PLPs across the coronavirus gena could be viewed as viable target to intervene in coronavirus immune evasion. Through biochemical and structural insights of the PEDV PLP, with the substrates Ubiquitin (Ub) and interferon-stimulated gene product 15 (ISG-15), we found that it is like *Betacoronaviruses* in its deubiquitinase activity with a preference for K48 di-Ub. Additionally, the PEDV PLP does not readily process ISG-15 unlike its *Betacoronavirus* counterparts giving insight into how the PEDV PLP interacts with innate immunity. A similar emergent threat to public health is CCHFV, a BSL-4 virus with a 5-40% mortality rate. Recently the monoclonal antibody (mAb) 13G8 has been shown to target the CCHFV glycoprotein GP38 and can protect against lethality

in a CCHFV mouse model. Here, we reveal the first time its GP38 epitope and how strain-strain differences among GP38s affect interactions with 13G8. Additionally, we discovered a higher affinity human derived mAb, CC5-17, that binds in a structurally divergent manner to that of 13G8 but overlaps its GP38 epitope. Coupled with sequence analysis, this new structural and in-vivo data blaze a new path to a broad-spectrum therapeutic use of these antibodies.

INDEX WORDS: Coronavirus, PEDV, Papain-like Protease, PLP, Crimean-Congo Hemorrhagic Fever, CCHFV, Non-Neutralizing, Antibody, mAb, GP38

ACROSS THE IMMUNE SYSTEM: FROM PATHOGENESIS TO THERAPEUTIC DEVELOPMENT FOR HIGH-RISK PATHOGENS

by

IAN ANDREW DURIE

B.S., University of Florida, 2014

M.B.B., University of Georgia 2017

A Dissertation Submitted to the Graduate Faculty of The University of Georgia in Partial Fulfillment of the Requirements for the Degree

DOCTOR OF PHILOSOPHY

ATHENS, GEORGIA

2022

© 2022

Ian Andrew Durie

All Rights Reserved

ACROSS THE IMMUNE SYSTEM: FROM PATHOGENESIS TO THERAPEUTIC DEVELOPMENT FOR HIGH-RISK PATHOGENS

by

IAN ANDREW DURIE

Major Professor:	Scott Pegan
Committee:	Eric Bergeron
	William Lanzilotta
	Ralph Tripp

Electronic Version Approved:

Ron Walcott
Vice Provost for Graduate Education and Dean of the Graduate School
The University of Georgia
August 2022

DEDICATION

To my wife and family.

Back in the fall of 2018 I was unsure if I would have a job in Athens, GA in 2019; I had just begun my relationship with my then girlfriend now wife Karson and we wanted to see where this journey would lead us. Thus, I applied to graduate school to obtain my PhD. In that time, we got engaged over pancakes and bacon on a Sunday morning during COVID lockdown. Six months later we married, and I am so incredibly lucky to have an Karson in my life. She has been a rock and has supported me throughout this entire process. It also helps that she already has her PhD in Chemistry so I had a secret weapon to get me through this. There were many a night Karson would look over my papers and presentation and she would say “this is my worst nightmare (biochemistry)”, but she stuck by my side and her input has been invaluable.

To my entire family, which includes my mom (Pam) and dad (Rick), my twin (Robert), and older brother (Allen) thank you for being a board to bounce ideas off as I got to try to explain highly detailed and complicated processes. Finally, my fantastic cousin Heather has become one of my closest family members in GA since my arrival in 2015, although we did not know each other too well because of our 16-year age gap, you have become an older sister to me, and I am so grateful to have you in my life. Georgia would have been miserable without you.

ACKNOWLEDGEMENTS

Once again, I have to acknowledge my wife Karson Durie through this process, because without her this journey would have been incredibly difficult and I would not have been able to do it without you. In addition to my wife, all the friends I have made along the way (James, Kirill, Preston, Jon, Rachel, Jason, Brandon, Nick, Kellee, Lincoln, and Priya) I appreciate you and thank you for being there.

To get to this point I have been incredibly privileged to have fantastic mentors. Before I was a scientist, I was a musician and self-proclaimed band nerd and those years practicing and performing clarinet laid the initial steps for me to get onto that stage. To my musical mentors over the years Wayne Camp, Paul Green, Mitchell Estrin, and Jason Thompson, you have had wide reaching impact on the individual I am today.

To my scientific mentors from undergraduate, Max Teplitski and Massimiliano Marvasi, thank you for taking a chance on me way back in 2012. You allowed me to flourish within your lab and your guidance and encouragement have gone a long way. During my master's I worked with Dr. Mark Eiteman in Biological Engineering who challenged my critical thinking skills. After my masters I got to work at Boehringer Ingelheim in Athens, and I got to work so many fantastic people which included but not limited to Justin Widener, Laurie Kreimeyer, Ernie Veal, Austin Schubach, and Adam Singer. Which brings to the larger acknowledgement of everyone I know in Athens, which includes all my racket sports groups (racquetball, squash, tennis, and badminton). At the end of a hard day, hitting a ball was a great relief.

Through my PhD journey my lab members were fantastic. I need to thank John Dziaminaski. Although he was a former graduate student and our time in lab never overlapped,

we had a surprising amount of communication. He would always make time if I had questions about procedures and techniques and he was integral to my understanding of my projects laid out in this dissertation. In addition to John, Brendan Freitas and Jack McGuire helped me adjust as I came into the lab, and we had some very long nights especially when we were on the forefront of COVID-19 research.

My second group of lab members resided at the CDC which included the best, brightest, and funniest group of people that made work fantastic. This includes Sergio Rodriquez, Florine Schlote, Jessica Spengler, Elif Karlassan, and Steve Welch. Not enough can be said about this group and if you have a chance to work with them take it.

Last, I need to thank my committee for the chance to prove myself and this path. Many times, committees are made up of people you gather in a room once a year, I was lucky in the regard that I was able to interact with everyone constantly. Dr. Lanzilotta and I go back before I started my PhD and he wrote a recommendation letter for me to get into ILS, his insight and bluntness while giving me my initial start in crystallography are pivotal. Eric, you have been a pleasure to work with and as a Co-PI your love of science and knowledge of the field have made you into a final boss in my mind to discuss and debate scientific ideas. Dr. Tripp although we haven't interacted as much you knew exactly what I needed and were able to find my gaps in knowledge, thank you for pushing me. Scott, this has been a wild ride from start to finish. In the back of my mind, I always wanted to work on a project involving a BSL-4 agent and luckily you put some faith in me, and I now get to cross this scientific milestone off my list. Thank you for letting me join your lab.

TABLE OF CONTENTS

Page

LIST OF TABLES

Page

LIST OF FIGURES

Page

CHAPTER 1

INTRODUCTION AND LITERATURE REVIEW

Throughout human civilization, viruses have become an everyday occurrence. While some are insignificant, others evade the immune system and cause significant damage and death. The body relies on two interdependent arms of the immune system, the innate and adaptive immune response, to fight off viral infections. Therefore, it is imperative to uncover the viral immune interaction to assist in therapeutic development.

How our bodies battle infections

Once viruses enter our body, there are two main ways our bodies handle and dispose of viruses: the innate and the adaptive system. Both rely on each other to function, with initial infection at 0-4 days handled through the innate immunity and the adaptive immunity playing a more prominent role from beyond 4+ days(*1*).

The Innate Immune Response

Innate immunity acts as the first line of defense against pathogens. This action revolves around mechanisms that prevent pathogens from spreading upon initial infection. In the case of viruses entering the body, innate immunity relies on damage-associated molecular patterns (DAMPS) or pathogen-associated molecular patterns (PAMPS)(*2*). PAMPS detect foreign structures (i.e., genetic material, proteins, and carbohydrates). This mechanism relies on structural similarity between pathogens. In contrast to DAMPS, cells that are damaged through pathogens release molecules inside or outside the cell that alerts the immune system to clear the damaged cells.

Some viruses can evade and antagonize innate immunity. For instance, Crimean-Congo Hemorrhagic Fever Virus (CCHFV) and Coronaviruses encode a viral ovarian de-ubiquitinase (vOTU) and a papain-like protease (PLP) which interact with ubiquitin (Ub) and ubiquitin-like molecules. Ubiquitin is a highly conserved 76-amino acid protein essential for posttranslational modification amongst eukaryotes and has a direct role in cell division, differentiation, and general homeostasis(*3*). Similarly, the ubiquitin-like protein, interferon-stimulated gene 15 (ISG-15), is also a posttranslational modification for cellular functions and plays a similar role in the innate response.

Ub and ISG-15 have similar functions and they also contain some structural similarities. They both contain a C-terminal LRLRGG motive but ISG-15 is twice as large and contains two-ubiquitin-like domains which can have a ~30% amino acid similarity between species(*2*). Both molecules can be covalently conjugated through enzymatic processes called Ubqiuitiniation and ISGylation via the enzymes E1, E2, E3(*4, 5*). Conjugation occurs on lysine residues of target proteins and can even occur on Ubiquitin molecules, which cause specialized branched Ub(*6*). For instance, K48 Di-Ub are known to regulate homeostasis and targeting proteins for degradation(*7*). These conjugations are essential to disrupt viral replication and/or function(*2, 3*).

The Adaptive Immune Response

Unlike innate immunity, which relies on similarity, adaptive immunity relies on its ability to recognize and adapt to new pathogen structures. Through this response, the body can also obtain 'memory' in which the body can clear infection if it encounters the same pathogen in the future. This response comprises of three different subsets of immune cells: $CD4^+$, $CD8^+$, and B lymphocytes(*8*).

Activation of the adaptive immune response relies on recognition of an antigen: a foreign-based substance, usually protein-derived, which binds to a T-Cell receptor, B-cell Receptor, or an antibody. The specific area of the antigen that binds to the receptors and antibody is called an epitope. Lymphocytes display membrane receptors that are unique between lymphocytes and can distinguish between different antigens and epitopes from pathogens. The diversity is the main determinant of antigen recognition and allows for pathogens to be selected against. Once recognition occurs through clonal selection, lymphocytes are activated and undergo clonal expansion. Mature lymphocytes are then able to clear infection through cell-mediated immunity or humoral immunity which clear the pathogen (Figure 1.1).

Humoral immunity relies on mature B cells which contain a B-cell receptor specific to the antigen. Once an antigen within the Antibody secreting cells (ASC) are differentiated cells from the B-cell lineage and appear during primary and secondary infections. These cells produce large amounts of antibodies within the blood and secondary organs. The antibodies can then assume several functions which clear pathogens. Production of either Humoral immunity or T-cell mediated immunity is the goal in vaccination.

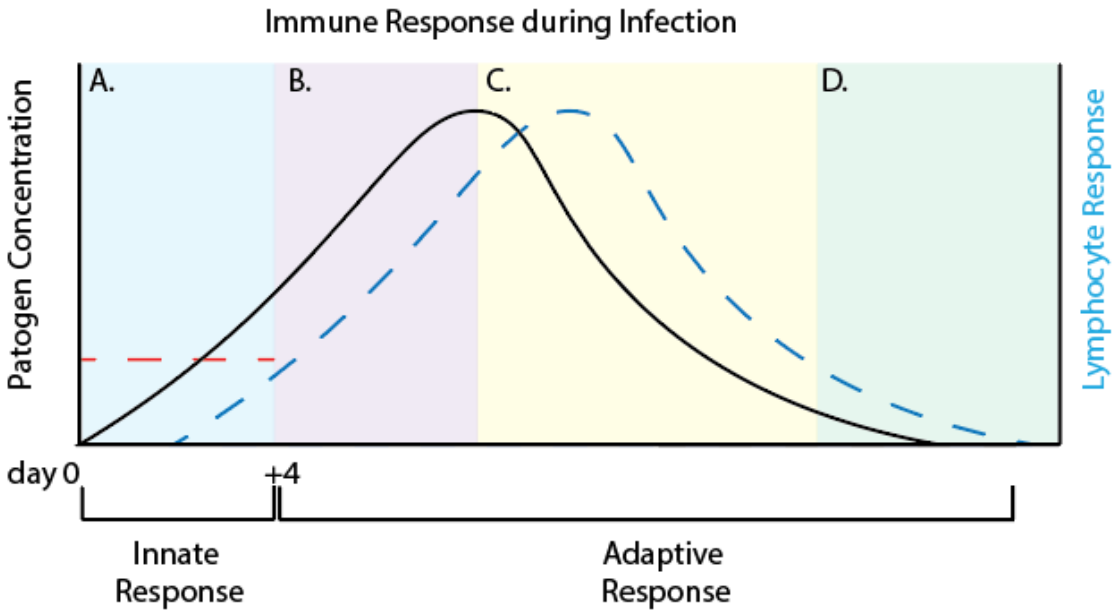

Figure 1.1: Immune Response during Infection: **(A)** Innate Immune Response trying to counteract pathogens in body **(B)** Adaptive immune response priming against pathogen **(C)** Maturation of Lymphocytes which induce humoral and cell-mediated immunity which clear pathogen **(D)** Memory induction to fight against similar pathogens in the future

Antibody Structure

Antibodies (Immunoglobulin Ig) are produced through B lymphocytes and can act as secreted molecules or membrane-bound antigen receptors. Secreted antibodies are classified into several isotypes that reside around the body, i.e., plasma fraction of blood (IgG), mucus (IgA), and intestinal fluids (IgM). In addition, other isotypes exist, such as IgE, which is associated with type I hypersensitivity and IgD, which is membrane receptor-bound responsible for antigen recognition. Secreted antibodies have two primary functions 1. Neutralization of pathogens and/or 2. Trigger effector functions (also referred to as non-neutralizing)(*1, 9*).

The main structure of Ig contains a heavy and light chain that contains several domains. In the case of IgG, the light chain is composed of two domains: a variable light domain, V_L, and a constant light domain, C_L, while the heavy chain consists of 4 domains: a variable heavy chain, V_H, and three constant domains, C_H1, C_H3, and C_H2 (Figure 2A). An IgG comprises two light chains and two heavy chains bound via disulfide bridges and is typically represented as a Y shape. The overall structure has two functional regions: the antigen-binding fragment (Fab) and the crystallizable fragment (Fc).

Every antibody isotype has a similar structural backbone, framework region, and highly flexible loops referred to as complementary defining regions (CDR), that protrude from the framework which are hypervariable. The Fab contains the antigen-binding structure, and in each variable domain, there are three (CDR) for a total of 6 loops that can encounter the antigen (Figure 1.2C). The recognition of the specific area of the antigen is referred to as the epitope. Antibody and antibody receptor variety is randomly selected through the process called VDJ recombination. This is the rearrangement of the variable (V), diversity (D), and joining (J) segments which create the diversity in the CDR. Most commonly, the heavy chain CDR3 is responsible for antigen binding. Even then it is suggested that on 20-33% of residues in the CDR interact with the antigen(*10*). Continued advancement and solvation of 3D antigen-antibody structures have also suggested that framework regions can also bind to antigens(*11*). Surrounded by the CDR's are the framework regions which constitutes several beta-sheets in parallel with each other on both the heavy and light chains (Figure 1.2B)(*12*).

The Fc is responsible for effector functions with activate other areas of adaptive immunity. The Fc can also be used to further classify an antibody via subclass (IgG1-4, IgA1, IgA2). These subclasses are associated with different functions and arise to different conditions, such as

deficiency of IgG2 the individual can be prone to bacterial infections(*13*). Additionally, the Fc region has two N-glycosylation sites near the hinge region. The glycosylation profile of antibodies can be used as an indication of disease state, but can also provide additional protection and benefit(*14*). For instance, antibody development against Ebola virus has shown that there is a correlation between Fc glycosylation and in vivo protection(*15*).

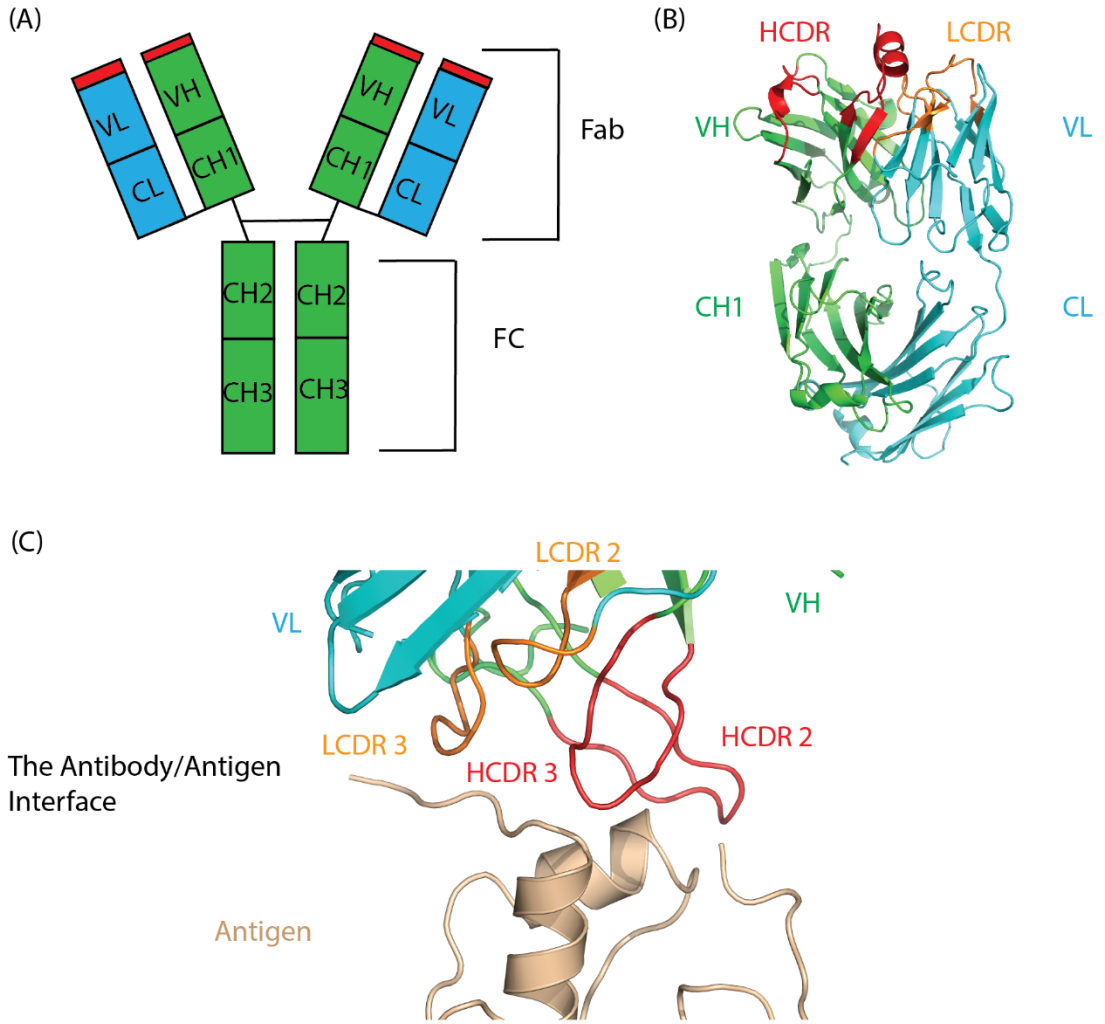

Figure 1.2: The Antibody Relationship **(A)** Overall 2D organization of IgG **(B)** The 3D organization of the Fab region of Ig **(C)** Example antibody/antigen interface which highlights the influence of CDRs on antigen binding

Antibody Functions

Neutralization is the most well-characterized of antibody functions because of its ease of measuring in-vitro and its general use as a correlate of protection(*16*). For neutralization to occur, the Fab region CDR binds to a specific toxin or a structural epitope on the protein. In the case of viruses, by binding to a specific epitope antibodies can interfere with the protein-receptor interaction, thereby blocking infection from the virus.

Non-neutralizing functions are more complicated because they do not 'neutralize' a virus from entering a cell and require a mediator to activate effector functions. The primary determinant of effector function is through the Fc region of the antibody that encounters different receptors and proteins for activation. Antibody-dependent cell-mediated cytotoxicity (ADCC), Antibody-dependent cellular phagocytosis (ADCP), and Complement activation require the interaction of the Fc region.

ADCC acts through FCγRIIIA, in which infected cells have antigen bound to their cell membrane, which then causes the association of specific IgG antibodies(*17*). Coating infected cells with IgG recruits immune cells like Natural Killer (NK) cells, monocytes/macrophages, NK T cells or γδ T cells, which then kill and clear the infected cells. Activation of the complement system requires similar conditions as ADCC, but instead of immune cells, complement proteins are recruited from circulating blood and tissues. Neutralizing and non-neutralizing antibodies work harmoniously when battling an infection. With highly fatal viruses like Ebola, neutralizing functions are needed, but non-neutralizing functions have been associated with clearance of viruses(*18*). Innate and Adaptive are necessary to combat the wide breadth of pathogens our body encounters.

Viruses

RNA viruses contain some of the most prevalent and deadly viruses, including Influenza, HIV, Coronavirus (CoV), Ebola, and Crimean-Congo Hemorrhagic Fever (CCHFV). Some of the aforenoted viruses, such as Influenza and HIV, have changed the antiviral development landscape because of their spread in the 20th century. The World Health Organization has listed several viruses, including CoV and CCHFV, as top priorities because of their potential spread and lack of vaccines and therapeutics to counterattack a possible epidemic(*19*).

Coronavirus

Coronaviruses are single-stranded positive-sense RNA viruses that belong to the Coronaviridae family. Within the Coronaviridae family the clinically important subfamily *Coronavirinae* contains four genra of coronaviruses: *Alphacoronavirus*, *Betacoronavirus*, *Gammacoronavirus*, and *Deltacoronavirus(20). Alphacoronaviruses* and *Betacoronaviruses* are known to infect mammals, and *Betacoronaviruses* are the recent cause of the COVID-19 pandemic and past outbreaks of SARS-1 and MERC-CoV. These coronaviruses have been hypothesized to originate from bat hosts(*21, 22*). Other coronaviruses like Gamma and Delta infect various animals. For example, Porcine Deltacoronavirus (PDCoV) and Gammacoronavirus have avian hosts. Interestingly coronaviruses in the same genre can have drastically different mechanisms of infection, such as those in the Betacoronaviruses. For example, SARS-1 and SARS-2 rely on the receptor angiotensin-converting enzyme 2 (ACE2), while MERS-CoV uses the dipeptidyl peptidase 4 (DPP4) as a receptor(*23, 24*).

After entry, the 26-32 Kb RNA genome is released and is translated into two large open reading frames, ORF1a and ORF1b. This genome translates into two polypeptides, pp1a and pp1ab. These polypeptides are then cleaved into 16 non-structural proteins (NSp1 to NSp16). The Nsp

forms a viral membrane-bound replicase complex(*25*). During the cleavage of the NSp, two proteases are released, the main protease and the Papain-like Protease (PLP). The main protease (3C-like protease) is responsible for cleaving Nsp4-Nsp16, while the PLP cleaves itself out of the polyprotein and cleaves Nsp1-Nsp3. Coronaviruses can encode up to two PLPs, but only one is enzymatically functional. For instance, the COVID-19 only encodes one PLPro while PEDV encodes two PLPro, but in the case of PEDV, only the PLP2 is functional(*26, 27*). In addition, the PLP has a secondary function that allows it to antagonize the innate immune system through the removal of Interferon Stimulated Gene Product 15 (ISG-15) or Ubiquitin (UB)(*2, 28*). The catalytic ability of the PLP has been found to be different between strains of coronaviruses, even within the same genra(*29*).

Because of these unique functions, the PLP has been proposed as a therapeutic target. Originally with SARS-CoV-1, the small molecule GRL-0617 was developed and shown to inhibit viral replication through targeting of the PLP active site(*30*). Soon after this molecule was repurprosed to target SARS-CoV-2 and was found to also be effective, in addition this active site was determined to be highly conserved across species especially those within the 2b subgroup of BetaCoronaviruses(*27, 31*). Interestingly the deubiquitinase and deISgylase functions are not just exclusive to the PLP, other viruses like those in the nairovirus family contain a vOTU with similar functions(*32*).

Crimean-Congo Hemorrhagic Fever

Bunyaviruses host a wide array of negative-sense RNA viruses. Of particular importance is the Nairovirus Crimean-Congo Hemorrhagic Fever (CCHFV). CCHFV has consistently been listed on WHO's blueprint of priority diseases because of its lack of approved prophylactics and therapeutics to combat it. Crimean-Congo Hemorrhagic Fever (CCHFV) is endemic to the

Eastern Hemisphere, where it has been documented in around ~50 countries, with high incidence rates in Turkey and Iran(*33-35*). Transmission of CCHFV occurs either through infected Ixodid tick bites or contact with contaminated blood from humans and animals. Upon onset of symptoms, patients can experience fatigue, nausea, and vomiting, with more severe cases causing hemorrhaging. With this wide array of symptoms, there is a 10-40% fatality rate, but some outbreaks have shown as high as 80% depending on strain and if the region has access to modern medical facilities(*36-38*).

As part of the *Nairoviridae* family, CCHFV is a tri-segmented negative-sense RNA virus. Each of the segments, Small (S), Medium (M), Large (L), encodes a different set of proteins that assist in viral replication and proliferation. The small segment encodes the nucleoprotein responsible for encasing genetic material. The medium segment encodes a glycoprotein precursor (GPC), which consists of a Mucin-like domain (MLD), GP38, Gn, Nsm, and Gc (Figure 1.3A)(*39-41*). Lastly, the large segment encodes the RNA-dependent RNA polymerase and a viral Ovarian Tumor De-ubiquitinase (vOTU) that is known to antagonize the innate immune system like the Coronavirus PLP(*42*).

Many aspects of the glycoproteins of CCHFV, including function, are still under investigation. Nevertheless, certain assumptions are made about how it acts as other viruses in the Bunyavirales Order. First, entry is assumed to be assisted via the glycoproteins Gn and Gc, which form a heterodimer that enters the cell via receptor-mediated endocytosis(*43*). Once inside the cell, an acidic environment causes the endosome to dissociate alongside the CCHFV glycoprotein surface. This dissociation allows the tri-segmented RNA to be released, replicated, and transcribed.

Of immunological and therapeutic importance is how the CCHFV GPC is processed, unlike many other viruses in Bunyavirus Order, CCHFV processing is more complex and has additional proteins of unknown function (MLD, GP38, NsM). Between the structural and non-structural proteins, the GPC contains one leader N-terminal signal peptide (SP), two internal SP, and five transmembrane domains (TMD) (Figure 1.3B). Initially the GPC is synthesized in the ER in which the GPC undergoes N-glycosylation at nine different asparagine residues on the MLD (3), GP38(2), G_n (1), and G_c(3). Glycosylation of Gn and GP38 are essential for localization and chaperoning of Gc while glycosylation of Gc is considered dispensible(*44*).

SPase cleaves the signal peptide off the GPC while also cleaving at two other distinct sites which yields PreGn (MLD, GP38, G_n), the NsM, and preG_c. The glycoproteins and then transported to the golgi in which the MLD in PreGn undergoes O-glycosylation at numerous sites. Although the function of the MLD is unknown, other viruses like Herpes Simplex Virus and Ebola use mucin domains as a barrier towards immune functions and assistance towards viral attachment(*45-47*).

Subsequently PreG_c and PreG_n are cleaved by a SK-1/S1P through a RRLL motif which separates MLD-GP38 (also referred to as GP85) from Gn(*40, 48*). Mature G_n and G_c are further processed to form the mature viron envelope. Of unknown functions are the variations of the MLD-GP38, which has been detected in three forms: 1. a dimerization of two MLD-GP38, GP180, 2. MLD-GP38 cleaved via a furin cleavage site yielding the MLD and GP38 or 3. Uncleaved MLD-GP38(*48*). It is unsure if GP85 or GP160 have any virology/pathological functions or if it is an artifact of the replication process.

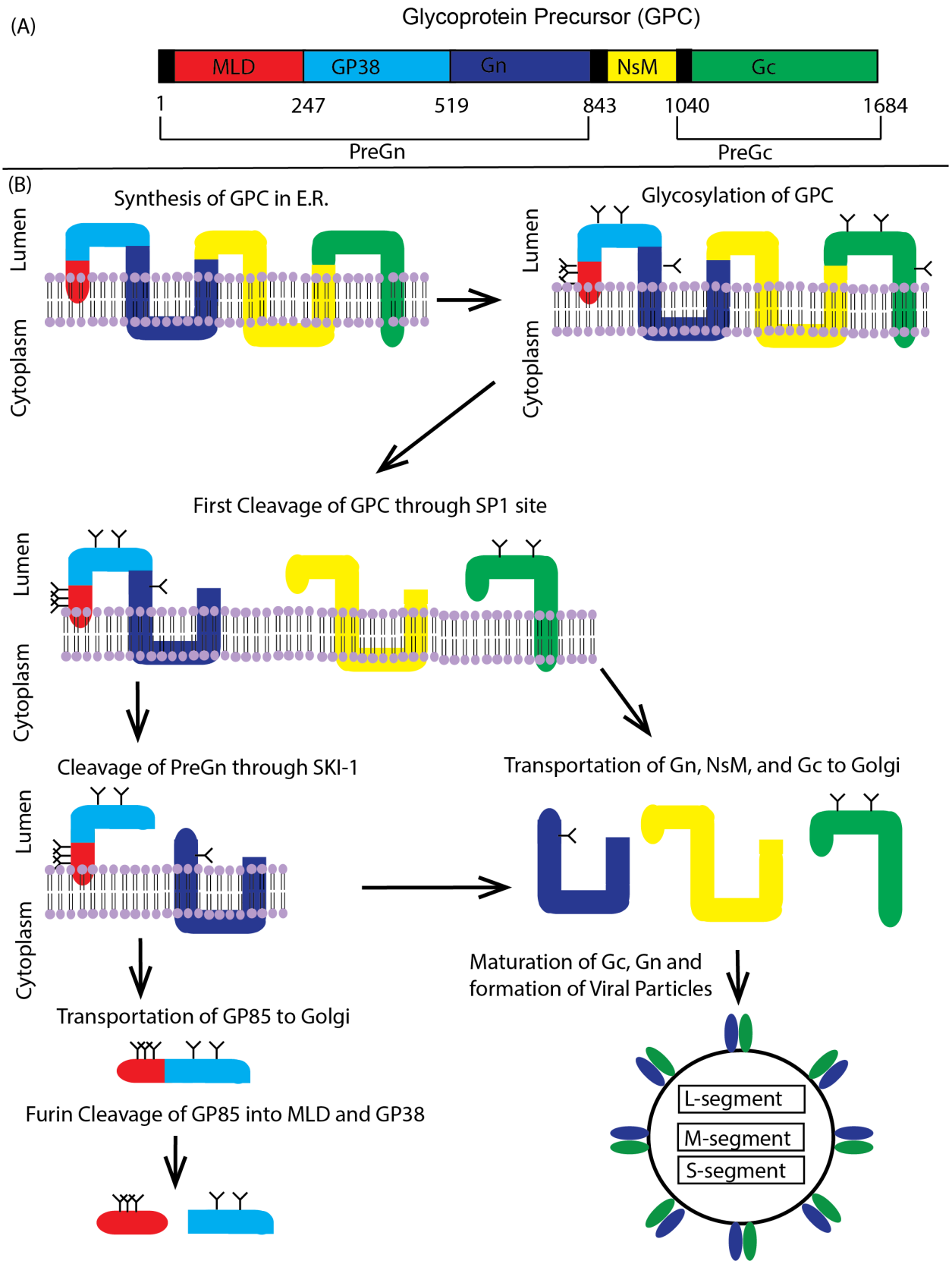
(A)
Glycoprotein Precursor (GPC)
MLD
GP38
Gn
NsM
Gc
1
247
519
843
1040
1684
PreGn
PreGc
(B)
Synthesis of GPC in E.R.
Glycosylation of GPC
Lumen
Cytoplasm
First Cleavage of GPC through SP1 site
Cleavage of PreGn through SKI-1
Transportation of Gn, NsM, and Gc to Golgi
Transportation of GP85 to Golgi
Maturation of Gc, Gn and
formation of Viral Particles
Furin Cleavage of GP85 into MLD and GP38
L-segment
M-segment
S-segment

Figure 1.3: CCHFV Glycoprotein Precursor processing **(A)** Organization of CCHFV GPC **(B)** How the GPC is processed through the cell to obtain mature viral particles

CCHFV GP38

Attempts to produce a neutralizing antibody that protected CCHFV proved to be a futile effort before 2020. Antibodies directed towards G_c showed neutralization in-vitro but did not provide protection in-vivo(*49*), while antibodies with no neutralizing ability provided protection. These non-neutralizing antibodies were initially classified as anti-G_n mAbs but were later found to target the CCHFV glycoprotein GP38(*50*). The function of GP38 is still under investigation but is necessary for GPC processing and maturation of viral particles.

The efficacy of non-neutralizing antibodies toward CCHFV is still under investigation, but the mAb 13G8 has proven to be insightful as a tool for future CCHFV mAb treatments and therapies. In table 1.1, several studies have used 13G8 against the CCHFV strains Ibar10200, Afg-09, and Turkey-2004. These three strains cover endemic regions where CCHFV is prevalent.

13G8	Timing	Dose	Strain	Cx dose	Route	Animal model	Survival
Mouse	-1 d	1mg	IbAr10200	100 PFU	SC	IFNAR -/-	60%
Mouse	-1 d / +3 day	1 mg	IbAr10200	100 PFU	SC	IFNAR -/-	90%
Mouse	+1 / +4 day	1 mg	IbAr10200	100 PFU	SC	IFNAR -/-	60%
Mouse	+2 / +5 day	1 mg	IbAr10200	100 PFU	SC	IFNAR -/-	20%
Mouse	-1 d / +3 day	1mg	Afg-09	100 PFU	SC	IFNAR -/-	20%
Mouse	+30min at same site as virus	5mg/ kg	Turkey2004	100 PFU	IP	STAT -/-	80%
Human	+30min at same site as virus	5mg/ kg	Turkey2004	100 PFU	IP	STAT -/-	100%

Human with AF	+30min at same site as virus	5mg/kg	Turkey2004	100 PFU	IP	STAT -/-	100%
Human with LALA Fc	+30min at same site as virus	5mg/kg	Turkey2004	100 PFU	IP	STAT -/-	60%
Human	-1 day	1mg	Ibar10200	100 PFU	IP	IFNAR -/-	80%
Human	+1 day	0.5mg	Ibar10200	100 PFU	IP	IFNAR -/-	0%
Human	+1 day	1mg	Ibar10200	100 PFU	IP	IFNAR -/-	10%

Table 1.1: Overview of the anti-GP38 mAb 13G8 in challenge studies in Blue were gathered and presented in Golden et al. 2019, Studies in orange were present in Mishra et al. 2020, Studies in light purple were presented in Fels 2021

CCHFV Vaccination efforts

Vaccination efforts are wide-ranging, with ~30 studies using a variety of vectors and methods to induce protection against CCHFV(*51*). In addition, animal models have been developed in conjunction with vaccination efforts because CCHFV cannot cause severe disease states in mice. The two main mice models used in CCHFV research are IFNAR -/- and STAT -/- mice. Both animal models rely on the knockout of innate functions, which causes severe disease in mice. Although many vaccines have been tested, the correlates of protection are not well understood or characterized (Table 1.2). With the recent advances towards the establishment of GP38 as an essential antigen. Vaccination studies were looked through to determine if there is a possible correlation in protection and if the inclusion of GP38 within vaccine constructs provided protection (Table 1.2). Of the 13 vaccination studies listed, nine include GP38, and of those nine, eight provided significant protection against lethal disease. Of the four that did not include GP38, only one provided complete protection if given two doses of a Small Segment derived mRNA-

based. Interestingly a recent GP38 DNA vaccine provided minimal protection, but interestingly the surviving mice had two log higher titers of anti-GP38 in their blood. This result could indicate that if anti-GP38 mAbs are given at a high enough dose or induced through a vaccine-based approach then survival can be obtained.

Vaccine	Route of Vaccination	Animal Model	Protection	Target/Antigens	Is GP38 included?	Are anti-GP38 titers measured?	Mechanism of Protection
MVA-GP(*52*)	IM	IFNAR -/-	100%	GPC	yes	no	No correlation with antibody titers tested
M-Segment DNA Vaccine(*53*)	IM-EP	IFNAR -/-	70-100%	GPC	yes	no	Neutralizing and total antibody titers do not correlate with protection
rVSV(*54*)	IP	STAT-1	100%	GPC	yes	No, but expression of GP38 was confirmed	Appearance of neutralizing titers, but the mechanism is unclear
VRP(*55-57*)	SC	IFNAR -/-	80-100%	GPC, Np	yes	no	Unclear, antibody titers are not tied toward protection
Subunit based on Gn or Gc ectodomain(*58*)	IP	STAT-1	0%	Only Gn or Gc	no	no	No correlates of protection
Gn Gc and NP DNA vaccine(*59*)	IM	IFNAR -/-	100%	preGn, preGc, Np	yes	no	unknown
GP38 DNA vaccine(*60*)	IM-EP	C57BL/6 with anti-IFN mAb	20%	GP38	yes	yes	Surviving mice had two log fold higher titers against GP38
VLP(*59*)	IM	IFNAR -/-	40%	GPC	yes	no	unknown
mRNA(*61*)	IM	IFNAR -/-	50% one dose,	Only S-segment	no	no	Increase in IgG1 and IgG2a titers

			100% two doses				
Adenovirus(*62*)	IM	IFNAR -/-	33-78%	NP	no	no	unknown
MVA-NP(*63*)	IM	IFNAR -/-	0%	NP	no	no	Not protective
Inactivated CCHFV(*64*)	IP	IFNAR -/-	60-80%	Entire virus	Yes	no	Unknown, but hypothesized for neutralizing antibodies against CCHFV
Mouse brain passaged inactivated CCHFV(*65*)	SC	IFNAR -/-	Not tested in animals	Entire virus	yes	no	unknown

Table 1.2: Overview of CCHFV vaccination studies Studies highlighted in light blue contain some part of the GPC, studies in purple contain the NP, and studies in borwn/orange use the whole virus

Development of Therapeutics for Pandemics

Recent proposals have that from discovery to proof-of-concept trials can be reduced from 5-6 months from traditional timelines of 10-12 months. This reduction in time has evolved from the COVID-19 pandemic, and knowledgebase surrounding production and research into mAbs have become more common over the past 5-10 years. Furthermore, because of the advancement of technology and production capabilities, risks can be taken to produce a mAb in a shorter amount of time.

On the other hand, small molecule therapeutics encounter more barriers before they can reach the marker. Development of small molecules with no previous literature or uses need to go through several different areas i.e. Toxicity, to prove their use. A more common approach to development towards pandemic level risk has been repurposing previously approved drugs for a secondary cause. A recent example has been the development of remdesivir towards COVID, after it was developed for Ebola and a host of other RNA viruses(*66*).

Overview of Dissertation

Through the following three chapters, various biochemical techniques will be used to categorize the viral proteins from CCHFV and the coronavirus PEDV. In chapter 2, the pathogenesis of the Alpha Coronavirus Porcine Epidemic Diarrhea Virus (PEDV) will be examined through the Papain-Like Protease and how it engages the substrates Ubiquitin and ISG-15. Following the analysis of PEDV, the following chapter will focus on the BSL-4 pathogen Crimean-Congo Hemorrhagic Fever and its secreted glycoprotein GP38. Here we uncover the biochemical differences between divergent strains of CCHFV to further antibody treatments against CCHFV. These chapters build a larger idea of how to develop therapeutics against these high-risk pathogens.

1. A. H. L. Abul K Abbas, Shiv, Pillai, *Cellular and Molecular Immunology*. (Philadelphia, ed. Tenth, 2021).

2. B. T. Freitas, F. E. M. Scholte, É. Bergeron, S. D. Pegan, How ISG15 combats viral infection. *Virus Research* **286**, 198036 (2020).

3. K. N. Swatek, D. Komander, Ubiquitin modifications. *Cell Research* **26**, 399-422 (2016).

4. K. M. Valerdi, A. Hage, S. van Tol, R. Rajsbaum, M. I. Giraldo, The Role of the Host Ubiquitin System in Promoting Replication of Emergent Viruses. *Viruses* **13**, (2021).

5. M. H. Glickman, A. Ciechanover, The Ubiquitin-Proteasome Proteolytic Pathway: Destruction for the Sake of Construction. *Physiological Reviews* **82**, 373-428 (2002).

6. E. Oh, D. Akopian, M. Rape, Principles of Ubiquitin-Dependent Signaling. *Annual Review of Cell and Developmental Biology* **34**, 137-162 (2018).

7. H. T. Kim *et al.*, Certain pairs of ubiquitin-conjugating enzymes (E2s) and ubiquitin-protein ligases (E3s) synthesize nondegradable forked ubiquitin chains containing all possible isopeptide linkages. *J Biol Chem* **282**, 17375-17386 (2007).

8. A. Sette, S. Crotty, Adaptive immunity to SARS-CoV-2 and COVID-19. *Cell* **184**, 861-880 (2021).

9. M. L. Chiu, D. R. Goulet, A. Teplyakov, G. L. Gilliland, Antibody Structure and Function: The Basis for Engineering Therapeutics. *Antibodies* **8**, (2019).

10. E. A. Padlan, Anatomy of the antibody molecule. *Molecular Immunology* **31**, 169-217 (1994).

11. I. Sela-Culang, V. Kunik, Y. Ofran, The Structural Basis of Antibody-Antigen Recognition. *Frontiers in Immunology* **4**, (2013).

12. R. J. Poljak *et al.*, Three-dimensional structure of the Fab' fragment of a human immunoglobulin at 2,8-A resolution. *Proc Natl Acad Sci U S A* **70**, 3305-3310 (1973).

13. Y. Muhammed, The Best IgG Subclass for the Development of Therapeutic Monoclonal Antibody Drugs and their Commercial Production: A Review. *Immunome Research* **16**, 1-12 (2020).

14. E. B. Irvine, G. Alter, Understanding the role of antibody glycosylation through the lens of severe viral and bacterial diseases. *Glycobiology* **30**, 241-253 (2020).

15. E. O. Saphire *et al.*, Systematic Analysis of Monoclonal Antibodies against Ebola Virus GP Defines Features that Contribute to Protection. *Cell* **174**, 938-952.e913 (2018).
16. A. VanBlargan Laura, L. Goo, C. Pierson Theodore, Deconstructing the Antiviral Neutralizing-Antibody Response: Implications for Vaccine Development and Immunity. *Microbiology and Molecular Biology Reviews* **80**, 989-1010.

17. M. C. Ochoa *et al.*, Antibody-dependent cell cytotoxicity: immunotherapy strategies enhancing effector NK cells. *Immunol Cell Biol* **95**, 347-355 (2017).

18. E. O. Saphire *et al.*, Systematic Analysis of Monoclonal Antibodies against Ebola Virus GP Defines Features that Contribute to Protection. *Cell* **174**, 938-952.e913 (2018).

19. S. Kuthyar, C. L. Anthony, T. Fashina, S. Yeh, J. G. Shantha, World Health Organization High Priority Pathogens: Ophthalmic Disease Findings and Vision Health Perspectives. *Pathogens* **10**, (2021).

20. J. Cui, F. Li, Z.-L. Shi, Origin and evolution of pathogenic coronaviruses. *Nature Reviews Microbiology* **17**, 181-192 (2019).

21. S. Su *et al.*, Epidemiology, Genetic Recombination, and Pathogenesis of Coronaviruses. *Trends in Microbiology* **24**, 490-502 (2016).

22. D. Forni, R. Cagliani, M. Clerici, M. Sironi, Molecular Evolution of Human Coronavirus Genomes. *Trends in Microbiology* **25**, 35-48 (2017).

23. W. Li *et al.*, Angiotensin-converting enzyme 2 is a functional receptor for the SARS coronavirus. *Nature* **426**, 450-454 (2003).

24. G. Lu *et al.*, Molecular basis of binding between novel human coronavirus MERS-CoV and its receptor CD26. *Nature* **500**, 227-231 (2013).

25. P. V'kovski, A. Kratzel, S. Steiner, H. Stalder, V. Thiel, Coronavirus biology and replication: implications for SARS-CoV-2. *Nature Reviews Microbiology* **19**, 155-170 (2021).

26. I. A. Durie *et al.*, Structural insights into the interaction of papain-like protease 2 from the alphacoronavirus porcine epidemic diarrhea virus and ubiquitin. *Acta Crystallographica Section D* **77**, 943-953 (2021).

27. B. T. Freitas *et al.*, Characterization and Noncovalent Inhibition of the Deubiquitinase and deISGylase Activity of SARS-CoV-2 Papain-Like Protease. *ACS Infectious Diseases* **6**, 2099-2109 (2020).

28. N. Barretto *et al.*, The papain-like protease of severe acute respiratory syndrome coronavirus has deubiquitinating activity. *J Virol* **79**, 15189-15198 (2005).

29. C. M. Daczkowski *et al.*, Structural Insights into the Interaction of Coronavirus Papain-Like Proteases and Interferon-Stimulated Gene Product 15 from Different Species. *Journal of Molecular Biology* **429**, 1661-1683 (2017).
30. K. Ratia *et al.*, A noncovalent class of papain-like protease/deubiquitinase inhibitors blocks SARS virus replication. *Proceedings of the National Academy of Sciences* **105**, 16119-16124 (2008).

31. B. T. Freitas *et al.*, Exploring Noncovalent Protease Inhibitors for the Treatment of Severe Acute Respiratory Syndrome and Severe Acute Respiratory Syndrome-Like Coronaviruses. *ACS Infectious Diseases* **8**, 596-611 (2022).

32. F. E. M. Scholte *et al.*, Crimean-Congo Hemorrhagic Fever Virus Suppresses Innate Immune Responses via a Ubiquitin and ISG15 Specific Protease. *Cell Reports* **20**, 2396-2407 (2017).

33. H. C. Maltezou *et al.*, Crimean-Congo hemorrhagic fever in Europe: current situation calls for preparedness. *Euro surveillance : bulletin européen sur les maladies transmissibles = European communicable disease bulletin* **15**, 19504 (2010).

34. O. Orkun, Z. Karaer, A. Cakmak, S. Nalbantoglu, Crimean-Congo hemorrhagic fever virus in ticks in Turkey: A broad range tick surveillance study. *Infect Genet Evol* **52**, 59-66 (2017).

35. Q. Mehmood, M. J. Tahir, A. Jabbar, A. R. Siddiqi, I. Ullah, Crimean-Congo hemorrhagic fever outbreak in Turkey amid the coronavirus disease 2019 (COVID-19) pandemic; a debacle for the healthcare system of Turkey. *Infect Control Hosp Epidemiol*, 1-2 (2021).

36. E. Ozkaya *et al.*, Molecular epidemiology of Crimean-Congo hemorrhagic fever virus in Turkey: Occurrence of local topotype. *Virus Res*, (2010).

37. A. C. Mishra, M. Mehta, D. T. Mourya, S. Gandhi, Crimean-Congo haemorrhagic fever in India. *Lancet* **378**, 372 (2011).

38. " Crimean-Congo haemorrhagic fever (CCHF) in Mauritania - Update," *Disease Outbreak Report* (World Health Organization, 2003).

39. A. J. Sanchez, M. J. Vincent, S. T. Nichol, Characterization of the glycoproteins of Crimean-Congo hemorrhagic fever virus. *J Virol* **76**, 7263-7275 (2002).

40. M. J. Vincent *et al.*, Crimean-Congo hemorrhagic fever virus glycoprotein proteolytic processing by subtilase SKI-1. *J Virol* **77**, 8640-8649 (2003).

41. S. Haferkamp, L. Fernando, T. F. Schwarz, H. Feldmann, R. Flick, Intracellular localization of Crimean-Congo Hemorrhagic Fever (CCHF) virus glycoproteins. *Virol J* **2**, 42 (2005).

42. E. Z. Eisenmesser *et al.*, Inherent dynamics within the Crimean-Congo Hemorrhagic fever virus protease are localized to the same region as substrate interactions. *Protein Sci* **24**, 651-660 (2015).

43. A. Albornoz, A. B. Hoffmann, P.-Y. Lozach, N. D. Tischler, Early Bunyavirus-Host Cell Interactions. *Viruses* **8**, (2016).

44. B. R. Erickson, V. Deyde, A. J. Sanchez, M. J. Vincent, S. T. Nichol, N-linked glycosylation of Gn (but not Gc) is important for Crimean Congo hemorrhagic fever virus glycoprotein localization and transport. *Virology* **361**, 348-355 (2007).

45. S. Pinzón Martín, P. H. Seeberger, D. Varón Silva, Mucins and Pathogenic Mucin-Like Molecules Are Immunomodulators During Infection and Targets for Diagnostics and Vaccines. *Frontiers in Chemistry* **7**, (2019).

46. X. Zhang *et al.*, T-Cell Immunoglobulin and Mucin Domain 1 (TIM-1) Is a Functional Entry Factor for Tick-Borne Encephalitis Virus. *mBio* **13**, e02860-02821.

47. M. Delguste *et al.*, Regulatory Mechanisms of the Mucin-Like Region on Herpes Simplex Virus during Cellular Attachment. *ACS Chemical Biology* **14**, 534-542 (2019).

48. A. J. Sanchez, M. J. Vincent, B. R. Erickson, S. T. Nichol, Crimean-congo hemorrhagic fever virus glycoprotein precursor is cleaved by Furin-like and SKI-1 proteases to generate a novel 38-kilodalton glycoprotein. *J Virol* **80**, 514-525 (2006).

49. A. Bertolotti-Ciarlet *et al.*, Cellular Localization and Antigenic Characterization of Crimean-Congo Hemorrhagic Fever Virus Glycoproteins. *Journal of Virology* **79**, 6152-6161 (2005).

50. J. W. Golden *et al.*, GP38-targeting monoclonal antibodies protect adult mice against lethal Crimean-Congo hemorrhagic fever virus infection. *Science Advances* **5**, eaaw9535 (2019).

51. S. E. Rodriguez *et al.*, Immunobiology of Crimean-Congo hemorrhagic fever. *Antiviral Research* **199**, 105244 (2022).

52. K. R. Buttigieg *et al.*, A Novel Vaccine against Crimean-Congo Haemorrhagic Fever Protects 100% of Animals against Lethal Challenge in a Mouse Model. *PLOS ONE* **9**, e91516 (2014).

53. A. R. Garrison *et al.*, A DNA vaccine for Crimean-Congo hemorrhagic fever protects against disease and death in two lethal mouse models. *PLOS Neglected Tropical Diseases* **11**, e0005908 (2017).

54. S. E. Rodriguez *et al.*, Vesicular Stomatitis Virus-Based Vaccine Protects Mice against Crimean-Congo Hemorrhagic Fever. *Sci Rep* **9**, 7755 (2019).

55. J. R. Spengler *et al.*, Heterologous protection against Crimean-Congo hemorrhagic fever in mice after a single dose of replicon particle vaccine. *Antiviral Res* **170**, 104573 (2019).

56. J. R. Spengler *et al.*, Viral replicon particles protect IFNAR−/− mice against lethal Crimean-Congo hemorrhagic fever virus challenge three days after vaccination. *Antiviral Research* **191**, 105090 (2021).

57. F. E. M. Scholte *et al.*, Single-dose replicon particle vaccine provides complete protection against Crimean-Congo hemorrhagic fever virus in mice. *Emerging microbes & infections* **8**, 575-578 (2019).

58. J. Kortekaas *et al.*, Crimean-Congo Hemorrhagic Fever Virus Subunit Vaccines Induce High Levels of Neutralizing Antibodies But No Protection in STAT1 Knockout Mice. *Vector-Borne and Zoonotic Diseases* **15**, 759-764 (2015).

59. J. Hinkula *et al.*, Immunization with DNA Plasmids Coding for Crimean-Congo Hemorrhagic Fever Virus Capsid and Envelope Proteins and/or Virus-Like Particles Induces Protection and Survival in Challenged Mice. *Journal of Virology* **91**, e02076-02016.

60. J. J. Suschak *et al.*, A CCHFV DNA vaccine protects against heterologous challenge and establishes GP38 as immunorelevant in mice. *npj Vaccines* **6**, 31 (2021).

61. T. Aligholipour Farzani *et al.*, Immunological Analysis of a CCHFV mRNA Vaccine Candidate in Mouse Models. *Vaccines* **7**, (2019).

62. M. Zivcec, D. Safronetz, D. P. Scott, S. Robertson, H. Feldmann, Nucleocapsid protein-based vaccine provides protection in mice against lethal Crimean-Congo hemorrhagic fever virus challenge. *PLOS Neglected Tropical Diseases* **12**, e0006628 (2018).

63. S. D. Dowall *et al.*, A Crimean-Congo hemorrhagic fever (CCHF) viral vaccine expressing nucleoprotein is immunogenic but fails to confer protection against lethal disease. *Hum Vaccin Immunother* **12**, 519-527 (2016).

64. N. Canakoglu *et al.*, Immunization of Knock-Out α/β Interferon Receptor Mice against High Lethal Dose of Crimean-Congo Hemorrhagic Fever Virus with a Cell Culture Based Vaccine. *PLOS Neglected Tropical Diseases* **9**, e0003579 (2015).

65. M. Mousavi-Jazi, H. Karlberg, A. Papa, I. Christova, A. Mirazimi, Healthy individuals' immune response to the Bulgarian Crimean-Congo hemorrhagic fever virus vaccine. *Vaccine* **30**, 6225-6229 (2012).

66. R. T. Eastman *et al.*, Remdesivir: A Review of Its Discovery and Development Leading to Emergency Use Authorization for Treatment of COVID-19. *ACS Central Science* **6**, 672-683 (2020).

CHAPTER 2

STRUCUTRAL INSIGHTS INTO THE INTERACTION OF THE PAPAIN-LIKE PROTEASE 2 FROM THE ALPHACORONAVIRUS PORCINE EPIDEMIC DIARRHEA VIRUS AND UBIQUITIN[1]

I. A. Durie *et al.*, Structural insights into the interaction of papain-like protease 2 from the alphacoronavirus porcine epidemic diarrhea virus and ubiquitin. *Acta Crystallographica Section D* 77, 943-953 (2021).[1] Reproduced with permission of the International Union of Crystallography

One Sentence Summary: Coronaviruses encode the papain-like protease (PLP) which is responsible for antagonizing the innate immune response; here we show the first known *Alphacoronavirus* PLP bound to its preferred substrate ubiquitin.

Abstract

Porcine epidemic diarrhea (PED) is a devastating porcine disease that is caused by the *Alphacoronavirus*, porcine epidemic diarrhea virus (PEDV). Like other members of the *Coronaviridae* family, PEDV encodes a multifunctional papain-like protease 2 (PLP2) that has the ability to process the coronavirus viral polyprotein to aid in RNA replication and antagonize the host innate immune response through cleavage of regulatory proteins Ub and/or ISG15 (deubiquitination and deISGylation, respectively). Because *Betacoronavirus* PLP's are well characterized, we sought to find out how PEDV PLP2 from *Alphacoronavirus* differentiated itself from it's related counterparts. The *Alphacoronavirus* PEDV PLP2 was first biochemically characterized, and then a 3.1 Å resolution crystal structure of PEDV PLP2 bound to Ub was solved giving insight as to how *Alphacoronavirus* PLPs bind to their preferred substrate, Ub. We found that PEDV PLP2 is a deubiquitinase and readily processes a variety of di-Ub linkages in comparison to its *Betacoronavirus* counterparts, which have a narrower range of di-Ub activity but process Ub and interferon-stimulated gene product 15 (ISG15).

Introduction

Porcine epidemic diarrhea (PED) is a devastating porcine disease that causes severe gastroenteritis and is currently threatening the safety and economics of the United States pork industry. The causative agent of PED, porcine epidemic diarrhea virus (PEDV), is an enveloped, positive-sense single stranded RNA (ssRNA) virus belonging to the *Alphacoronavirus* genus within the *Coronaviridae* family. PEDV was first observed in 1971 in the United Kingdom and continued to re-emerge through the years throughout Europe causing mild outbreaks (*1*). It was not until 2010 when a new highly virulent strain of PEDV emerged in China that cases were beginning to be seen throughout the rest of the world. Cases of PEDV were first confirmed in North American swine in April of 2013 and within just 14 months had spread to 30 different states affecting almost 50% of swine herds resulting in almost 7 million pigs lost (*2-4*). Compounding the devastation, PEDV has an astounding mortality rate close to 100% in neonatal pigs (*2*). Recently it was estimated that the total economic impact for the US alone could range from an astonishing $900 million to $1.8 billion (*5, 6*). Vaccines are currently available for PEDV; however, the efficacy and safety of these vaccines has recently been questioned (*7-9*). In addition, PEDV is often seen to co-infect with related coronaviruses, that cause almost identical clinical symptoms, transmissible gastroenteritis virus (TGEV), porcine deltacoronavirus (PDCoV), and the newly emerged swine acute diarrhea syndrome coronavirus (SADS-CoV), which has caused complications in diagnoses of these viruses (*10*). With continued outbreaks and re-emergence of PEDV and emergence of new porcine coronaviruses, understanding how these viruses interact with their host will be key in the development of new therapeutics.

CoVs are known to infect a wide variety of species including mammals and birds with viruses from the *Alpha-*, *Beta-*, and *Deltacoronavirus* genera readily infecting porcine. The genome of PEDV is 28 kb long and like other positive single-stranded RNA viruses encodes two cysteine proteases, the papain-like protease (PLP) and the 3C-like protease or main protease (3CLpro; M^{pro}). PEDV, as well as several other members of *Alpha-* and *Betacoronavirus,* encode two copies of the PLP and are denoted as PLP1 and PLP2; when a single PLP is encoded it is denoted at PLpro (Figure 2.1) (*11*). Together, these proteases are responsible for the proteolytic processing of the long polyprotein into the respective 16 different nonstructural proteins (nsps), which are essential for the formation of the membrane-bound replicase complex utilized during RNA replication (*12-16*). The PLP is responsible for cleaving nsps 1-3 while the 3C-like protease cleaves 4-16; however, the CoV PLP has been observed to play additional roles other than promoting viral replication (*13, 17*).

Several CoV PLPs, such as the PLpro from severe acute respiratory syndrome coronavirus (SARS CoV), severe acute respiratory syndrome coronavirus 2 (SARS CoV-2), Middle East respiratory syndrome coronavirus (MERS-CoV), avian infectious bronchitis virus (IBV) and the PLP2 from mouse hepatitis virus (MHV), have been suggested to down regulate the innate immune system by cleaving post-translational modifications of host proteins by ubiquitin (Ub) and Ub-like interferon stimulated gene product 15 (ISG15) (*14, 18-20*). The processes of ubiquitination and ISGylation of viral and host proteins are essential for several pathways within the innate immune system, which is understood as the first line of defence against viral infections (*21, 22*). As part of this defence, induction of these pathways include interferons (IFNs), within the type I interferon response (IFN-1), interferon stimulated genes (ISGs) and cytokines as well as an inflammatory

response through the NFκB pathway (*23, 24*). The combined activities of deubiquitination and deISGylation by the PLP have been observed to antagonize the IFN-1 response suggesting the PLP to be a virulence factor that can be manipulated for therapeutic purposes. This has been demonstrated through the disruption of deubiquitinating and deISGylating activities from the MERS-CoV PLpro, which subsequently resulted in the partial suppression of Ub-dependent mitochondrial antiviral-signalling protein (MAVS) mediated signalling leading to removal of the antagonized IFN-I response (*25*). In addition, destabilizing mutations within the MHV PLP2, which diminished both activities, resulted in a reversal of the antagonism of IFN-1 response (*15*). Taken together, these results demonstrate the need to further understand the PLPs from re-emerging coronaviruses, especially CoVs infecting swine like PEDV, to better understand this key viral evasion mechanism and associated pathogenicity.

The biochemically characterized CoV PLPs, have been observed to possess varying degrees of deubiquitinase and deISGylase activities. Ubiquitination, and subsequent deubiquitinase activity, is not limited to a single mono-Ub event but includes polyubiquitination at one of the seven available lysine positions on Ub (positions 6, 11, 27, 29, 33, 48, and 63) (*26, 27*). Both mono- and polyubiquitination of viral and host proteins are essential in several different signalling pathways. For example, K63-linked poly-Ub has been observed to be directly involved in the activation of retinoic acid-inducible gene I and mitochondrial antiviral signalling protein, which is a critical innate immune pathway in recognizing foreign single-stranded RNA (ssRNA) (*28, 29*). Also, K48-linked poly-Ub has been observed to be involved in triggering the degradation of IκB in the NFκB pathway and K11-linked poly-Ub has recently been implicated in TNF signalling (*30-34*).

However, the exact role of deubiquitination activities in promoting CoV PLPs as antagonists of the IFN pathway is still unknown.

Work on the PEDV PLP2 in cells has demonstrated that the PEDV PLP2 is directly involved in the antagonism of the IFN response and can cleave poly-Ub chains from RIG-I and stimulator of interferon genes (STING); however, the exact catalytic activity and substrate preference has yet to be reported (*35*). Here the biochemical characterization of the PLP2 in regard to its deubiquitinating and deISGylating activities from PEDV is described in detail. In addition, this study reveals the first structure of an *Alphacoronavirus* PLP2 bound to its preferred substrate, unlocking potential keys to understanding host-viral interactions.

Results

Deubiquitinating and DeISGylating activity of PEDV PLP2

Previously, viral deubiquitinases (DUBs) and deISGylases have been shown to vary in their substrate specificity even between virus strains (*20, 38*). To investigate the substrate preferences of PEDV PLP2, the full-length protease containing both the catalytic domain as well as the UBL, was expressed and purified. Single point kinetic parameters were assessed utilizing a 7-amino-4-methylcoumarin (AMC) fluorophore conjugated to the C-terminal end of Ub, human ISG15, and a short peptide sequence, RLRGG, which is the shared recognition sequences of the two prior substrates. The peptide is used as a control in order to examine overall catalytic efficiency of the protease. Deubiquitinating and deISGylating substrate preference was determined by monitoring the release of the AMC fluorophore over time. Curiously, PEDV PLP2 turns over Ub-AMC at 0.29 ± 0.0014 molecules/min, which is three orders of magnitude above what was seen for the

deISGylase activity at 3.2 x 10^{-4} ± 0.000039molecules/min (Figure 1a/b). The overall peptide-AMC activity is similar to that of its deISGylase activity and was assessed as 1.0 X 10^{-2} molecules/min (Figure 1c). PEDV PLP2 appears to principally be a DUB, which intriguingly sets it apart from its *Betacoronavirus* counterparts, SARS CoV-2 and MERS CoV. In comparison to other DUBs at the same substrate concentration, PEDV PLP2 has similar DUB activity to SARS CoV-2 PLP, while it's deISGylase function resembles the vOTU of porcine reproductive and respiratory syndrome virus (PRRSV) modified live vaccine (Ingelvac PRRS® MLV)(*37*).

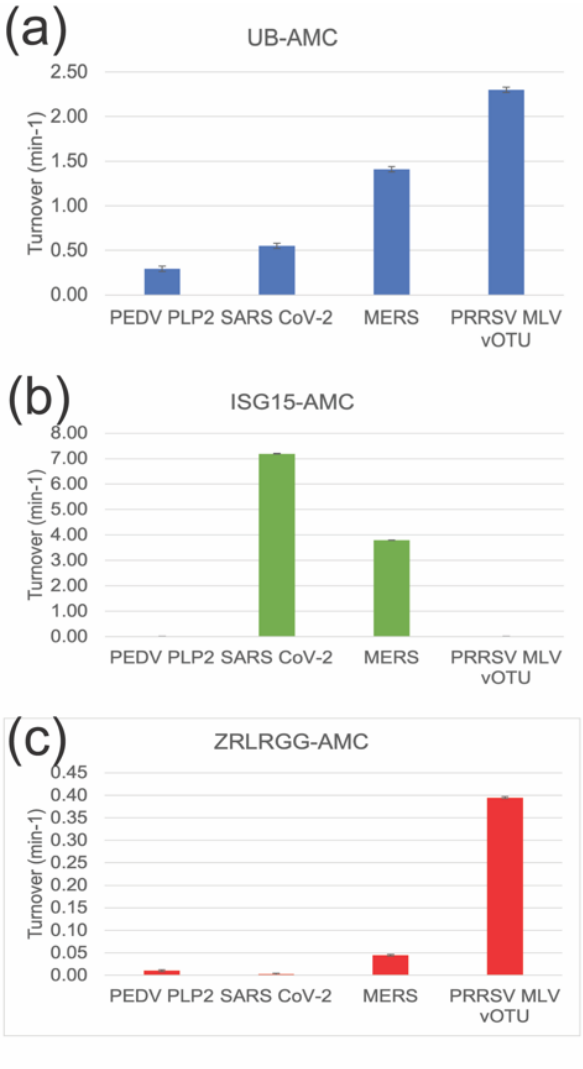

Figure 2.1 Enzymatic Activity Comparison of Deubiquitinating Enzymes. Protease activity of PEDV PLP2 in comparison to SARS CoV-2 PLP, MERS-CoV PLP, and PRRSV-MLV vOTU. All enzymes were assessed utilizing single concentrations at (a). 1 µM Ub-AMC, (b). 1 µM ISG15-AMC, and (c). 50 µM ZRLRGG-AMC. Readout is measured via an increase in fluorescence over time and is reported as turnover (molecules/min). Error is reported as standard deviation. Specific activity data was taken from (*20, 36, 37*).

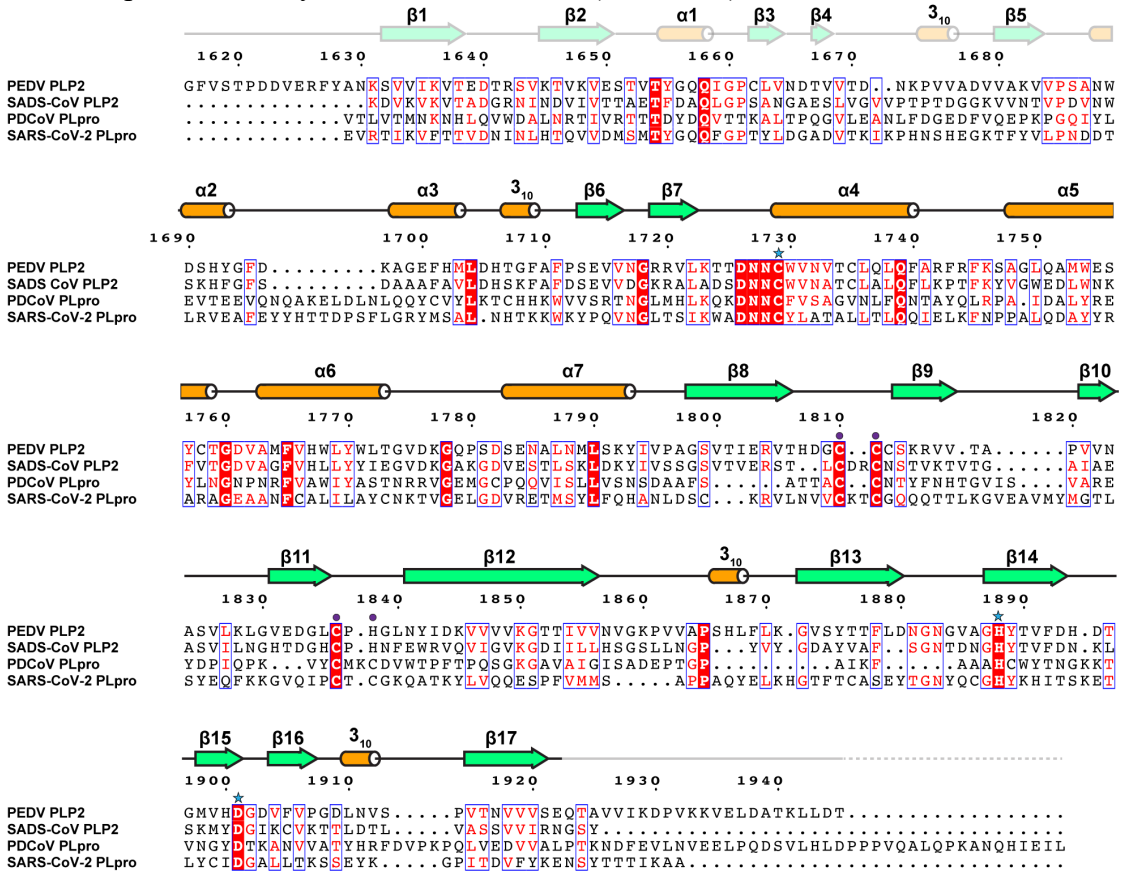

Figure 2.2 Sequence alignment of PLpros and PLP2s from coronaviruses. The PLP2 from PEDV PLP2 (accession number AHA38151.1), SADS CoV PLP2 (accession number ASK51716.1), PDCoV PLpro (accession number AIP90485.1), and SARS CoV-2 PLpro (accession number QKG86869.1). The residue numbering is based on the polyprotein 1a of PEDV. The faded out secondary structure above the sequence alignment denotes the secondary structure of the UBL from SARS CoV-2 (RCSB 6W9C). The colored in secondary structure was calculated by DSSP from experimental data and denotes the catalytic core that was used for crystallization. Residues that form the catalytic triad are denoted by stars in sky blue, while the zinc finger residues are marked by purple circles.

1.1. Structure of PLP2 from the *Alphacoronavirus* PEDV

With limited structural information available related to PEDV PLP2 and how it engages its preferred substrate, a structure of the protease complex was sought. Initial attempts to crystallize full length PEDV PLP2 with or without Ub proved unsuccessful. However, screening just the catalytic core of PEDV PLP2 short with the Ub-PA substrate yielded a 3.1 Å dataset(*44*). Using molecular replacement with a previously deposited unbound PEDV PLP2 short structure, a structural solution was found in space group P212121. The asymmetric unit contained eight copies of the protease-Ub complex along with fourteen zinc ions. A dictionary of protein secondary structure (DSSP) analysis of the catalytic core of PEDV PLP2 short reveals a mix of seven α-helices, three 3_{10} turns, and seventeen β-strands (Figure 2.2 and 2.3A). Eight of zinc ions were associated with the finger domain of PEDV PLP2 whereas six zinc ions formed electrostatic bridges between chains of PEDV PLP2. Four of the zinc ions formed bridges with chain A, C, G, E residues His1688, His1692, and chain O,M,I,K residue Cys1812 (Figure 2.3C). The other two zinc ions formed bridges with chain C, E Glu1803, Cys1812, with Chain A,G Glu1803, and Cys1812 (Figure 2.3C). An overlay comparison of the eight copies revealed very little global structural differences between the chains (Figure 3b).

Overall, the secondary structure elements of PEDV PLP2 give rise to the classic features of *Coronaviridae* PLPs' catalytic domain (the finger domain, the palm domain, the thumb domain) (Figure 3a). As with other *Coronaviridae* PLPs, like MERS-CoV and SARS CoV, the PEDV PLP2 can assume two states: an open state when unbound or a closed state when bound to substrate (such as Ub or ISG15) (*25, 36*). To ascertain common features and points of difference that can occur within *Alphacoronavirus* PLPs, our closed conformation PEDV PLP2 structure

alongside an open conformation PEDV structure (RCSB 6NOZ) was overlayed with the recently solved *Alphacoronavirus* PLP2 of swine acute diarrhea syndrome, SADS (RCSB 6L5T) (*45*) (Figure 2.3D). Both *Alphacoronavirus* PLP2 structures were solved without their UBL domain and the overlay shows that *Alphacoronavirus* PLP2's has similar secondary structures. SADS and PEDV PLP2 have a 44% pairwise identity. Even though *Coronaviridae* PLPs have similar functions and folds, the difference in sequence identity can drastically change the binding affinity of a PLP with ISG15 and Ub. The finger and palm domain contain key regions that are responsible for binding of Ub. The overlay of SADS and PEDV have shown some differences between the two structures particularly in the finger domain of their PLP2.

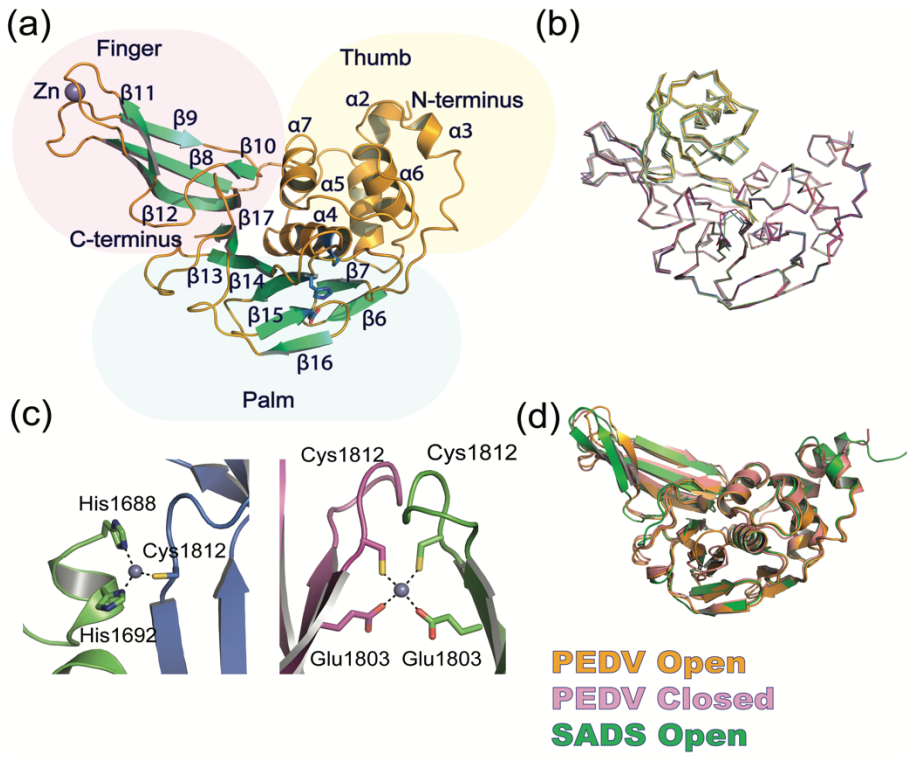

Figure 2.3 Structure of PEDV PLP2 (a). Cartoon rendering of the PEDV PLP2 with the α-helixes in orange and β-strands in lime green, the catalytic triad is represented by sticks in sky blue. The structural domains of PEDV PLP2 consist of the fingers (pale pink), palm (pale teal), and thumb (pale yellow). (b). Ribbon overlay of the eight PEDV PLP2 Ub complex chains which make up the asymmetric unit. RMSD of overlaid chains did not exceed 0.42 (c). Zn ion crystal

contacts between chains in the asymmetric unit. (d). Overlay of PEDV PLP2 open and closed with SADS-CoV PLpro (PDB accession number 6NOZ and 6L5T) The root mean square deviation (RMSD) of PEDV closed to SADS Open is 1.33, and PEDV closed to PEDV open is a RMSD of 0.9727. Dashed lines represent hydrogen bond distances less than 3.5Å.

They both contain six alpha helixes while PEDV PLP2 has twelve β-strands in comparison to the SADS PLP2 thirteen β-strands that comprise the palm, finger, and thumb domains. They both contain four β-strands that form the finger domain. In comparison with *Betacoronaviruses* and *Deltacoronaviruses* the finger domain does not appear to pack as tightly against the hydrophobic region in the palm domain (*36*). Within the finger domain the β-strands 11 and 12 contain a Cys1810-Cys1811-Cys1836-His1838 motif that bind to a Zn^{2+} ion. This is conserved among *Alphacoronaviruses* in comparison to *Betacoronaviruses* and *Deltacoronaviruses* which have a zinc finger binding motif that is formed from four-cysteine residues. The loop between β-strands 8 and 9 have some differences that affect the zinc binding motif. Although they both contain a Cys-Cys-Cys-His motif that bind to a Zn^{2+} ion, SADS has an additional two amino acids, Asp and Arg, that reside between the PEDV Cys1810-Cys1811 (Figure 2.1). Both PLP2s have an Asp residue in hydrogen bonding proximity to Cys1811, which appears to stabilize the loop between β-strands 8 and 9 when bound to Zn^{2+}. When comparing the open to the closed conformation of PEDV PLP2 there is a 2.95Å shift in movement in the finger domain when moving from an unbound to a bound conformation.

Moving away from the finger to the palm domain there is an additional four amino acids in PEDV PLP2 between β-strand 12 and β-strand 13. As part of the palm domain, three of these amino acids compose a 3_{10} Helix between β-strand 12 and β-strand 13. *Coronaviridae* PLPs have a highly conserved alpha helix within the palm domain denoted within our Figure 1 as α-helix 4.

This α-helix is in proximity to the catalytic triad denoted by Cys-1729, His-1888, and Asp-1901, and contains a Trp-1730 that is conserved among PEDV, SADS, and human coronavirus (HCoV). In *Betacoronaviruses* the Trp is replaced with a Tyr which can be exploited as an anchor for drug inhibition (*20*). With these subtle differences between SADS and PEDV PLP2, this replacement could result in a difference in affinity to Ub and ISG15.

Ubiquitin interaction with PEDV PLP2

Previous work has used the suicide substrate Ub-PA to covalently bind PLPs and other deubiquitinases to aid in the study of their interactions with Ub (*36, 44*). Upon obtaining the first bound *Alphacoronavirus* PLP2 with the suicide substrate Ub-PA, we observed three main regions that confer important binding interactions: the finger domain, a hydrophobic region located in the palm domain, and the ubiquitin LRLRG binding site which is also located in the palm domain (Figure 2.4). These three regions are found within other PLPs and serve a similar function(*25, 46*).

In the PEDV finger domain, two interactions stand out in the interface of PEDV PLP2 and Ub. The first is the terminal nitrogen of PEDV Arg-1815 located in β-strand 9 which interacts with Ub Ala-46, and the second is an electrostatic interaction between PEDV Asp-1833 from β-strands11 and Ub-PA His-68 (Figure 2.4B). Asp-1833 is conserved among the *Alphacoronavirus's* SADS and PEDV. The electrostatic interaction between Asp-1833 and His-68 force a conformational shift of β-strand 11 towards Ub-PA which leads to an energetically favourable interaction between the Ub-PA hydrophobic region and the PEDV hydrophobic region denoted by residues 1821-1824, and 1855-1858 (Figure 2.4C). These observed interactions between PEDV PLP2 and Ub can also provide initial insight into PEDV PLP2's low

deISGylase activity. For instance, the ISG15 counterparts of Ub His68 tend to be large bulky or hydrophobic residues such as phenylalanine, tyrosine, and isoleucine that would be incompatible with PEDV PLP2's D1833. Additionally, the Ile44 and Val70 of Ub responsible for the hydrophobic interface with PEDV PLP2 tend to be hydrophilic residues in ISG15. Specifically, the ISG15 counterpart of Ile44 is typically a serine or threonine, whereas the ISG15 counterpart of Val70 is typically an asparagine or histidine.

The Ub-PA LRLRG tail rests in the PLP2 active site between the finger and hydrophobic region. To facilitate Ub processing, the PEDV PLP2 catalytic triad consisting of Cys-1729, His-1888, and Asp-1901 are responsible for DUBs' enzymatic mechanism of action. In the case of our substrate Ub-PA, only Cys-1729 from PEDV PLP2 forms a covalent interaction while His-1888 and Asp-1901 have no discernible interactions with the Ub-PA tail. Otherwise, the Ub-PA mainchain consists of five main interactions. Ser-1781 forms three hydrogen bonding interactions with the Ub tail backbone, Arg-72 and Gly-75. The other two interactions involve a hydrogen bond interaction between Ub-PA Arg-74 to PEDV PLP2 Asp-1887, and the interactions between Asp-1782 and the Ub-PA tail mainchain (Figure 2.4D).

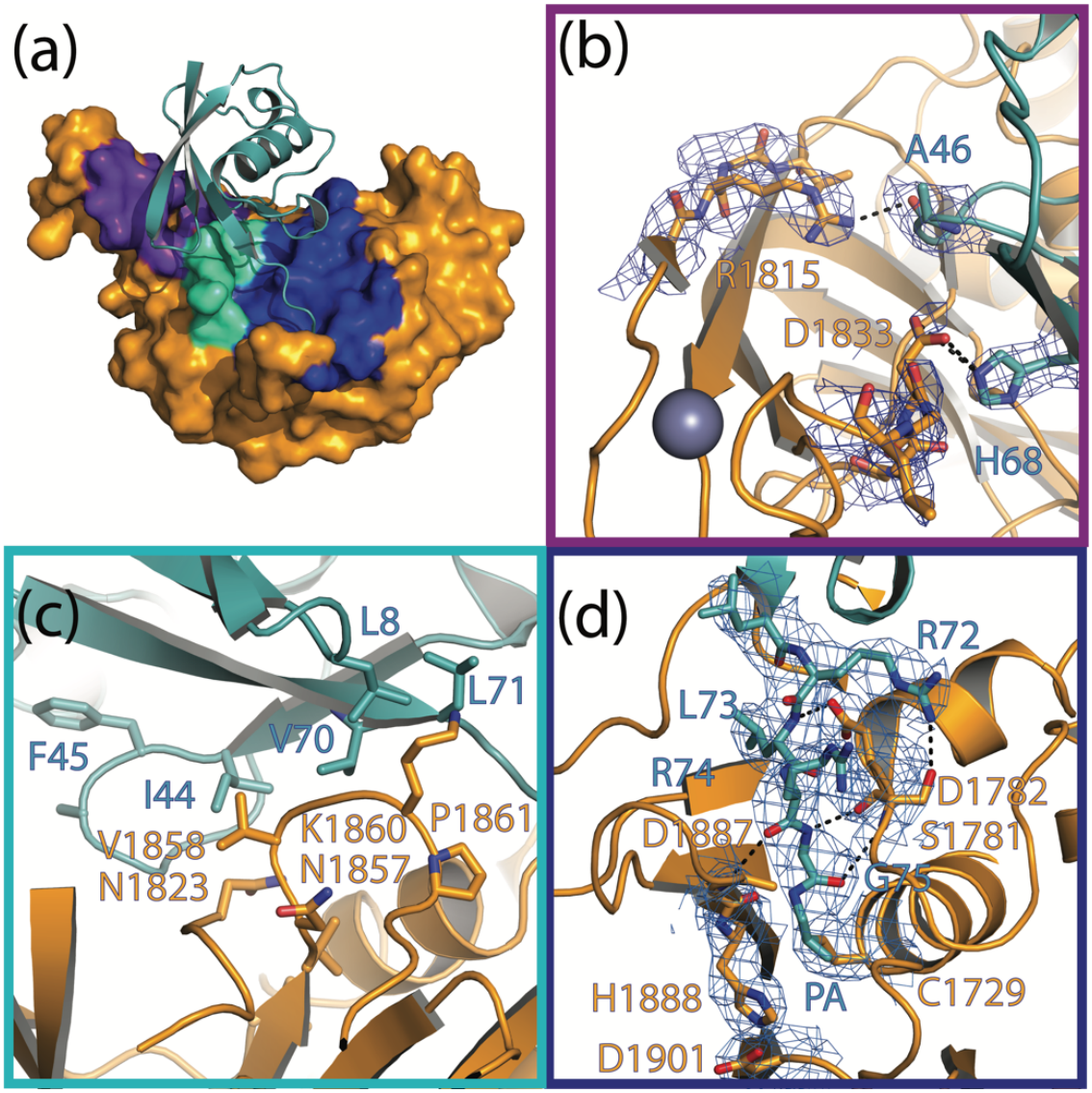

Figure 2.4 PEDV PLP2 regions responsible for binding of Ub PEDV PLP2 surface interactions with ribbon ubiquitin in teal, (a). purple denoting the finger domain interaction with Ub, green cyan denoting the hydrophobic region interaction between PEDV PLP2 and Ub, and blue which denotes the Ub tail binding site (b). hydrogen bonding between the finger domain and ubiquitin with $2F_o$-F_c density map overlaid over key residues (c). Hydrophobic interactions between PEDV PLP2 and ubiquitin (d). Ubiquitin recognition sequence LRLRGG in PEDV PLP2 active site with $2F_o$-F_c density map to show key interactions in the active site. Dashed lines represent hydrogen bond distances less than 3.5Å.

To characterize the bound (closed) conformation of PEDV PLP2, an overlay was computationally performed with the deposited PEDV PLP2 unbound (open) conformations (RCSB 6NOZ) to visualize the differences between open and closed conformations of PEDV PLP2. As with other PLPs, three main areas are observed that contort to account for a closed conformation as previously seen with bound PLPs (Figure 2.5I)(*36*). The finger binding domain moves towards the palm domain (Figure 2.5II). The shift of β-strand 11 and β-strand 12 towards the palm domain is facilitated by the electrostatic interaction between PEDV PLP2 Asp-1833 and Ub His-6. With this movement it forces a slight shift of β-strand 8 and β-strand 9 with the Zn^{2+} ion towards β-strands 11 and 12.

At the palm domain there are two main areas that constitute the closed conformation, the movement of the BL2 loop which occurs from the binding of the Ub-PA tail in the PEDV PLP2 active site Cys1729 (Figure 2.5III, 2.5IV). Some differences are usually found the BL2 loop located between β-strand 14 and β-strand 15. Usually, the BL2 loop has been observed in many PLPs as being highly flexible and electron density does not usually appear unless it is influenced by the packing of the crystal lattice or depending on the type of substrate bound. Surprisingly, the open conformation of PEDV yielded density to support how the BL2 loop moves (Figure 2.5III). When Ub-PA is locked into position, a similar conformation shift like in the finger domain occurs but with Ub Arg-74 and PEDV PLP2 Asp1887. When moving from an open to closed conformation, Asn-1883 moves 5.95Å upwards towards the PEDV active site and Ub LRLRG tail.

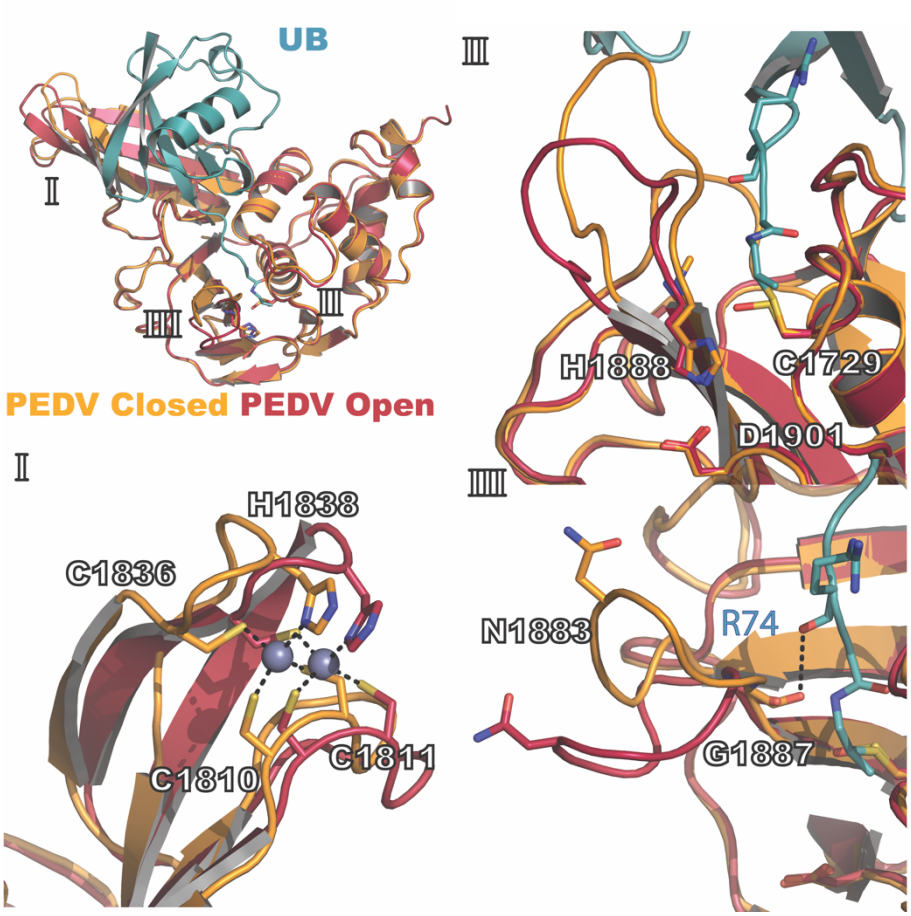

Figure 2.5 Closed vs Open conformations of PEDV PLP2 Comparison and overlay of PEDV PLP2 closed and open structures I. Zn Finger movement II. PEDV PLP2 catalytic triad interactions with Ub RLRG III. Conformation changes of the BL2 loop regarding the Ub RLRG tail. Dashed lines represent bond distances less than 3.5Å.

These changes in conformation may help account for the more stringent substrate specificity observed between *Alphacoronavirus* and *Betacoronaviruses*. To gain further insight into the closed conformation between bound PLPs, Ub-bound MERS CoV, SARS CoV-2, and our PEDV PLP2 structure were overlaid (Figure 2.6). The overall fold of the three PLPs are nearly identical except for the finger domain. It appears that PEDV PLP2 is more rigid than its *Betacoronavirus*

counterparts including its finger domain and the BL2 loop. The PEDV finger domain does not come towards the palm domain nearly as much as that of SARS CoV-2 (RCSB 6XAA) and MERS CoV (RCSB 5V69). There is a dramatic shift of 16.45 Å from a closed PEDV PLP2 finger domain to the closed MERS CoV finger domain. This shift in the finger domain alongside residue differences could affect substrate specificity for Ub and ISG15.

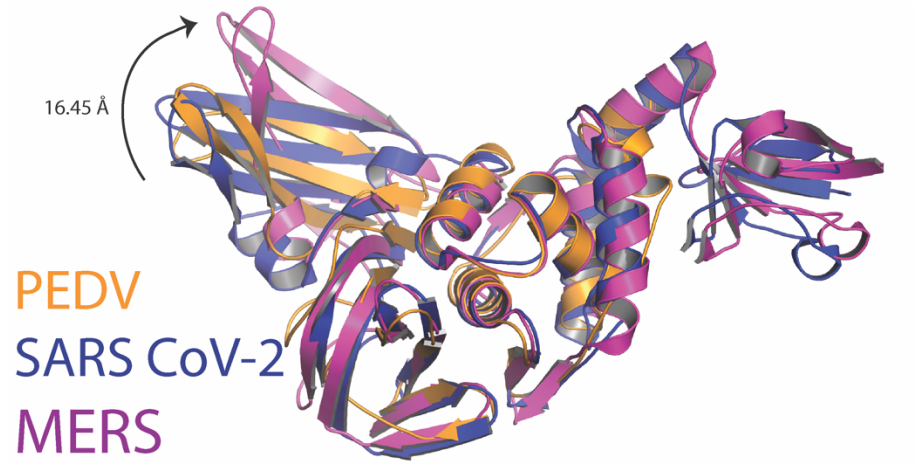

Figure 2.6 Closed conformations of PLPs Comparison and overlay of bound (closed) PLP's. A mix of *Alphacoronavirus* and *Betacornaviruses* bound to ubiquitin were overlaid on one another the ubiquitin was taken out to visualize the closed conformation of PLPs. Our PEDV structure was overlaid with the *Betacoronaviruses* SARS CoV-2 (RCSB 6XAA) in blue and MERS PLP (RCSB 5V69) in magenta. The RMSD of bound PEDV PLP2 to bound SARS CoV-2 PLP is 2.7 Å, and bound PEDV PLP2 to bound MERS CoV PLP is 2.5 Å.

Poly-ubiquitin and PEDV PLP2

In some cases, DUBs can have higher turnover rates for poly-Ub linkages compared to mono-Ub potentially due to an increase in favourable contacts between the larger Ub substrate (*44*). To further investigate and characterize PEDV PLP2's DUB activity a panel of seven lysine linked di-Ub (K6, K11, K27, K29, K33, K48, and K63) and linear di-Ub were tested via gel shift assay (Figure 2.7A). Over a span of 60 minutes, PEDV PLP2 was observed to have significant activity for K63, K48, K11, and K6 di-Ub. In the past, PLPs have been observed to prefer K48-linked

poly-Ub linkages (*20, 47*). Similarly, PEDV PLP2 was observed to have significant activity towards K48-linked di-Ub. Intriguingly, significant activity was also observed for K63-, K11-, and K6-linked di-Ub which shares similarity to the di-Ub K63 and K48 cleavage from MERS-CoV PLP and mouse hepatitis coronavirus PLP2 (MHV) (*25*).

After initial di-Ub activity assays, K48- and K63- linked di-Ub fluorescence resonance energy transfer (FRET) substrates were used to quantify PEDV PLP2 activity. The activity toward each FRET substrate was monitored by an increase in fluorescence via the proteases' ability to cleave the di-Ub molecule, which separates the FRET pairing. The overall di-Ub FRET activity for PEDV PLP2 was low for K48- and K63-linkages compared to what was seen with the cleavage assays using Ub-AMC and ISG15-AMC, likely suggesting the FRET pair positioning interfered with the protease's interaction with the substrates. Subsequent tests revealed that positioning of the FRET pairing had a large impact on turnover with preferences of K11 position 4, K48 position 3, and K63 position 3 (Figure 2.7B).

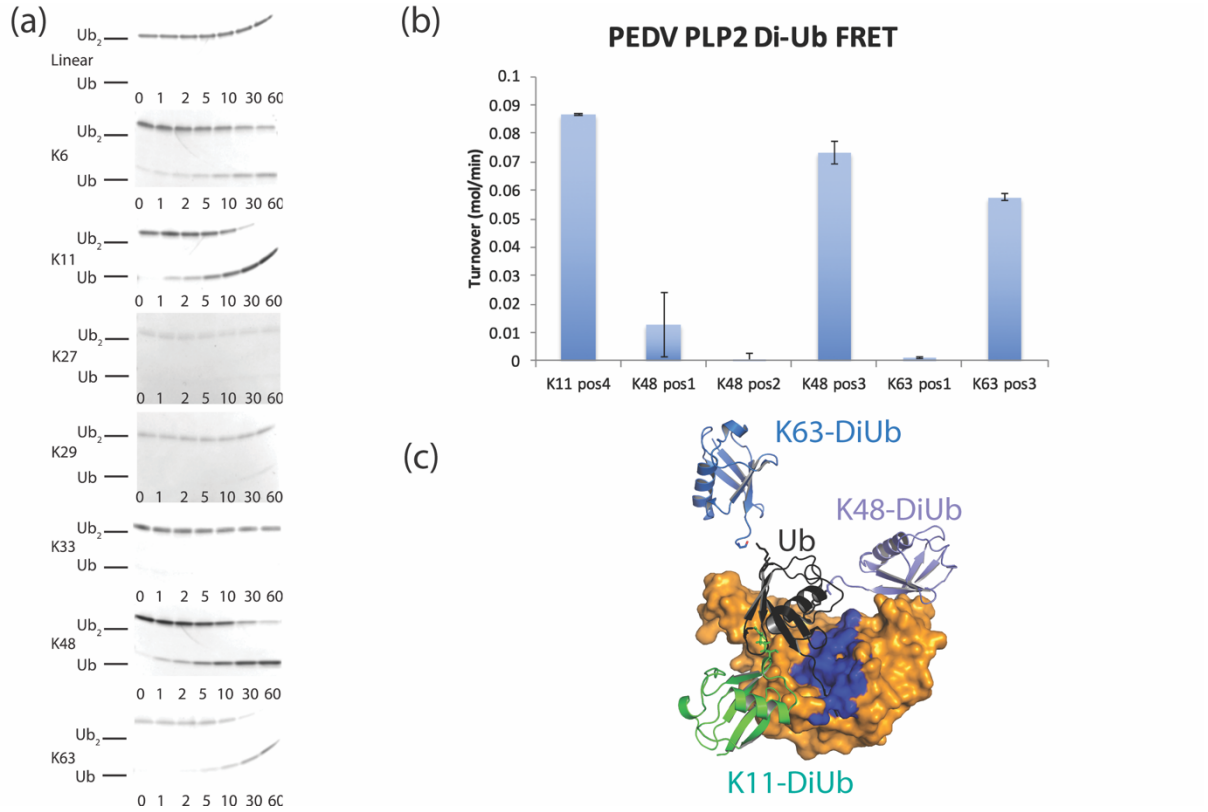

Figure 2.7 PEDV PLP2's ability to cleave Di-Ub linkages (a). Di-Ub linkages (10 μM) were incubated with PEDV PLP2 (200 nM) at 37 °C for 60 min. Seven time points were taken and analysed on a 10% Mini-Protean Tris-Tricine precast gel (Bio-Rad). (b). PEDV PLP2 was tested against di-Ub substrates (c). Overlay of di-Ub substrates to a bound PEDV PLP2. The blue region highlighted on the surface depicts the Ub binding site, K48 from (RCSB 5E6J) in light purple, K11 from (RCSB 2MBQ) in light green, K63 from (RCSB 3H7P) in light blue.

Within the antiviral innate immune response pathway K11-, K48- and K63-linked poly-Ub are heavily implicated to be involved, providing a potential link that PLPs such as PEDV PLP2 can be involved in suppressing the innate immune response via deubiquitination. Specifically, K48-linked poly-Ub is responsible for activation of the inflammatory response through the NF-κB pathway via proteasomal degradation of inhibitor of nuclear factor κB (IκB). K63-linked poly-Ub has been directly linked to antiviral signaling by RIG-I/MAVS, which induces type-I IFNs (*29, 36, 39*). Lastly, K11-linked poly-Ub has been recently shown to be involved in the ubiquitination

of STING and TNF signaling, which induces pro-inflammatory cytokines in response to a viral infection (*32, 33*).

To gain some insight to explain the substrate preferences of PEDV PLP2, we used our solved complex structure to overlay K48 di-Ub (RCSB 5E6J), K11 di-Ub (RCSB 2MBQ) and K63 di-Ub (RCSB 3H7P) (Figure 2.7C). A previous study shows that K48 has a distinctive interaction with the UBL of the SARS CoV PLP during crystal formation (*46*). Although our construct did not express the PLP2 UBL, it appears that K48 would play a role in forming interactions with the thumb domain. K11 di-Ub was overlayed on our closed conformation PEDV PLP2 significant interactions are seen in K11-distal which interacts significantly with the finger and palm domain. The orientations of both K63, K48, and K11 do not sterically clash with our PEDV PLP2 structure. The ubiquitin binding is distinctive and different between coronaviruses, and for PEDV its processing of K6 and K11 makes it unique among coronaviruses. Taken together, the ability of the PEDV PLP2 to process several different Ub-linkages might suggest a link to the increased pathogenicity of PEDV.

Conclusion

Here we report the first bound structure of an alphacoronavirus PLP2 with the substrate Ub. As with other coronaviruses we see a common theme among PLPs with the Ub having significant interactions with the finger, palm, and thumb domain. In comparison to *Betacoronavirus* PLPs, the finger domain of *Alphacoronaviruses* PLPs has a less significant role in its interaction with Ub, which may explain its inability to process ISG15. The *Alphacoronavirus* zinc finger domain contorts itself away from Ub in comparison to structures like MERS or SARS CoV-2 PLP bound to Ub or ISG15. This could explain its non-selectivity towards di-Ub linkages with preferences

towards K63-, K11-, and K6 molecules, while having extremely low affinity towards ISG15. Substrate specificity of Ub or ISG15 has major roles in viral immune suppression, and by characterizing PEDV PLP2 further studies can pave the way to fully understanding its role in immune suppression.

Materials and Methods

Expression and Purification of the PLP2 Domain from PEDV for Biochemical Characterization

The construct for the PLP2 domain originating from PEDV polyprotein 1a consisting of residues 1616-1945 with an engineered 6xHis tag was cloned into the pET15b expression vector (GenScript) and transformed into *E. coli* BL21 (DE3) competent cells (New England Biolabs) via heat shock. The subsequent cells were grown overnight in 250mL LB broth supplemented with 100 μg/mL ampicillin at 37 °C. 10 mL of the overnight culture was added to 1.5L LB broth autoinduction media [Autoinduction Media: LB broth supplemented with β-lactose, glucose, glycerol, KH_2PO_4, Na_2HPO_4 pH 8.0] and grown at 25 °C for 24 hr. Cells were collected via centrifugation at 10,000g for 15 min and stored at -80 °C for purification. For purification, cell pellets were resuspended in Buffer A [5 M guanidine, 500 mM NaCl, 100 mM Tris pH 8.0, 10% (v/v) glycerol], supplemented with lysozyme. The cell suspension was then sonicated on ice at 80% power with a 50% duty cycle for a total of 8 min using a Fisher Scientific series 150. The cell lysate was centrifuged at 70,600g for 30 min at 4 °C and the subsequent supernatant filtered using a 0.8 μM filter for further purification. The filtered supernatant was flowed over high-density nickel agarose beads (Gold Biotechnology) pre-equilibrated with cold Buffer A, washed with 5 CV of Buffer A supplemented with 30 mM imidazole and eluted with 5 CV of Buffer A

supplemented with 300 mM imidazole. The eluted protein was dialyzed overnight in Buffer B [1 M L-arginine, 100 mM NaCl, 100 mM Tris pH 8.0, 0.1 mM $ZnCl_2$] at 4 °C and dialyzed a second time in Buffer C [300 mM NaCl, 20 mM Tris pH 8.0, 0.1 mM $ZnCl_2$, 2 mM DTT, 5% (v/v) glycerol] for a minimum 12 hr to remove the L-arginine. The protein was further purified by size-exclusion chromatography using Superdex 200 resin (GE healthcare) equilibrated with Buffer D [150 mM NaCl, 10 mM HEPES pH 8.0, 0.1 mM $ZnCl_2$, 2 mM DTT]. The fractions with protein, confirmed by SDS-PAGE, were pooled for biochemical assays.

Analysis of Enzymatic Activity of PEDV PLP2 towards Ub and ISG15

To assess the PEDV PLP2 protease steady-state kinetic parameters, fluorescence assays were performed as previously described (*36-38*). Briefly, purified PEDV PLP2 was tested against Ub, ISG15, and Z-RLRGG peptide conjugated to the fluorescence molecule 7-amino-4-methylcoumarin (AMC) and di-Ub fluorescence resonance energy transfer (FRET) linkage substrates K11, K48, and K63 (Boston Biochem). Assays were performed in duplicate in assay buffer [100 mM NaCl, 50 mM HEPES pH 7.5, 0.01 mg/mL bovine serum albumin (BSA), 5 mM DTT] with the change in relative fluorescence as a function of time (RFU/min) monitored within the steady-state region. For the di-Ub FRET assays, the turnover was determined by measuring the increase in fluorescence as a result of the separation of the FRET TAMRA/QXL pair, in which QXL acts as a quencher. Additional di-Ub FRET positions were tested that contained the fluorophore-quencher FRET pair at different positions to account for steric interference. The concentrations used for the assays were Ub- and ISG15-AMC at 1 μM, Z-RLRGG-AMC at 50 μM, di-Ub FRET pairings at 1 μM and the PEDV PLP2 protease at 50 nM.

di-Ub Cleavage Assays

To perform the di-Ub cleavage assays, the eight different di-Ub linkages, K6, K11, K27, K29, K33, K48, K63, and N-terminal linear form were purchased (Boston Biochem) to assess the PEDV PLP2 ability to cleave the different di-Ub chains to mono-Ub. The assay was performed at 37 °C in the prementioned assay buffer, minus BSA, with the substrates present at 10 μM and PEDV PLP2 present at 100nM in a total assay volume of 70 μL. The reactions were quenched 1:1 with 9 μL of 2 x SDS-tricine sample buffer at seven different time points [0, 1, 2, 5, 10, 30, and 60 min] and then boiled at 95 °C for 5 min. Samples were analyzed via SDS-PAGE on a 10-20% Mini-Protean Tris-Tricine precast gel (Bio-Rad).

Expression and Purification of the Catalytic PLP2 Domain from PEDV for Complexation and Crystallization

A shortened PLP2 (PEDV PLP2 short) domain without the ubiquitin-like domain (UBL, residues 1616-1690) consisting of residues 1691-1920 of the nsp3 from PEDV with an engineered 6xHis tag was cloned into the pET15b expression vector (Genscript) and transformed into *E. coli* T7 Express competent cells (New England Biolabs) via heat shock. The subsequent cells were grown overnight in 250mL LB broth supplemented with 100 μg/mL ampicillin at 37 °C. 10 mL of the overnight culture was added to 1.5L LB broth and grown at 37 °C until the culture O.D was 0.6 and then induced with 0.5 mM isopropyl β-D-thiogalactopyranoside (IPTG), and the culture was incubated at 18 °C overnight. Cell were collected via centrifugation at 5,200 G for 10 min and stored at -80 °C.

The cell pellet was resuspended in 125ml of lysis buffer (500 mM NaCl, 20 mM Tris pH 7.4, 10 mM beta-mercaptoethanol (BME)) with lysozyme for 40 minutes. The cell suspension was then

sonicated on ice at 50% power with a 50% duty cycle for a total of 6 min using a Fisher Scientific series 150. Immediately after the lysate was centrifuged at 23000 RPM for 20 min. The supernatant was then filtered using a 0.8 μM-pore-size-filter, and the subsequent solution was poured over 2ml of high-density nickel agarose beads (Gold Biotechnology). The resin was subjected to 10 column volumes of lysis buffer, 10 column volumes of buffer supplemented with 10 mM imidazole, and then 10 column volumes of buffer supplemented with 300 mM imidazole. The eluted protein was subsequently dialyzed in size exclusion buffer (150 mM NaCl, 10 mM HEPES pH 7.4, 2 mM DTT, and 0.1 mM $ZnCl_2$) overnight. After the dialyzed protein was injected over a size exclusion Superdex 75 column (GE Healthcare). Purity of fractions were confirmed using gel electrophoresis.

Expression and Purification of Ub for Complexation

Ub (1-75) in the vector pTYB2 was expressed, purified, and derivatized with propargylamine to generate a suicide substrate (Ub-PA) as detailed in previous methods(*39*). PEDV PLP2 short was saturated with Ub-PA and incubated at room temperature for 4 hours. To remove excess Ub-PA, the complex was run over a high-density nickel agarose beads (Gold Biotechnology). The column was washed with 30 mM imidazole, and then eluted off with 300 mM imidazole. Thrombin was added to the eluted fraction to remove the His-6x tag and then dialyzed for 4 hours in a buffer consisting of 150 mM NaCl, 25 mM HEPES pH 7.4, 2 mM DTT, and 0.1 mM $ZnCl_2$. The protein complex was then concentrated to 6-7 mL and purified over a size exclusion Superdex 200 column (GE Healthcare) in a running buffer of 100 mM NaCl, 5 mM HEPES pH 7.4, 5 mM DTT, and 0.1 mM $ZnCl_2$. Purity of fractions were confirmed using gel electrophoresis.

Crystallization of PEDV PLP2 in Complex with Ubiquitin

The covalent PEDV PLP2 short–Ub complex was concentrated to 8.4 mg/mL and subsequently screened against 768 crystal conditions from a series of NeXtal suites using a TTP Labtech Mosquito (TTP Labtech, Herfordshire, UK). The screen used a 0.4 nL hanging drop comprised of a 1:1 ratio of protein solution and reservoir solution. Within 3-7 days square-plated crystals formed from in a solution containing 0.2M $MgCl_2$, 0.1M Tris, and 30% PEG 4k. The condition was further optimized by setting trays with 0.30M $MgCl_2$, 0.1M Tris, and 16% PEG 4k in a 500µL well solution and setting up a hanging drop that combined 2 µL of well solution with 2 µL of a 9 mg/ml PEDV PLP2-Ub protein solution.

Data Processing and Structure Solution

Crystals were flash cooled in liquid nitrogen using 18% PEG 4K with 5% solution containing equal parts Ethylene Glycol, DMSO and Glycerol (EDG) as a cryoprotectant. Data was collected under a dry N_2 stream on the 16M Eiger detector at Brookhaven National Laboratory. The data set was indexed, integrated, and scaled using HKL-2000(*40*). The structure was solved by molecular replacement using Phaser via the solved apo structure of PEDV (PDB entry 6NOZ)(*41*). Successive rounds of manual model building, and refinement were done using Coot and PHENIX(*42, 43*).

SUPPLEMENTARY INFORMATION

Table S2.1 Data collection and refinement statistics

Values in parentheses are for the highest resolution shell

Data collection	
Wavelength	1.0
Resolution range	48.34 - 3.099 (3.21 - 3.099)
Space group	P 21 21 21
Unit cell	98.138 136.873 193.348 90 90 90
Unique reflections	46738 (4185)
Multiplicity	6.1 (5.6)
Completeness (%)	97.21 (88.58)
Mean I/sigma(I)	4.66 (1.0)
Overall *B* factor from Wilson plot	56.45
R-merge	0.231 (0.849)
R_{meas}	0.253 (0.936)
R_{pim}	0.102 (0.387)
$CC_{1/2}$	0.972 (0.614)
Reflections used in refinement	46723 (4182)
Reflections used for R-free	2349 (218)
Final R_{work}	0.2003 (0.2778)
Final R_{free}	0.2577 (0.3338)
Number of non-hydrogen atoms	19153

macromolecules	19098
ligands	46
solvent	9
Protein residues	2465
RMS(bonds)	0.007
RMS(angles)	0.40
Ramachandran favored (%)	97.11
Ramachandran allowed (%)	2.89
Ramachandran outliers (%)	0.00
Rotamer outliers (%)	0.05
Clashscore	4.79
Average B-factor	53.91
macromolecules	53.89
ligands	63.94
solvent	34.19

References

1. M. Antas, G. Woźniakowski, Current Status of Porcine Epidemic Diarrhoea (PED) in European Pigs. *J Vet Res* **63**, 465-470 (2019).

2. G. W. Stevenson *et al.*, Emergence of Porcine epidemic diarrhea virus in the United States: clinical signs, lesions, and viral genomic sequences. *J Vet Diagn Invest* **25**, 649-654 (2013).

3. D. Goede *et al.*, Previous infection of sows with a "mild" strain of porcine epidemic diarrhea virus confers protection against infection with a "severe" strain. *Vet Microbiol* **176**, 161-164 (2015).

4. D. Goede, R. B. Morrison, Production impact & time to stability in sow herds infected with porcine epidemic diarrhea virus (PEDV). *Prev Vet Med* **123**, 202-207 (2016).

5. L. L. Schulz, G. T. Tonsor, Assessment of the economic impacts of porcine epidemic diarrhea virus in the United States. *J Anim Sci* **93**, 5111-5118 (2015).

6. P. L. Paarlberg, "Updates estimated economic welfare impacts of porcine epidemic diarrhea virus (PEDV)," (Purdue University, Deptartment of Agricultural Economic, 2014).

7. D. Song, B. Park, Porcine epidemic diarrhoea virus: a comprehensive review of molecular epidemiology, diagnosis, and vaccines. *Virus Genes* **44**, 167-175 (2012).

8. D. Song, H. Moon, B. Kang, Porcine epidemic diarrhea: a review of current epidemiology and available vaccines. *Clin Exp Vaccine Res* **4**, 166-176 (2015).

9. S. Subramaniam *et al.*, Vaccination of sows with a dendritic cell-targeted porcine epidemic diarrhea virus S1 protein-based candidate vaccine reduced viral shedding but exacerbated gross pathological lesions in suckling neonatal piglets. *J Gen Virol* **99**, 230-239 (2018).

10. F. Zhang *et al.*, Prevalence and phylogenetic analysis of porcine diarrhea associated viruses in southern China from 2012 to 2018. *BMC Vet Res* **15**, 470 (2019).

11. P. C. Y. Woo *et al.*, Discovery of Seven Novel Mammalian and Avian Coronaviruses in the Genus Deltacoronavirus Supports Bat Coronaviruses as the Gene Source of Alphacoronavirus and Betacoronavirus and Avian Coronaviruses as the Gene Source of Gammacoronavirus and Deltacoronavirus. *Journal of Virology* **86**, 3995-4008 (2012).

12. V. Thiel *et al.*, Mechanisms and enzymes involved in SARS coronavirus genome expression. *Journal of General Virology* **84**, 2305-2315 (2003).

13. N. Barretto *et al.*, The papain-like protease of severe acute respiratory syndrome coronavirus has deubiquitinating activity. *J Virol* **79**, 15189-15198 (2005).

14. K. Ratia *et al.*, Severe acute respiratory syndrome coronavirus papain-like protease: Structure of a viral deubiquitinating enzyme. *Proceedings of the National Academy of Sciences* **103**, 5717-5722 (2006).

15. A. M. Mielech *et al.*, Murine Coronavirus Ubiquitin-Like Domain Is Important for Papain-Like Protease Stability and Viral Pathogenesis. *Journal of Virology* **89**, 4907-4917 (2015).

16. B. H. Harcourt *et al.*, Identification of Severe Acute Respiratory Syndrome Coronavirus Replicase Products and Characterization of Papain-Like Protease Activity. *Journal of Virology* **78**, 13600-13612 (2004).

17. K. Ratia, A. Kilianski, Y. M. Baez-Santos, S. C. Baker, A. Mesecar, Structural Basis for the Ubiquitin-Linkage Specificity and deISGylating Activity of SARS-CoV Papain-Like Protease. *PLoS Pathog* **10**, e1004113 (2014).

18. H. A. Lindner *et al.*, Selectivity in ISG15 and ubiquitin recognition by the SARS coronavirus papain-like protease. *Archives of Biochemistry and Biophysics* **466**, 8-14 (2007).

19. L. Kong, N. Shaw, L. Yan, Z. Lou, Z. Rao, Structural View and Substrate Specificity of Papain-like Protease from Avian Infectious Bronchitis Virus. *The Journal of Biological Chemistry* **290**, 7160-7168 (2015).

20. B. T. Freitas *et al.*, Characterization and Noncovalent Inhibition of the Deubiquitinase and deISGylase Activity of SARS-CoV-2 Papain-Like Protease. *ACS Infect Dis* **6**, 2099-2109 (2020).

21. M. E. Davis, M. U. Gack, Ubiquitination in the antiviral immune response. *Virology* **479-480**, 52-65 (2015).

22. A. J. Sadler, B. R. Williams, Interferon-inducible antiviral effectors. *Nat Rev Immunol* **8**, 559-568 (2008).

23. M. Frieman, K. Ratia, R. E. Johnston, A. D. Mesecar, R. S. Baric, Severe acute respiratory syndrome coronavirus papain-like protease ubiquitin-like domain and catalytic domain regulate antagonism of IRF3 and NF-kappaB signaling. *J Virol* **83**, 6689-6705 (2009).

24. S. G. Devaraj *et al.*, Regulation of IRF-3-dependent Innate Immunity by the Papain-like Protease Domain of the Severe Acute Respiratory Syndrome Coronavirus. *Journal of Biological Chemistry* **282**, 32208-32221 (2007).

25. B. A. Bailey-Elkin *et al.*, Crystal structure of the Middle East respiratory syndrome coronavirus (MERS-CoV) papain-like protease bound to ubiquitin facilitates targeted disruption of deubiquitinating activity to demonstrate its role in innate immune suppression. *J Biol Chem* **289**, 34667-34682 (2014).

26. D. Komander, M. J. Clague, S. Urbe, Breaking the chains: structure and function of the deubiquitinases. *Nat Rev Mol Cell Biol* **10**, 550-563 (2009).

27. Y. Kulathu, D. Komander, Atypical ubiquitylation - the unexplored world of polyubiquitin beyond Lys48 and Lys63 linkages. *Nat Rev Mol Cell Biol* **13**, 508-523 (2012).

28. K. S. Faaberg, J. Han, Y. Wang, Molecular dissection of porcine reproductive and respiratory virus putative nonstructural protein 2. *Adv Exp Med Biol* **581**, 73-77 (2006).

29. W. Zeng *et al.*, Reconstitution of the RIG-I pathway reveals a signaling role of unanchored polyubiquitin chains in innate immunity. *Cell* **141**, 315-330 (2010).

30. I. Alkalay *et al.*, Stimulation-dependent I kappa B alpha phosphorylation marks the NF-kappa B inhibitor for degradation via the ubiquitin-proteasome pathway. *Proc Natl Acad Sci U S A* **92**, 10599-10603 (1995).

31. Z. Chen *et al.*, Signal-induced site-specific phosphorylation targets I kappa B alpha to the ubiquitin-proteasome pathway. *Genes Dev* **9**, 1586-1597 (1995).

32. C. A. Castaneda, T. R. Kashyap, M. A. Nakasone, S. Krueger, D. Fushman, Unique structural, dynamical, and functional properties of k11-linked polyubiquitin chains. *Structure* **21**, 1168-1181 (2013).

33. J. N. Dynek *et al.*, c-IAP1 and UbcH5 promote K11-linked polyubiquitination of RIP1 in TNF signalling. *EMBO J* **29**, 4198-4209 (2010).

34. D. Wang *et al.*, The nonstructural protein 11 of porcine reproductive and respiratory syndrome virus inhibits NF-kappaB signaling by means of its deubiquitinating activity. *Mol Immunol* **68**, 357-366 (2015).

35. Y. Xing *et al.*, The papain-like protease of porcine epidemic diarrhea virus negatively regulates type I interferon pathway by acting as a viral deubiquitinase. *Journal of General Virology* **94**, 1554-1567 (2013).

36. C. M. Daczkowski, O. Y. Goodwin, J. V. Dzimianski, J. J. Farhat, S. D. Pegan, Structurally Guided Removal of DeISGylase Biochemical Activity from Papain-Like Protease Originating from Middle East Respiratory Syndrome Coronavirus. *J Virol* **91**, (2017).

37. S. M. Bester, C. M. Daczkowski, K. S. Faaberg, S. D. Pegan, Insights into the Porcine Reproductive and Respiratory Syndrome Virus Viral Ovarian Tumor Domain Protease Specificity for Ubiquitin and Interferon Stimulated Gene Product 15. *ACS Infectious Diseases* **4**, 1316-1326 (2018).

38. M. K. Deaton, A. Spear, K. S. Faaberg, S. D. Pegan, The vOTU domain of highly-pathogenic porcine reproductive and respiratory syndrome virus displays a differential substrate preference. *Virology* **454-455**, 247-253 (2014).

39. M. K. Deaton *et al.*, Biochemical and Structural Insights into the Preference of Nairoviral DeISGylases for Interferon-Stimulated Gene Product 15 Originating from Certain Species. *Journal of Virology* **90**, 8314-8327 (2016).

40. Z. Otwinowski, W. Minor, in *Methods in Enzymology*. (Academic Press, 1997), vol. 276, pp. 307-326.

41. A. J. McCoy *et al.*, Phaser crystallographic software. *J Appl Crystallogr* **40**, 658-674 (2007).

42. P. Emsley, K. Cowtan, Coot: model-building tools for molecular graphics. *Acta Crystallogr D Biol Crystallogr* **60**, 2126-2132 (2004).

43. D. Liebschner *et al.*, Macromolecular structure determination using X-rays, neutrons and electrons: recent developments in Phenix. *Acta Crystallographica Section D* **75**, 861-877 (2019).

44. G. C. Capodagli, M. K. Deaton, E. A. Baker, R. J. Lumpkin, S. D. Pegan, Diversity of Ubiquitin and ISG15 Specificity among Nairoviruses' Viral Ovarian Tumor Domain Proteases. *Journal of Virology* **87**, 3815-3827 %! Diversity of Ubiquitin and ISG3815 Specificity among Nairoviruses' Viral Ovarian Tumor Domain Proteases (2013).

45. L. Wang, W. Hu, C. Fan, Structural and biochemical characterization of SADS-CoV papain-like protease 2. *Protein Science* **29**, 1228-1241 (2020).

46. M. Békés *et al.*, Recognition of Lys48-Linked Di-ubiquitin and Deubiquitinating Activities of the SARS Coronavirus Papain-like Protease. *Mol Cell* **62**, 572-585 (2016).

47. K. Ratia, University of Illinois at Chicago, (2008).

CHAPTER 3

STRUCTURAL AND MECHANISTIC CHARACTERIZATION OF NON-NEUTRALIZING ANITBODIES TARGETING CRIMEAN-CONGO HEMORRHAGIC FEVER

Durie, Ian. Submitted to Nature Communications

One Sentence Summary: Non-neutralizing antibodies target the non-structural protein GP38 from Crimean-Congo Hemorrhagic Fever Virus (CCHFV), here we show the first structural characterization of these mAbs while also determining their therapeutic use across a wide range of CCHFV strains.

Abstract:

Crimean-Congo Hemorrhagic Fever Virus (CCHFV) causes a debilitating illness typically up to 40% mortality rate. With a 2017 outbreak in Spain illustrating CCHFV's continued ability to expand its endemic area and no approved vaccine or therapeutics available, CCHFV is viewed as a priority public health threat by the WHO. Recently, the non-neutralizing monoclonal antibody (mAb) 13G8 has been shown to target the CCHFV glycoprotein GP38 and protect against lethality in a CCHFV mouse model pre- and post-exposure respectively. Here for the first time, we biochemically and structurally reveal the 13G8 epitope on GP38 and examine the broad-spectrum potential of 13G8 as well a newly human derived mAb CC5-17 that is competitive with 13G8. We also determine the practicality of these mAbs for use against the closely related Aigai virus. This information coupled with *in vivo* efficacy data paves the way for an effective future monoclonal antibody therapeutic towards a wide swatch of CCHFV strains.

Introduction

Crimean-Congo Hemorrhagic Fever Virus (CCHFV), a tick-borne virus from the *Nairoviridae* family, causes a debilitating hemorrhagic fever and death in 5-40% of cases(*1, 2*). This deadly virus is found throughout the Eastern hemisphere and because of its propensity to spread WHO has outlined CCHFV as a salient public health risk that is lacking in approved vaccines and/or therapeutics(*1*). Among CCHFV there are several strains that are classified along five clades: I–III(endemic in Africa), IV (Asia), V (Eastern Europe/Europe 1) . This is down from six due to the reclassification by the ICTV of the rarely disease-causing strain AP92 and other genogroup VI viruses like the Pentalofos strain, into the closely associated Aigai virus(*3*). As part of the *Nairoviridae* family, CCHFV possesses a negative sense tri-segmented RNA genome, consisting

of a Large (L), Medium (M), and Small (S) segment(*1, 4, 5*). Most therapeutic and vaccine development efforts have focused on utilizing the many proteins of the M-segment, which include two structural proteins Gn and Gc, two previously classified secreted proteins GP38 and mucin-like domain (MLD), and one non-structural protein (Nsm)(*6-12*).

In the case of CCHFV, therapeutic development of neutralizing mAbs against the structural proteins G_c or G_n have proven difficult. Recent strides towards anti-G_c mAbs have shown efficacy before infection but need to be engineered as a bispecific antibody to provide narrow spectrum therapeutic efficacy after infection(*8*). These developments track with the trend that antibodies have been characterized as poorly neutralizing in CCHFV patients and not considered the main correlate of protection(*13-15*). At the same time, previously considered anti-G_n mAbs were found not to target mature G_n. Instead, they target glycoprotein 38 (GP38) found in the pre-G_n encoded directly after the mucin like domain (MLD) (*8, 10*). These anti-G_n mAbs were originally raised against the CCHFV strain IbAr10200 and were observed to provide protection in neonatal mice lacking mature immune systems, which do not display typical CCHFV pathogenesis(*16*). Two of these anti-GP38 antibodies,13G8 and 10E11, were later retested in the more sophisticated CCHFV IFNAR $^{-/-}$ mouse model, and only 13G8 was found to provide protection in a non-neutralizing manner(*9*). Soon 13G8 became an antibody of interest and was tested for its prophylactic potential against the CCHFV strains IbAr10200(Clade III), Afg-09(Clade IV), and Turkey-2004(Clade V)(*10, 17*). These challenge experiments soon proved that 13G8 can provide high levels of protection.

GP38's role in viral replication and pathogenesis is still being elucidated but GP38 is shown to be essential in maturation of CCHFV viral particles(*18*). Additional studies have observed that GP38 may be secreted or localizes to the outside of infected cells and the CCHFV viral envelope(*10*).

Recently, GP38 has proven useful as an antigen in a DNA vaccine study of necessary CCHFV M-segment proteins(*19*). Partial protection was seen when encoding only GP38, in addition the surviving group had two-fold higher titers of anti-GP38 mAbs, indicating the use of GP38 in future vaccines. While GP38's role is not very well understood, a recent X-ray structure of a laboratory isolate, IbAr10200, has provide some initial insight into the origins of GP38. Specifically, GP38 and Gn have some structural and sequence homology that has spurred speculation of GP38 originating from a gene duplication event(*17*). While the CCHFV IbAr10200 provided initial insights into the fold of GP38, a GP38-antibody complex has yet to be described. The lack of structural and molecular basis for how protective non-neutralizing mAb's bind to GP38 has stymied further development of viable broad-spectrum anti-GP38 mAbs.

In this study we are the first to solve a structure of a clinically relevant strain of GP38 alone and in complex with mAb 13G8. Next, we identified 7 new anti-GP38 mAbs from human CCHFV survivors and in doing so identified two new antigenic sites on GP38. We also solved a complex of GP38 with one of the human derived mAbs, CC5-17. Interestingly, 13G8 and CC5-17 compete at the same antigenic site, but CC5-17 outcompetes 13G8 with a three orders of magnitude difference in KD. Attesting to broad spectrum potential of 13G8 and CC5-17, we characterized key amino acid sites that are responsible for the mAbs robust affinity across the five phenological clades of CCHFV, but not that of closely related Aigai virus. To explore whether the higher affinity of CC5-17 relative to 13G8 equated to greater protection, we treated pre- and post-challenged $IFNAR^{-/-}$ mice with CCHFV Turkey-2004. Surprisingly, while both mAbs offer a level of protection, 13G8 is more efficacious than CC5-17. This structural information coupled with efficacy data further characterizes GP38 as an antigen of interest for vaccination studies while also advancing mAb development towards CCHFV.

Results

13G8 has different affinities towards CCHFV GP38s and closely related Aigai virus

GP38 can have up to 20% difference in amino acid sequence between CCHFV strains, because of this variability the strain-to-strain differences that influence 13G8 binding to GP38 need to be understood (Figure S3.1/S3.2B). Previous studies determined 13G8's KD against IbAr10200 GP38 to be $9.29x10^{-11}$ M(*10*). To standardize 13G8, it was engineered it to have a human IgG1 backbone and thus denoted it as c13G8. This chimeric c13G8 was initial testing using BioLayer Interferometry (BLI) to measure its binding affinities against GP38's from CCHFV strains IbAr10200, Turkey-2004, and Kosovo/Hoti (further referred to as Hoti) which account for the major clinically relevant Clades). A similar nano-Molar affinity was observed and comparable amongst Clades III-V when c13G8 was tested against IbAr10200 GP38 ($4.27x10^{-10}$ M), Turkey-2004 GP38 ($5.23x10^{-10}$ M), and Hoti GP38 ($5.57x10^{-10}$ M) (Figure 3.1 A-C). To explore if c13G8 had broad-spectrum potential beyond CCHFV, c13G8's was tested against the Aigai virus strain Pentalofos, a close relative of CCHFV. Interestingly, binding was completely abolished and could not be detected via BLI, when c13G8 encountered GP38 from Pentalofos (Figure 3.1D).

Structure of a GP38 originating from the CCHFV strain Hoti

With c13G8 showing nanomolar or better affinity towards various CCHFV strains, but not those of the Aigai virus, the molecular factors behind this phenomenon were sought out. To provide the most clinical relevance to the study, the CCHFV circulating strain Hoti was used. This strain is one of the two strains that can be used to elicit human disease like symptoms in a non-human primate model (*20-25*). Additionally, CCHFV Hoti has a 15% sequence identify difference with that of the IbAr10200 isolate that might reveal any major differences in tertiary structures or surface composition between CCHFV GP38s. Crystals of the CCHFV Hoti GP38 were readily

obtained and shortly thereafter a structure was solved to a resolution of 3.2Å with a R_{work}/R_{free} of 0.26/0.30 in the space group C_2 (Table S1). Both the structures of GP38 originating from the IbAr10200 and Hoti strains followed the same global fold to include the same number of beta sheets. However, some differences were present such as an additional alpha helix detected through the DSSP server (*26, 27*). This helix is located between beta strands 2 and 3, that resides closer to the N-glycosylation sites (Figure S3.2). Also, a divergent loop conformation is observed in amino acid region 490-500. Like the IbAr10200 structure there was no electron density for the amino acid region 330-345 suggesting this loop is highly flexible.

Complex structure of 13G8-Fab with GP38 Hoti

With no major tertiary structural differences between GP38 originating from the IbAr10200 and Hoti strains, a complex structure with 13G8 was sought to gain insight into its GP38 epitope. To this end, a CCHFV GP38 originating from the Hoti strain, with the Fab region of 13G8 was crystallized. Subsequently, a low resolution 3.6Å data set in the P43212 space group was obtained. From initial solution via molecular replacement and through iterative rounds of refinement a final R_{work}/R_{free} of 0.28/0.31was obtained (Figure 3.1G, Table S3.1). Upon examination, the electron density around the binding interface is well defined, and the 13G8 site I epitope can be clearly identified (Figure S3.3A). Using PISA, a surface area of 783.8 $Å^2$ was calculated for the 13G8-GP38 interface(*28*). Two main components of this interface are also identified. The first is the light chain CDR3 that interacts with the GP38 N-terminus (Figure 3.1H). Unlike the previously solved GP38 Apo structures of the Hoti and IbAr10200 strains that have a flexible N-terminus tail, the Hoti GP38 N-terminus tail within the complex is shifted and stabilized by 13G8. The other main interaction region is where the 13G8 heavy chain CDR3 interacts with the GP38 α-helix 2 and fits within a larger hydrophobic pocket in GP38 (Figure 3.1H).

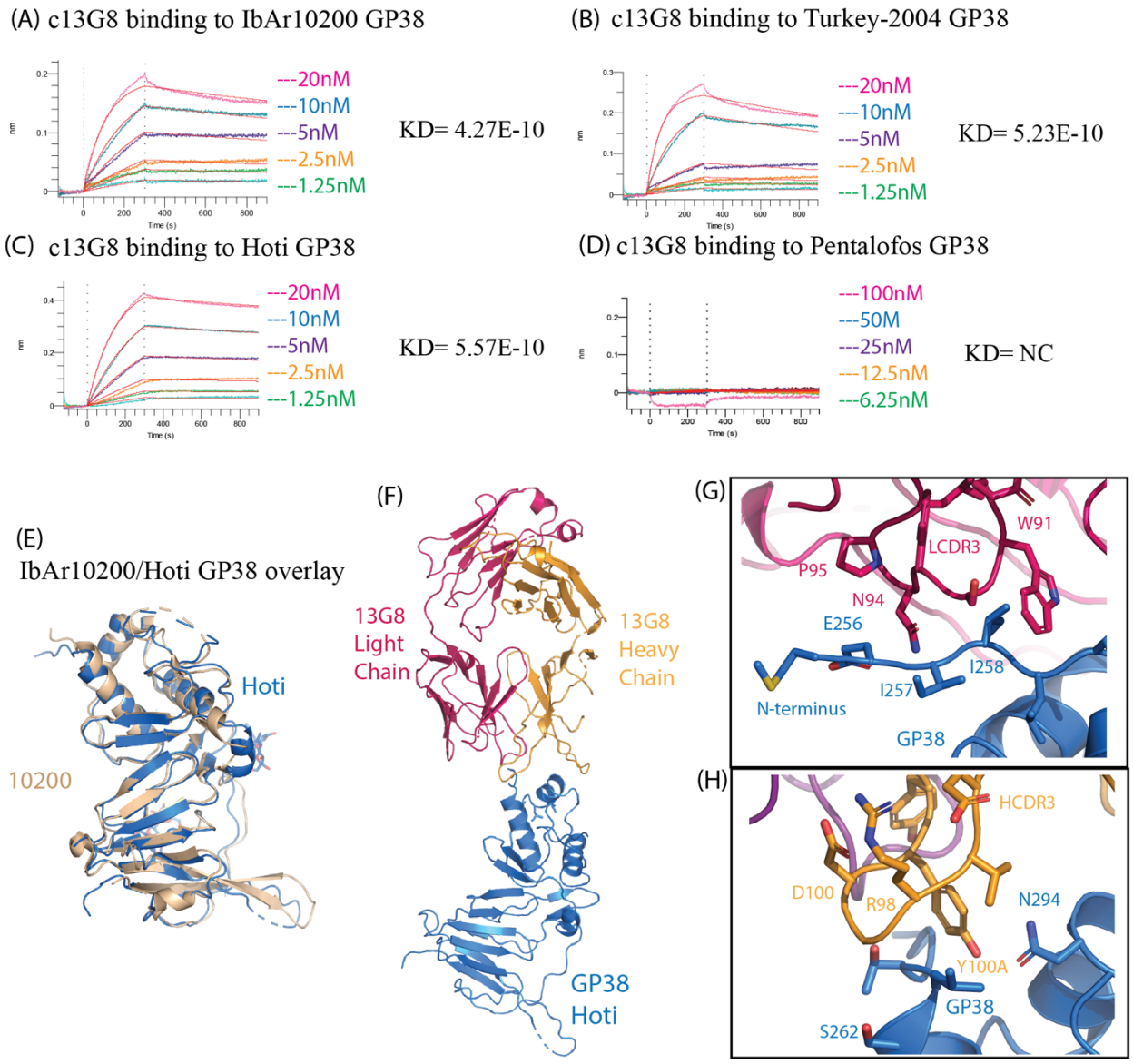

Figure 3.1 c13G8 interactions across Nairovirus GP38 (**A** to **D**) BLI binding of c13G8 mAb with GP38 from (**A**) CCHFV IbAr10200 (**B**) CCHFV Turkey-2004 (**C**) CCHFV Hoti (**D**) Aigai Virus Pentalofos (**E**) Overlay of CCHFV IbAr10200 GP38 (RCSB 6VKF) with our own solved CCHFV Hoti GP38 Structure (**F**) c13G8 fab with GP38 Hoti (**G**) LCDR3 interaction with Hoti GP38 (**H**) HCDR3 interaction with Hoti GP38

Isolation of anti-GP38 mAbs from previously infected human donors

Previously only two anti-GP38 mAbs have been tested for efficacy, 13G8 and 10E11 in the lethal CCHFV challenge models of IFNAR$^{-/-}$ and STAT$^{-/-}$ mice(*10, 17*). Although 13G8 and 10E11 were

found to compete at the same antigenic site through BLI, only 13G8 provided protection against CCHFV. The lack of protection in 10E11 was attributed to 10E11's lower binding affinity of $5.22x10^{-10}$ M (*10*). With ELISA data showing that plasma from CCHFV survivors react towards GP38, the human antibody repertoire may offer an alternative to the mouse derived 10E11 and 13G8. As a minimum, such mAbs would also allow further insights into the protection provided by 13G8. To obtain a bevy of such mAbs, patients were recruited from a high-risk area with known epidemics. Turkey was selected as an outbreak there started in in 2002 resulting in >10,000 cases by 2016. The current reported case load is >200 cases annually(*29-32*). To determine the antibody repertoire against CCHFV GP38 in human survivors, six verified survivors of CCHFV infection had their blood drawn and separated in PBMCs and plasma. Their plasma was used in an ELISA to test for overall anti-GP38 reactivity against Turkey-2004 GP38 (Figure 3.2B). Variable plasma reactivity was found throughout the six patients towards GP38, with the highest seen in patient CC5.

Patient CC5's antibody repertoire was subsequently analyzed through a transcriptomics and genomics approach(*33*). Antibody isolation involved affinity purification of the IgG, enzyme digestion of the antibodies, and mass spectrometry of the peptide fragments. This peptide data was reconciled to a patient-specific database from their memory B cells. Of the 11 antibodies produced seven bound to Turkey-2004 GP38 which includes CC5-6, CC5-12, CC5-14, CC5-16, CC5-17, CC5-20, CC5-25 (Figure 3.2C). Of these mAbs, there is relatively low somatic hypermutation (SHM) (<14%) between the mAbs isolated, with overall higher mutation rates within the heavy chain (Table 3.1).

Table 3.1: Antibody gene usage for non-neutralizing anti-GP38 mAbs

mAb	Gene family V	Gene family D	Gene family J	CDR3 Length	%SHM
CC5-17	IGHV5-51*01	IGHD3-10*01	IGHJ4*02	23	3%
	IGKV1-39*01	-	IGKJ1*01	7	9%
CC5-16	IGHV4-31*03	IGHD3-10*01	IGHJ4*02	15	13%
	IGLV2-11*01	-	IGLJ3*02	10	12%
CC5-6	IGHV4-31*03	IGHD3-3*01	IGHJ6*02	14	14%
	IGKV1-5*03	-	IGKJ1*01	8	7%
CC5-25	IGHV3-33*01	IGHD3-9*01	IGHJ6*02	15	5%
	IGLV3-1*01	-	IGLJ3*02	11	7%
CC5-12	IGHV4-34*01	IGHD6-25*01	IGHJ4*02	10	0%
	IGLV1-47*01	-	IGLJ1*01	12	5%
CC5-14	IGHV1-69*17	IGHD3-22*01	IGHJ5*02	20	14%
	IGLV1-40*01	-	IGLJ2*01	11	3%
CC5-20	IGHV1-69D*01	N/A	IGHJ6*02	15	7%
	IGKV3-20*01	-	IGKJ1*01	9	5%

*The gene family data was extracted from IgBLAST (https://www.ncbi.nlm.nih.gov/igblast/)

Characterization of human derived anti-GP38 mAbs

Following the reconciliation and initial ELISA binding characterization of CC5's antibodies, their binding affinity towards Turkey-2004 GP38 was determined using SPR. In comparison to c13G8 which had a KD of 10^{-9}, the CC5 antibodies either matched or had a higher binding affinity at 10^{-12} with the best binders being CC5-6, CC5-16, CC5-17 (Table 3.2). Next the CC5 antibodies were characterized via the epitope they target. A BLI competition assay was used to test how CC5 mAbs competed against mAbs of the known site I, site II, and site III represented by mouse derived antibodies 13G8, 8F10, and 7F5/C611 respectively. Of the seven mAbs isolated, three directly competed with 13G8, which were CC5-17, CC5-6, and CC5-12. It appears that CC5-16 distinctively binds between sites I and II and was thus classified as a site V mAb. Curiously, the previously characterized site III antibody C611 directly competed with the site II mAb 8F10 but

did not compete with the site III mAb 7F5. CC5-25 directly competed with the site III antibody 7F5. Lastly the mAbs CC5-14 and CC5-20 directly competed with each other and little else thus identifying a new antigenic site referred to as Site IV (Figure 3.2C).

Table 2. SPR Binding Characterization of anti-GP38 mAbs against Turkey-2004 GP38

	Ka (1/Ms)	Kd (1/s)	KD (M)
c13G8	1.73×10^{6}	2.9×10^{-3}	$1.68 \times 10^{--9}$
CC5-17	3.93×10^{5}	2.58×10^{-7}	2.54×10^{-12}
CC5-16	8.7×10^{6}	3.1×10^{-5}	3.5×10^{-12}
CC5-6	7.4×10^{4}	4.6×10^{-7}	6.2×10^{-12}
CC5-25	6.5×10^{5}	2.9×10^{-5}	4.4×10^{-11}
CC5-12	1.1×10^{6}	2.7×10^{-4}	2.4×10^{-10}
CC5-14	1.5×10^{7}	1.0×10^{-2}	7.4×10^{-10}
CC5-20	2.4×10^{6}	3.47×10^{-3}	1.6×10^{-9}

Structure of CC5-17 with GP38 Hoti

Because of CC5-17's ability to directly compete with 13G8 with a three orders of magnitude higher affinity, a structure of GP38-CC5-17 was sought to gain insights into how this high affinity anti-GP38 mAb interfaced with Site I. Crystals were obtained of CCHFV GP38 originating from the Hoti strain in complex with the Fab of CC5-17. A low resolution 3.8Å structure was subsequently solved in the P43212 space group with a R_{work}/R_{free} of 0.31/0.34 (Figure 3.2E, Table S3.1). As with our other complex structure, the binding interface was well characterized (Figure S3B). Using PISA analysis, a surface area of 776.5$Å^{2,}$ was calculated, which was like our 13G8-GP38 Hoti

complex. At first glance, CC5-17 appears to globally bind to a similar area, and there are three main determinants that confer binding. The first is light chain CDR3 which partially interacts with the N-terminus, and secondly interacts with GP38's α-helix 2. The third interaction is the heavy chain CDR3 which interacts with a larger hydrophobic pocket on top of GP38, and the large 20 AA flexible loop (Figure 3.2E).

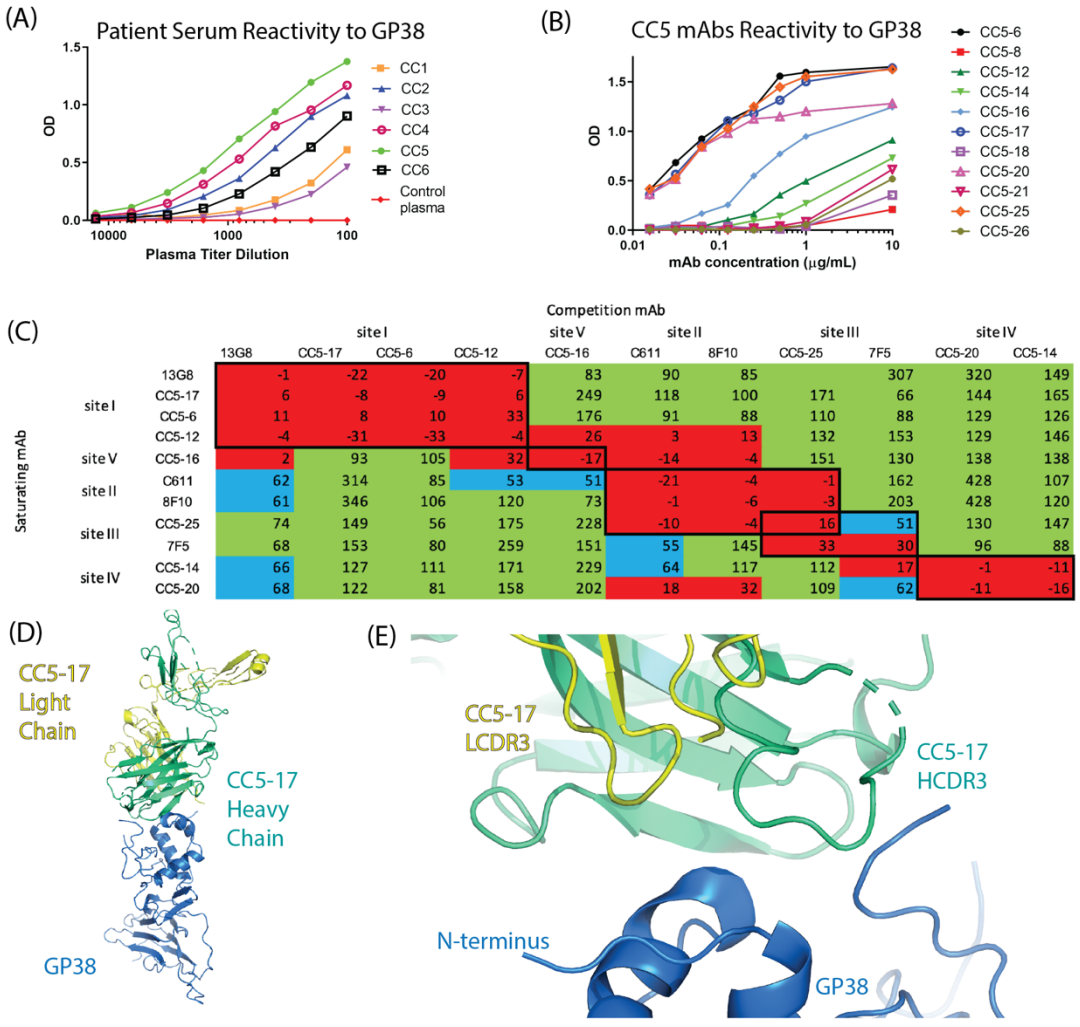

Figure 3.2 Generation of human derived anti-GP38 mAbs: (**A**) 6 patients who previously had CCHFV in Trabzon (Turkey) were recruited and their plasma was used to determine their anti-GP38 titers (**B**) Patient CC5 was selected, and their plasma was used to mine 11 mAbs which were then retested against GP38 (**C**) Seven CC5 antibodies were then tested against known Group 1, Group 2 and Group 3 antibodies. <33% binding indicates competition, 34-66% indicate partial

competition, >67% indicate no competition (**D**) Overall structure of GP38 Hoti with CC5-17 Fab (**E**) HCDR3 binding and LCDR3 binding interactions with GP38 Hoti

Comparison of how 13G8 and CC5-17 bind GP38 Hoti

Comparison of 13G8's and CC5-17's interaction with site I reveals on a macro level different angles of engagement with GP38. This is observed by the 22° difference between core axis of the Fabs from 13G8 and CC5-17 (Figure 3.3A). As previously mentioned, these antibodies rely on three areas of GP38 (residues 253-261, 289-294, and 343-349). The overall binding interface is conserved through the two antibodies and have minor differences between them (Figure 3.3B). But through the 22° shift is what enables CC5-17 to engage GP38 more thoroughly than that of 13G8. The first major engagement is how CC5-17's LC CDR3 engages with α-helix 2, several residues appear to interact at this sight, including a salt bridge between GP38's E289 and CC5-17's LCDR3 R93, and the LCDR3 Y92 proximity to GP38 can engage either with the hydrophobic pocket or cause hydrogen bonding events with α-helix 2(Figure S3.4B). The other way in which CC5-17's interacts is through the HCDR3 in which this loop penetrates the hydrophobic pocket, and then causes the highly flexible 20 AA loop of GP38 to shift outward and a different conformation of residues 340-345 is observed, in comparison to not only our complex 13G8-GP38 Hoti structure, but that of our Apo GP38 Hoti and the apo IbAr10200 GP38 (Figure S3.4A).

13G8 and CC5-17 target diverse CCHFV strains

With 13G8's ability to target GP38s originating from at least most major clades of CCHFV, CC5-17's cross clade binding potential was explored to see if it was comparable to that of c13G8 or, if its selectivity included GP38 from the Aigai virus strains like Pentalofos. BLI was used again to measure the KD of CC5-17 against GP38 from CCHFV IbAr10200, Turkey-2004, and Hoti and the Aigai virus Pentalofos. Curiously the same pattern as c13G8 was observed, in which CC5-17

bound to GP38 from CCHFV IbAr10200, Turkey-2004, and Hoti but it did not engage with Pentalofos GP38(Figure S3.5).

To elucidate what was the molecular basis for this difference in affinity at site I for both 13G8 and CC5-17, the site I epitopes of these two mAbs were compared across CCHFV Clades I-V and Aigai Virus Pentalofos. When comparing the sequences of IbAr10200, Turkey-2004, Hoti, and Pentalofos there are several deviations between Pentalofos and the other strains that reside along α-helix 2 at residues 292, 294, and 296 (Figure 3.4C). At site 292 a lysine is replaced by a threonine, while at site 294 an asparagine is now either a valine (CCHFV Clade I/II) or a threonine (Pentalofos). Site 296 has the most variety between the evaluated viruses. Instead of a glycine found in three of the five CCHFV clades, it can be a glutamine (Clade I), glutamic acid (Clade II), or a lysine (Pentalofos). Investigating the location of these GP38 amino acid sites within the interface of GP38 and the two mAbs, reveals that a change of the glycine at position 296 to a larger charged residues such as a lysine, or negatively charged side chain amino acid maybe problematic for interactions with CC5-17. Whereas position 296 lay on the edge of the GP38-mAb epitope for 13G8 where a larger sidechain could find space in the bulk solvent, it was located centrally in the CC5-17 interface (Figure S3.6). Hence, suggesting that larger residues at this site could lead to diminished affinity for CC5-17 but not necessarily 13G8.

To probe this assertion and the roles of other sites of variation within the site I epitope, single amino acid mutations were introduced into Hoti GP38 to abolish binding. The reverse was also performed by introducing the single mutations into Pentalofos GP38 to re-establish binding. BLI was used to calculate binding affinities of 13G8 and CC5-17 against the new mutant GP38s to evaluate amino acid sites 292, 294, and 296.

The impact of GP38 Hoti containing single mutations drawn from Aigai strain Pentalofos on the affinity of 13G8 appeared to be limited. The dissociation constant 3.31 $x10^{-9}$ M and 4.09 $x10^{-7}$ M for K292T and G296K respectively were relatively close to that of the control at 5.38 $x10^{-9}$. Although the impact of the K292T mutation was also largely negligible with a dissociation constant of 1.67 x 10^{-9} M versus that of the control at 2.00 x 10^{-9} M, this was not the case for the G296K mutant. As expected from the position of G296 within the GP38-CC5-17 interface, mutation to lysine had a significant impact on CC5-17 affinity lowering it by two orders of magnitude, 1.26 x 10^{-7} M. Altogether, this data suggests more than one alteration within site I at these amino acid positions would be necessary for 13G8 to lose significant activity whereas having a glycine at position 296 is necessary for robust CC5-17 binding.

While many of the mutations in GP38 from the CCHFV Hoti strain had minimal impact in lowering 13G8 and CC5-17 affinity for GP38, larger impacts were observed when adapting equivalent Pentalofos GP38 sites 299, 301 and 303 to those of the CCHFV Hoti strain. As previously observed the affinity of 13G8 and CC5-17 for GP38 encoded by the Aigai virus strain Pentalofos were not calculable. However, Pentalofos GP38 carrying individual mutations at T299K, K303G, and T301N have measurable dissociation constants of 1.34$x10^{-4}$ M, 3.32$x10^{-6}$ and 4.09$x10^{-7}$ M respectively with 13G8. The same mutations have a greater impact on CC5-17 binding to Pentalofos GP38 altered at T299K, K303G, and T301N. Their dissociation constants are 3.64 x 10^{-7} M, 1.41 x 10^{-7} and 1.08 x 10^{-7} M respectively. These trends reinforce the suggestion that the lack of 13G8 affinity for GP38 from the Aigai strain Pentalofos is largely due to a synergistic effect of multiple differences within site I. In the case of CC5-17, altering any of the individual amino acid positions within site I of the Pentalofos GP38 can restore generally higher affinity some positions like that of T301 and K303 hold greater sway.

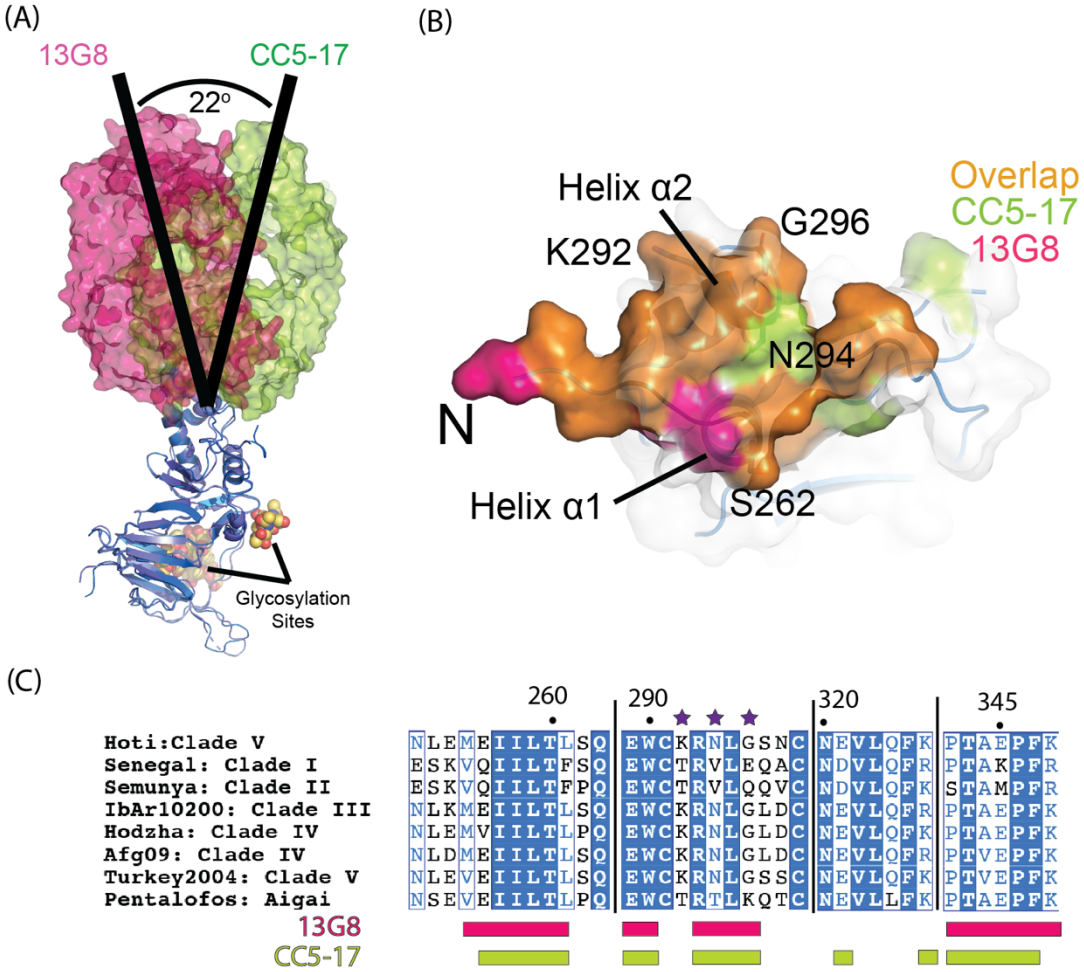

(D)

	Hoti GP38			Pentalofos GP38			
	Hoti GP38 WT	K292T	G296K	Pentalofos GP38 WT	T299K	K303G	T301N
13G8	5.38E-09	3.31E-09	4.09E-09	NC	1.34E-04	3.32E-06	4.09E-07
CC5-17	2.00E-09	1.67E-09	1.26E-07	NC	3.64E-07	1.41E-07	1.08E-07

KD values displayed are (M)

Figure 3.3 GP38 Site 1 investigation **(A)** Comparison of 13G8 vs CC5-17 and how it engages Site I epitope **(B)** Surface Area comparison of Site 1 Epitope, Magenta showing surface area of 13G8 engagement, Lime denoting surface area of CC5-17 engagement, and Orange denoting the shared surface area of the two Fabs **(C)** Sequence Alignment of relevant residues on GP38, purple stars denote sites of interest **(D)** Single mutations were conducted at GP38 Hoti sites 292 and 296 and Pentalofos GP38 sites 299, 301, and 303. These mutant proteins were then tested via BLI to obtain their binding kinetics

Affinity of non-neutralizing antibodies is not the sole driver of efficacy

With the discovery of CC5-17, which binds tighter and to the same sight as 13G8, their binding affinity was explored to determine if it is a major contributor to efficacy. To examine this notion, c13G8 and CC5-17 were tested side-by-side in an animal challenge study. $IFNAR^{-/-}$ mice were challenged with CCHFV Turkey2004 because of its low passage number, previous use in a 13G8 animal challenge, and our new human-derived antibody was isolated from patients in Turkey. Groups of mice (n = 6 per group) were injected via the IP route with 100 $TCID_{50}$ of CCHFV Turkey-2004. Antibody dosing was split into four groups, and mice were dosed 30 min with either 0.25mg or 1.0mg of mAb after infection or given two-dose regiment +1/+4 days with 0.25mg or 1.0mg mAb after infection to fully understand the therapeutic potential.

From previous studies a 1mg dose of 13G8 confers somewhere between 60-80% protection when given 24 hours before infection(*8, 10*). During our studies when 1 mg of c13G8 was given 30 min after infection we saw 83% survival. When c13G8 was given at +1/+4 days, a similar efficacy rate of 66%, a difference of one mouse, was seen (Figure 3.4A). When dosing down to 0.25mg, a similar efficacy is seen between the two groups at 50% (+30 min) and 66% (+1/+4 day) (Figure 3.4B).

Alongside our c13G8 studies, CC5-17 was tested within the same study. Interestingly an overall decrease in efficacy was seen when mice were given CC5-17. A 50% survival rate was observed at the 1mg dose given at 30min post infection and/or when given at +1/+4 days post infection (Figure 3.4A). While when dosing down CC5-17 to 0.25mg, the mice reached endpoint criteria by day 7 and it did not afford any protection(Figure 3.4B).

CC5-17 and 13G8 both provide partial protection when given at 1.0 mg, while more surprisingly CC5-17 provides no protection when given at 0.25mg in comparison to the partial protection given

by c13G8 (Figure 4). Irrespective of the antibody and dose there are a few commonalities. Clinical signs of animals when given mAbs 30min post infection see a delayed response to illness and clinical signs become apparent days 6/7, while when given the dual dose treatment clinical signs are worse at days 4/5. But with the dual dose there are notable clinical signs of recovery with mAb treatment. Even though the 30 min treatment provides partial protection, the +1/+4 group with a 1mg dose recovered quickly after receiving their second dose and clinical scores rapidly decrease past day 5. Clearly there is a dose dependency of mAb needed to prevent severe disease in animals and further solidifies the use of these antibodies as future options towards CCHFV.

As seen in other trials 13G8 provides protection before infection, and in our studies, we further establish c13G8's ability to provide protection after infection. The path to establish a more efficacious mAb through competition assays and binding affinity have proven complicated as seen with CC5-17. The current thought of increasing binding affinity to contribute to efficacy was incorrect and we bring up new questions about the characteristics needed for non-neutralizing mAbs and binding affinity is not a sole determinant of protection.

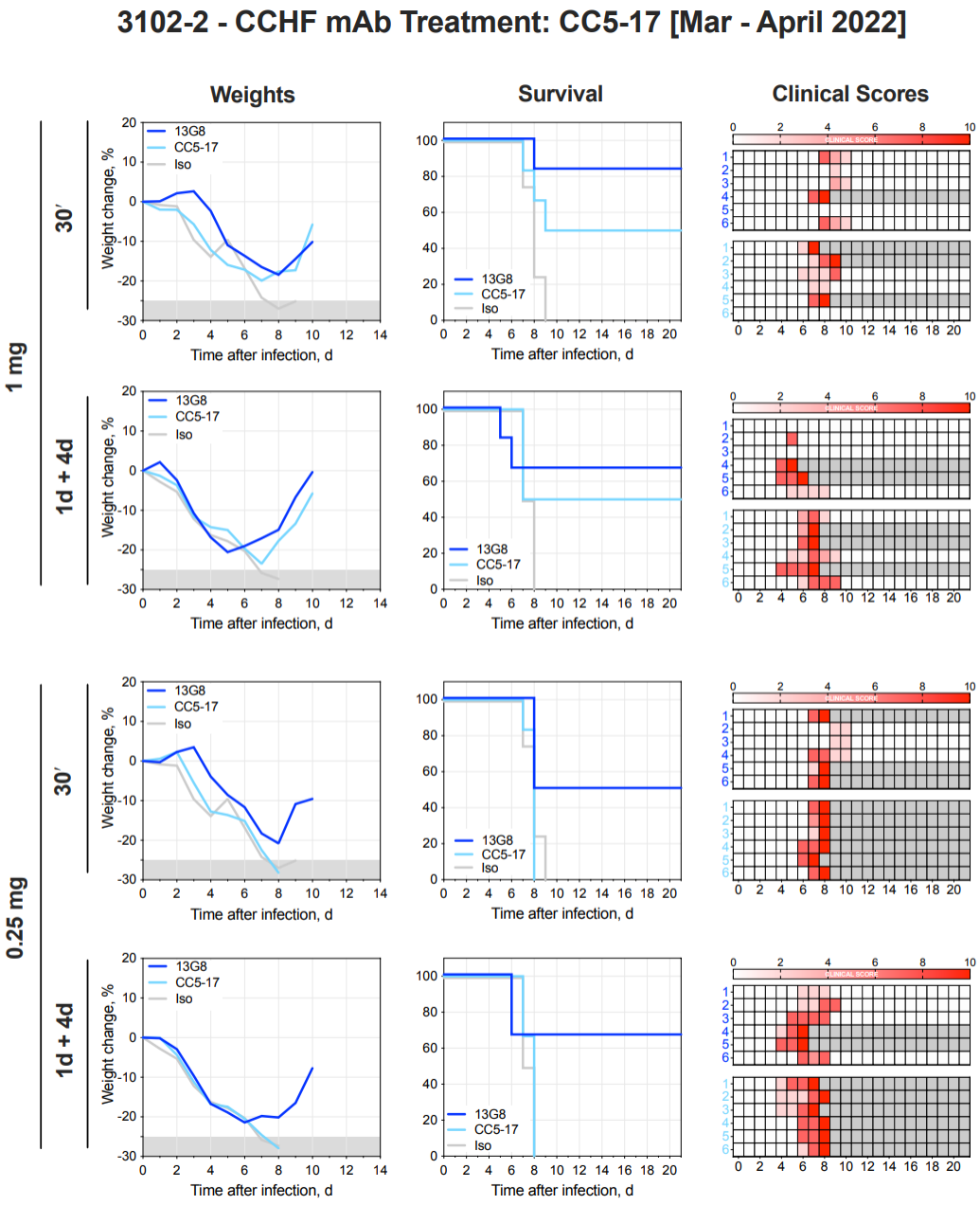

Figure 3.4 Animal Efficacy Study of Site 1 Antibodies (**A**) 1mg dose treatment of 13G8, CC5-17, or Isotype were given at 30 min or +1/+4 days after challenge (**B**) 0.25mg mAb dose treatment of 13G8, CC5-17, or Isotype were given at 30 min or +1/+4 days after challenge

Discussion

What are the drivers of protection for non-neutralizing Site I mAbs?

Neutralizing antibodies have been considered a golden standard in years past especially with recent work highlighting COVID-19(*34-36*). With more high-risk pathogens like Ebola, Lassa, and Nipah there is a turn to analyze and consider non-neutralizing activities and their influence towards preventing severe disease(*37-41*). As like those high-risk pathogens, therapeutic development towards CCHFV has proven difficult, but with the recent progress of a GP38 based DNA vaccine and anti-GP38 mAbs, GP38 has become an antigen of interest. Here we show the first complex structure of GP38 with that of 13G8 and the human derived mAb CC5-17.

Although the human derived mAb boasted a 1000-fold increase over its mouse derived counterpart, 13G8, CC5-17 was observed to have lower efficacy *in vivo*. While this highlights that affinity is not the sole driver of efficacy when it comes to the efficacy of non-neutralizing anti-GP38 mAbs, it also suggests that other factors are likely at play. As seen structurally, the epitope between 13G8 and CC5-17 is largely the same. However, these two antibodies approach GP38 at two different angles which contribute to the KDs. Although, CC5-17 had a 1000-fold increase in KD, its Ka had a 10-fold lower Ka than that of c13G8 ($3.93x10^5$ to $1.73x10^6$ (1/Ms)). Because GP38 is thought to localize to the outside of viral particles and infected cells it could be possible that the increase in association rate assists in clearance of not only virus but infected cells. In comparison to anti-G_c mabs, they both have a pM affinity while also having a Ka like CC5-17 (10^5 1/Ms)(*8*). If not for the association rate, how GP38 localizes to the outside of these particles needs to be considered and if the orientation of the localized GP38 could influence binding of mAbs.

This would also need to be considered through the mAbs that target sites II-V and if they provide any efficacy.

Of interest structurally and biochemically is that both 13G8 and CC5-17 partially bind to the N-terminus. Through processing of the CCHFV GPC, GP85 is cleaved through the enzyme furin, yielding GP38 and the MLD, this leads to another possibility that site I antibodies may interfere with this processing. With antigenic sites I-V being distinct as well as in some cases having overlapping epitopes between groups, this array of mAbs would be useful in the future to tease out whether there is an epitope dependency on efficacy and if so why and how. For instance, if efficacy of GP38 mAb were limited those binding the N-terminus, this may provide insights that focus future mAb development efforts. If not, this human and mouse derived mAbs array appears to have the breath to probe the practicality of developing mAbs at sites other than the N-terminus. For example, antigenic sites that may bind closer the GP38's two N-glycosylation sites that could also lead to a decrease in function. These sites are already known to be necessary for maturation of GP38 and Gn(*42*). Likewise, glycosylation is used by several viruses like SARS-CoV-2 and Influenza A which to block antibodies from conserved epitopes that play a role in binding and entering of cells(*43-45*). If the binding is not a major determinant for protection, then the Fc would need to be explored more thoroughly. In the original 13G8 challenge study, mice with either a Fc receptor $^{-/-}$ or C3 $^{-/-}$ were used and the FcR $^{-/-}$ mice survived while the C3$^{-/-}$ perished(*10*). Following up on this study, the reverse was performed in which the LALA mutation was introduced into the 13G8 Fc region which abolishes any effector function, and 60% survival was observed in mice(*17*). The Fc seems to be a partial determinant of protection, but it is not fully understood, and possibly GP38 could contribute to the pathogenesis of CCHFV.

The search for a broad spectrum CCHFV therapeutic

The isolation of human derived antibodies like CC5-17 that provide partial protection in animals further solidifies the immunogenicity importance of GP38. Additionally, we observed from patient CC5 they had a relatively low somatic hypermutation rate in their antibody repertoire. High hypermutation rates are seen within debilitating infections like Human Immunodeficiency Virus (HIV), where the somatic hypermutation (SHM) rates are 30-50% in comparison to our patients SHM rates of 3-14%. This is promising as it appears that human immune systems can deliver protective antibodies against CCHFV with low SHM rates. Alongside if GP38 were to be used in future vaccinations, this can be done with relative ease as other vaccination efforts with multiple doses against viruses like HPV have SHM around 8-10%(*46, 47*). The ability of both mice and humans to generate antibodies that have substantial cross-protection potential by targeting a conserved site I on GP38 also bodes well for developing GP38 inspired antigens for vaccine platforms. This could take the form of chimeric GP38s, GP38 cocktails, or GP38 miniproteins (*48, 49*).

From a broad-spectrum therapeutic perspective, the structural insights gained via the GP38-13G8 and GP38-13G8 structures suggests that anti-GP38 mAbs can have a considerable cross protection potential. This may be of considerable benefit given that neutralizing G_c mAbs appear to be limited in breath of protection when it comes to the five phenological clades of CCHFV. Recently, a bispecific mAb DVD-121-801 has shown robust post-exposure protection against IbAr 10200(*8*). While it shown to have strong neutralization against the CCHFV laboratory isolate IbAr10200 and its Oman counterpart, weak neutralization was observed for Kosovo/Hoti and Turkey-2004. The limitations largely being linked to the use of a Fab from anti-Gc mAb ADI-37801, which binds to the highly strain-strain variable conformation nonpolar host–membrane insertion surface within

the G_C fusion region(*8, 50*). In contrast, 13G8 can protect against the major clinically relevant CCHFV strain Turkey-2004. (Clade V), and past studies confirmed it can protect against IbAr10200 (Clade III) (*10, 17, 50*). Through our structural and biochemical studies, we confirm how site I antibodies bind across the major clinical strains of CCHFV (Clades III-V). Antibody development towards CCHFV also needs to target highly conserved antigenic sites, as to prevent viral mutations from making the mAb obsolete with new variants. Through our studies we have shown that several mutations need to occur in GP38's α-helix 2 to cause the obsolescence of 13G8 and CC5-17 as therapeutic options. In comparison to our broad-spectrum non-neutralizing anti-GP38 mAbs, the

Through our work we have established the structural and biochemical characteristics of GP38's antigenic site I, with a mouse derived anti-GP38 mAb and a human derived anti-GP38 mAb. The characterization of this site can lead to these site I mabs as a therapeutic option, in addition this site can be utilized for future vaccination methods to fully cover the spectrum of CCHFV clades I-V and potentially other nairoviruses.

Materials and Methods

CCHFV GP38 Expression

Plasmids for GP38 were based on residues 0- 517 CCHFV M-segment viral strains. The plasmid was codon-optimized in a P-twist plasmid with a HRV3C protease cleavage site with an 8x HisTag and a Twin-Step Tag. HEK-293 cells (ATCC) were maintained in HEK-293 Expi Media (Thermo Fischer) based on their specifications. All transfections were followed based on the FectoPro protocol.

CCHFV GP38's were produced using a 1:4 transfection of Furin plasmid to GP38 plasmid in HEK expi cells. Four hours after transfection kifunesine was added to a final concentration of 5μM to

inhibit the processing of complex glycans which could interfere in the crystallization process. The transfection was monitored over 5-8 days and when cell viability dropped below 50% then the supernatant was spun down to remove cell debris using a Beckman coulter centrifuge at 2000 g for 60 min. The supernatant was then run through a 0.2 μm filter and then adjusted to a pH of 7.4, 200mM NaCl, and 20mM Tris-HCl. Supernatant was then run over a His-Excel column (Cytiva) and eluted using 400mM Imidazole. Fractions were then analyzed via SDS-Page and fractions containing GP38 were collected. GP38 was then dialyzed in 200mM NaCl, 4mM Tris-HCl with additional HRV3C protease to cleave the affinity tags. Digestion took place overnight and was then flowed over a His-Excel column and subsequently flowed over a S200 column to obtain a pure cleaved GP38.

Anti-GP38 mAb and Fab Expression

HEK Expi cells (ATCC) were maintained in HEK Expi Media (Thermo Fischer) based on the Thermo's specifications. Cells were transfected based on the FectoPro protocol (VWR). A 1:1 ratio of Heavy to Light chain plasmid was transfected into HEK-expi. The transfection was monitored over 5-8 days and when cell viability dropped below 50% then the supernatant was spun down to remove cell debris using a Beckman coulter centrifuge at 2000 g for 60 min.

Fab supernatant was equilibrated and purified as previously mentioned in GP38 purification. Fractions were analyzed via SDS-Page and dialyzed into 200mM Nacl, 4mM Tris-HCl at a pH of 7.4 overnight. Fab's were then flowed over a S200 column and fractions were confirmed via SDS-Page.

mAb supernatant was equilibrated to a pH of 7.4, 200mM NaCl, and 40mM Sodium Phosphate dibasic and then was flowed over a mAb Select Sure column (Citivia). Bound protein was eluted via 100% elution buffer (100mM sodium Citrate pH 3.4) and 1ml fractions were neutralized using

200mM of Tris-Base pH 10.0. Fractions were confirmed using SDS-Page and then dialyzed to 200mM Nacl, 4mM Tris-Hcl pH 8.0 for use in BLI studies.

Crystallization of GP38-Fab complexes

Proteins were equilibrated to 4mM Tris-HCl pH 8.0, 200mM NaCl, A 1:1.2 ratio of GP38 to Fab was incubated for 4 hours. After incubation the complex was purified over a S200 column using a Biorad NGC. Fractions were collected and run using SDS-Page to confirm purity. Fractions containing the complex were then concentrated to 10-13mg/ml using a 10K Vivaspin Centrifugal Concentrator. Nextel crystal screens solutions were plated via a SPT Lab Tech Mosquito using a 1:1 ratio of protein to well solution hanging drop to a total volume of 600nL. Drops were checked over 2-3 weeks for crystal formation. GP38 Hoti formed in a solution of 20% PEG3350, 0.4M NH_4I. 13G8Fab-GP38Hoti was formed in a solution of 1.1M sodium malonate, 0.1M HEPES pH 7.0, and 0.5% Jeffamine ED-2001, while CC5-17 Fab-GP38Hoti was formed in a solution of 20% PEG1000, and 0.1M HEPES pH 6.4. Crystals were then flash frozen in liquid nitrogen.

Data Collection, Processing and Refinement

Data was collected at the Advanced Photon Source (APS) beamlines 19-BM. Data Processing was performed using HKL-2000. Molecular Replacement was performed using Phaser out of the Phenix suite of programs. To phase the complexes 13G8 Fab and CC5-17 Fab models were generated using SWISS-MODEL, while the GP38-Hoti model was generated using MODELLER (PDB 6VKF)(*51, 52*). After phasing structures went through multiple rounds of refinement in Coot and Phenix(*53, 54*).

BLI Kinetics Assay

Anti-hIgG Fc Capture (AHC) BLI sensors from Sartorius which was dipped into baseline 1x Octet kinetics buffer for 60s. Sensors then encountered a 1µg/mL antibody solution of either c13G8 or

CC5-17 for 150s as a loading step, following loading they were then dipped into a second baseline containing 1x Octet Kinetics buffer. Sensors were then dipped into varying nM concentrations (0.3125, 0.625, 1.25, 2.5, 5.0, 10.0, 20.0) of either IbAr10200, Turkey-2004, Hoti, and Pentalofos GP38 for 300s as an association step, and then transferred back to 1x Octet kinetics buffer for 600s as a dissociation step. KD's were calculated via the Sartorius software.

Patient Recruitment

Patients infected with CCHFV who were admitted to Farabi Hospital (Karadeniz Technical University, Trabzon, Turkey) and in the convalescence phase were recruited. Blood was drawn and separated into PBMCs and Plasma. All patients signed informed consent and the study was approved by IRBs in Karadeniz Technical University and University of Maryland, Baltimore.

Anti-GP38 antibody ELISA

The microtiter Immulon 2 HB 96-well flat bottom plates (Immuno Chemistry Technologies, Bloomington, MN) were coated with 0.2 μg of the gp38 antigen (HOTI strain)-overnight and blocked with 10% dried milk in TBS and 0.1% NP-40 (Blotto solution). Serially diluted samples were added to the wells and incubated 1 hour at 37°C. After washing the wells 6 times, the substrate (BluePhos® Microwell, Seracare, Milford, MA) was added to each well for 15 min at 37°C. Then the signal was read at 650 nm. The tests were done in duplicates, and the average of the background subtracted results reported.

Isolation and Generation of anti-GP38 antibodies

The antibody was isolated from a donor CC5 (recruited as noted above). A combined transcriptomics and genomics approach was used for the identification of the specific antibodies. The circulating anti-gp38 antibodies in plasma were isolated using sequential affinity chromatography. The isolated antibodies were digested with proteases (trypsin, chymotrypsin, and

Glu-C) and the resulted peptides subjected to Mass spectrometry to construct a proteomics library. For the genomics analysis, the memory B cells were isolated from PBMC using EasySep™ Human Memory B Cell Isolation Kit (Cat#17864), then the single cell suspension was loaded onto the 10x Genomics Chromium Controller, microfluidics chip and the VDJ library were prepared based on manufacturer's instruction. The sequence of the matched paired heavy and light chains found in both libraries, were used for production of the mAbs. For this purpose, the variable regions of the antibodies were cloned in the plasmids contained constant regions of the IgG1 or IgG3 and k or λ. The paired heavy and light chain plasmids were co-transfected into the FreeStyle-293 cells, and recombinant antibodies purified from culture supernatants by Protein A or G affinity chromatography.

BLI Competition Assay

Site I, II, and III antibodies were bought from BEI resources. BLI competition was done by soaking PentaHis Sartorius probes into a solution of 10 μg/ml Turkey2004 GP38-his/strep for 60s. Following loading of the probe these were then dipped into Sartorius 1x kinetics buffer for 30 seconds. Probes were then dipped into the first antibody solution 10 μg/ml for 600s to saturate. Probes were then dipped into kinetics buffer for 30s and then dipped into competing a 10 μg/ml antibody solution for 300s. Following competition, the probes were then regenerated in 10mM glycine for 10s and then dipped into kinetics buffer to wash the probes for 10s. This step was done three times to fully dissociate the previous proteins.

Processing was performed by taken by the maximum signal during each step involving the antibody. Calculation of percent inhibition was performed by taking the competing antibodies signal and dividing by the max signal by the same antibody during when it was used as a saturating

step. This number was multiplied by a 100 to give a percentage inhibition, lower percentages indicate less shift in nm and more competition between two antibodies.

Generation of 13G8 and CC5-17 for animal studies

c13G8 and CC5-17 were expressed by transient transfection of expiCHO-S cells. Briefly, expiCHO-S cells were transfected with plasmids of the heavy and light chains of antibodies and expressed according to the manufacturer's instructions for 10 days. Culture supernatants were collected and clarified, and antibodies were purified with HiTrap MabSelect Sure pcc (Cytiva) protein A affinity chromatography column on AKTA start fast protein liquid chromatography (FPLC) system. The CC5-17 antibody was eluted with pH2.2 glycine and c13G8 was eluted using IgG Elution Buffer (Thermo Scientific). Eluted fractions were neutralized with 2M Tris. Following neutralization fractions containing antibodies were applied to HiLoad 26/600 Superdex 200pg column to both improve the purity and buffer exchange to PBS. Pure fractions of antibodies were pooled, quantified by Nanodrop 2000c (Thermo Scientific), and stored at -20°C. For the animal experiments, aliquots of mAbs were diluted in sterile PBS pH 7.4 at 0.25mg/ml and 1mg/ml for c13G8 and CC5-17 and 1mg/ml for the isotype control. Diluted antibodies were further quantified using BLI in Octet R8 (Sartorius) with Protein A biosensors to confirm accuracy of the doses.

CCHFV Animal Challenge study comparing c13G8 vs CC5-17

B6.129S2-*Ifnar1*^{tm1Agt}/Mmjax mice (MMRRC Stock No: 32045-JAX) were infected subcutaneously (SC) in the interscapular region with 100 µL of CCHFV Turkey-200406546 (passaged 1× suckling mouse brain and 1× in SW13 cells; GenBank: KY362517, KY362519, KY362515) under isoflurane anesthesia (target dose: 100 $TCID_{50}$; back-titer dose: 63 $TCID_{50}$). The virus stock was verified by next-generation sequencing and confirmed mycoplasma free. Viral

stock titers and inoculum back-titers (calculated as $TCID_{50}$) were determined by a method based on that of Reed and Muench on BSR-T7/5 cells fixed and stained at 5 dpi (rabbit anti-CCHFV NP pAb, IBT Bioservices 04-0011; 1:2500) and Alexa-488 goat anti-rabbit secondary antibody. Groups of 8 mice (4 female and 4 male) were subsequently treated intraperitoneally (IP; 500 μL total volume) with monoclonal antibody (13G8 or CC5-17) 30 min post-challenge or at both 1- and 4-days post-challenge with 0.25 or 1.0 mg of antibody. Groups of 4 mice (2 female and 2 male) were mock treated IP with IgG1 isotype control (1.0 mg dose). Baseline weights were obtained at day 0, prior to inoculation, and mice were monitored daily for 21 dpi. Clinical signs in mice were scored based on 14 parameters: 2 points each for quiet, dull, responsive (QDR) disposition, hunched back or ruffled coat; 3 points each for dehydration or abnormal huddling/hypoactivity; 5 points each for ataxia/circling/tremors/paresis, abnormal breathing, or anemia; 7 points for weight loss of >20%; 10 points each for inability to bear weight, paralysis, frank hemorrhage or bleeding, moribund state, or weight loss of >25%. Animals were humanely euthanized when end-point criteria were reached (clinical score ≥10) or at study completion (21 dpi). Mean clinical scores were calculated by dividing the daily sum of all scores in an experimental group by the total by the number of animals remaining.

References

1. S. S. Al-Abri *et al.*, Current status of Crimean-Congo haemorrhagic fever in the World Health Organization Eastern Mediterranean Region: issues, challenges, and future directions. *Int J Infect Dis* **58**, 82-89 (2017).

2. J. R. Spengler, É. Bergeron, C. F. Spiropoulou, Crimean-Congo hemorrhagic fever and expansion from endemic regions. *Current Opinion in Virology* **34**, 70-78 (2019).

3. A. Papa *et al.*, History and classification of Aigai virus (formerly Crimean-Congo haemorrhagic fever virus genotype VI). *J Gen Virol* **103**, (2022).

4. E. Bergeron, M. J. Vincent, S. T. Nichol, Crimean-Congo hemorrhagic fever virus glycoprotein processing by the endoprotease SKI-1/S1P is critical for virus infectivity. *J Virol* **81**, 13271-13276 (2007).

5. M. Zivcec, F. E. M. Scholte, C. F. Spiropoulou, J. R. Spengler, É. Bergeron, Molecular Insights into Crimean-Congo Hemorrhagic Fever Virus. *Viruses* **8**, (2016).

6. S. D. Dowall *et al.*, A Crimean-Congo hemorrhagic fever (CCHF) viral vaccine expressing nucleoprotein is immunogenic but fails to confer protection against lethal disease. *Human Vaccines & Immunotherapeutics* **12**, 519-527 (2016).

7. S. D. Dowall, M. W. Carroll, R. Hewson, Development of vaccines against Crimean-Congo haemorrhagic fever virus. *Vaccine* **35**, 6015-6023 (2017).

8. J. M. Fels *et al.*, Protective neutralizing antibodies from human survivors of Crimean-Congo hemorrhagic fever. *Cell* **184**, 3486-3501.e3421 (2021).

9. A. R. Garrison *et al.*, A DNA vaccine for Crimean-Congo hemorrhagic fever protects against disease and death in two lethal mouse models. *PLOS Neglected Tropical Diseases* **11**, e0005908 (2017).

10. J. W. Golden *et al.*, GP38-targeting monoclonal antibodies protect adult mice against lethal Crimean-Congo hemorrhagic fever virus infection. *Science Advances* **5**, eaaw9535 (2019).

11. D. W. Hawman *et al.*, A DNA-based vaccine protects against Crimean-Congo haemorrhagic fever virus disease in a Cynomolgus macaque model. *Nature Microbiology* **6**, 187-195 (2021).

12. F. E. M. Scholte *et al.*, Single-dose replicon particle vaccine provides complete protection against Crimean-Congo hemorrhagic fever virus in mice. *Emerg Microbes Infect* **8**, 575-578 (2019).

13. S. E. Rodriguez *et al.*, Immunobiology of Crimean-Congo hemorrhagic fever. *Antiviral Research* **199**, 105244 (2022).

14. K. Ergunay *et al.*, Antibody responses and viral load in patients with Crimean-Congo hemorrhagic fever: a comprehensive analysis during the early stages of the infection. *Diagnostic Microbiology and Infectious Disease* **79**, 31-36 (2014).

15. A. J. Shepherd, R. Swanepoel, P. A. Leman, Antibody Response in Crimean-Congo Hemorrhagic Fever. *Reviews of Infectious Diseases* **11**, S801-S806 (1989).

16. A. Bertolotti-Ciarlet *et al.*, Cellular localization and antigenic characterization of crimean-congo hemorrhagic fever virus glycoproteins. *J Virol* **79**, 6152-6161 (2005).

17. A. K. Mishra *et al.*, Structure and Characterization of Crimean-Congo Hemorrhagic Fever Virus GP38. *J Virol* **94**, (2020).

18. N. Freitas *et al.*, The interplays between Crimean-Congo hemorrhagic fever virus (CCHFV) M segment-encoded accessory proteins and structural proteins promote virus assembly and infectivity. *PLOS Pathogens* **16**, e1008850 (2020).

19. J. J. Suschak *et al.*, A CCHFV DNA vaccine protects against heterologous challenge and establishes GP38 as immunorelevant in mice. *npj Vaccines* **6**, 31 (2021).

20. R. W. Cross *et al.*, Crimean-Congo hemorrhagic fever virus strains Hoti and Afghanistan cause viremia and mild clinical disease in cynomolgus monkeys. *PLoS Negl Trop Dis* **14**, e0008637 (2020).

21. E. Haddock *et al.*, A cynomolgus macaque model for Crimean-Congo haemorrhagic fever. *Nat Microbiol*, (2018).

22. D. W. Hawman *et al.*, A DNA-based vaccine protects against Crimean-Congo haemorrhagic fever virus disease in a Cynomolgus macaque model. *Nat Microbiol* **6**, 187-195 (2021).

23. D. W. Hawman *et al.*, Efficacy of favipiravir (T-705) against Crimean-Congo hemorrhagic fever virus infection in cynomolgus macaques. *Antiviral Res* **181**, 104858 (2020).

24. D. R. Smith *et al.*, Persistent Crimean-Congo hemorrhagic fever virus infection in the testes and within granulomas of non-human primates with latent tuberculosis. *PLoS Pathog* **15**, e1008050 (2019).

25. C. E. Arnold *et al.*, Host response transcriptomic analysis of Crimean-Congo hemorrhagic fever pathogenesis in the cynomolgus macaque model. *Scientific Reports* **11**, 19807 (2021).

26. W. G. Touw *et al.*, A series of PDB-related databanks for everyday needs. *Nucleic Acids Res* **43**, D364-368 (2015).

27. W. Kabsch, C. Sander, Dictionary of protein secondary structure: pattern recognition of hydrogen-bonded and geometrical features. *Biopolymers* **22**, 2577-2637 (1983).

28. E. Krissinel, K. Henrick, Inference of macromolecular assemblies from crystalline state. *J Mol Biol* **372**, 774-797 (2007).

29. H. C. Maltezou *et al.*, Crimean-Congo hemorrhagic fever in Europe: current situation calls for preparedness. *Euro surveillance : bulletin européen sur les maladies transmissibles = European communicable disease bulletin* **15**, 19504 (2010).

30. T. K. Burki, Ticks and Turkey. *Lancet* **380**, 1897-1898 (2012).

31. O. Orkun, Z. Karaer, A. Cakmak, S. Nalbantoglu, Crimean-Congo hemorrhagic fever virus in ticks in Turkey: A broad range tick surveillance study. *Infect Genet Evol* **52**, 59-66 (2017).

32. Q. Mehmood, M. J. Tahir, A. Jabbar, A. R. Siddiqi, I. Ullah, Crimean-Congo hemorrhagic fever outbreak in Turkey amid the coronavirus disease 2019 (COVID-19) pandemic; a debacle for the healthcare system of Turkey. *Infect Control Hosp Epidemiol*, 1-2 (2021).

33. M. M. Sajadi *et al.*, Identification of Near-Pan-neutralizing Antibodies against HIV-1 by Deconvolution of Plasma Humoral Responses. *Cell* **173**, 1783-1795 e1714 (2018).

34. M. M. Sauer *et al.*, Structural basis for broad coronavirus neutralization. *Nature Structural & Molecular Biology* **28**, 478-486 (2021).

35. L. B. Shrestha, N. Tedla, R. A. Bull, Broadly-Neutralizing Antibodies Against Emerging SARS-CoV-2 Variants. *Front Immunol* **12**, 752003 (2021).

36. C. O. Barnes *et al.*, SARS-CoV-2 neutralizing antibody structures inform therapeutic strategies. *Nature* **588**, 682-687 (2020).

37. E. O. Saphire *et al.*, Systematic Analysis of Monoclonal Antibodies against Ebola Virus GP Defines Features that Contribute to Protection. *Cell* **174**, 938-952.e913 (2018).

38. H. R. Wagstaffe *et al.*, Antibody-Dependent Natural Killer Cell Activation After Ebola Vaccination. *The Journal of Infectious Diseases* **223**, 1171-1182 (2021).

39. T. Abreu-Mota *et al.*, Non-neutralizing antibodies elicited by recombinant Lassa–Rabies vaccine are critical for protection against Lassa fever. *Nature Communications* **9**, 4223 (2018).

40. L. Foster Stephanie *et al.*, A recombinant VSV-vectored vaccine rapidly protects nonhuman primates against lethal Nipah virus disease. *Proceedings of the National Academy of Sciences* **119**, e2200065119 (2022).

41. J. T. Earnest *et al.*, The mechanistic basis of protection by non-neutralizing anti-alphavirus antibodies. *Cell Reports* **35**, 108962 (2021).

42. B. R. Erickson, V. Deyde, A. J. Sanchez, M. J. Vincent, S. T. Nichol, N-linked glycosylation of Gn (but not Gc) is important for Crimean Congo hemorrhagic fever virus glycoprotein localization and transport. *Virology* **361**, 348-355 (2007).

43. J. Brun *et al.*, Assessing Antigen Structural Integrity through Glycosylation Analysis of the SARS-CoV-2 Viral Spike. *ACS Central Science* **7**, 586-593 (2021).

44. I. T. Schulze, Effects of Glycosylation on the Properties and Functions of Influenza Virus Hemagglutinin. *The Journal of Infectious Diseases* **176**, S24-S28 (1997).

45. I. Kosik *et al.*, Influenza A virus hemagglutinin glycosylation compensates for antibody escape fitness costs. *PLOS Pathogens* **14**, e1006796 (2018).

46. E. M. Scherer *et al.*, Characteristics of Memory B Cells Elicited by a Highly Efficacious HPV Vaccine in Subjects with No Pre-existing Immunity. *PLOS Pathogens* **10**, e1004461 (2014).

47. M. A. Moody *et al.*, HIV-1 gp120 vaccine induces affinity maturation in both new and persistent antibody clonal lineages. *Journal of virology* **86**, 7496-7507 (2012).

48. B. E. Correia *et al.*, Proof of principle for epitope-focused vaccine design. *Nature* **507**, 201-206 (2014).

49. Y. N. Lee *et al.*, Protection against respiratory syncytial virus by inactivated influenza virus carrying a fusion protein neutralizing epitope in a chimeric hemagglutinin. *Nanomedicine* **12**, 759-770 (2016).

50. A. K. Mishra *et al.*, Structural basis of synergistic neutralization of Crimean-Congo hemorrhagic fever virus by human antibodies. *Science* **375**, 104-109 (2022).

51. S. Bienert *et al.*, The SWISS-MODEL Repository—new features and functionality. *Nucleic Acids Research* **45**, D313-D319 (2017).

52. A. Waterhouse *et al.*, SWISS-MODEL: homology modelling of protein structures and complexes. *Nucleic Acids Research* **46**, W296-W303 (2018).

53. D. Liebschner *et al.*, Macromolecular structure determination using X-rays, neutrons and electrons: recent developments in Phenix. *Acta Crystallographica Section D* **75**, 861-877 (2019).

54. P. Emsley, K. Cowtan, Coot: model-building tools for molecular graphics. *Acta Crystallogr D Biol Crystallogr* **60**, 2126-2132 (2004).

55. M. Goujon *et al.*, A new bioinformatics analysis tools framework at EMBL–EBI. *Nucleic Acids Research* **38**, W695-W699 (2010).

56. F. Sievers *et al.*, Fast, scalable generation of high-quality protein multiple sequence alignments using Clustal Omega. *Molecular Systems Biology* **7**, 539 (2011).

57. X. Robert, P. Gouet, Deciphering key features in protein structures with the new ENDscript server. *Nucleic Acids Research* **42**, W320-W324 (2014).

Supplementary Information

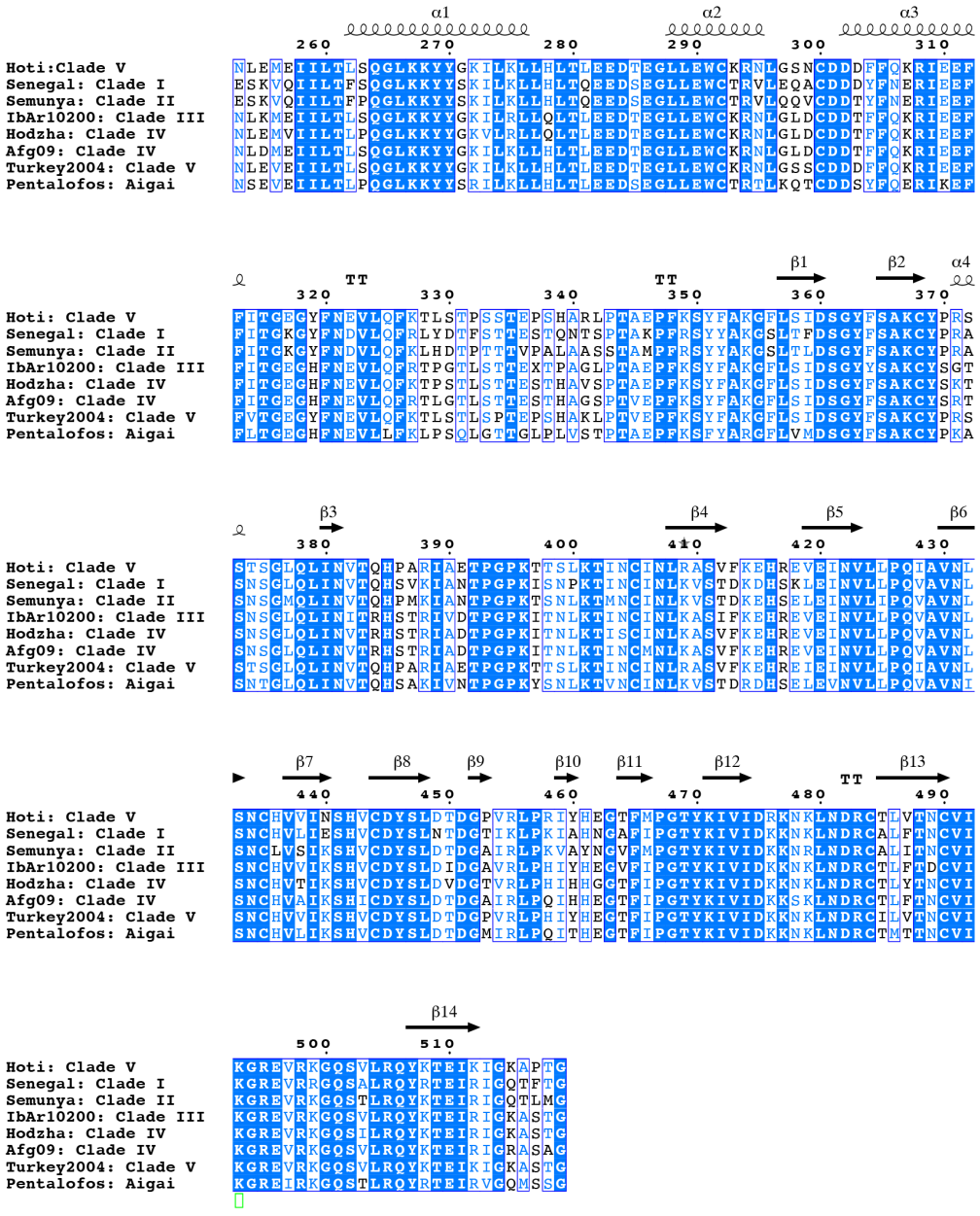

Figure S3.1 Sequence Alignment of Nairovirus GP38. Hoti (Accession number AWX63617.1), Senegal (Accession number ABB30027.1), Semunya (Accession number AAZ94860.1), IbAr10200 (Accession number AWX63620.1), Hodza (Accession number AAP29978.1), Afg-09 (Accession number ADQ57289.1) Turkey2004 (Accession number ASW22359.1), and Aigai Virus: Pentalofos (Accession number AVO00706.1). Similarity and alignment calculations were

performed using Clustal Omega(*55, 56*). General outline and graphic was generated using EsPript(*57*). Residue positions of high conservation are highlighted in Blue.

Table S3.1. Data collection and refinement statistics

	GP38 Hoti	GP38 Hoti complex with 13G8 Fab	GP38 Hoti complex with CC5-17 Fab
Data collection			
Space group	C_{121}	$P4_32_12$	$P4_32_12$
Wavelength (Å)	1.0	1.0	1.0
Cell dimensions			
a, *b*, *c* (Å)	171.633 75.322 62.218	175.957 175.957 93.224	175.676 175.676 92.158
a, *b*, γ (°)	90 110.411 90	90 90 90	90 90 90
Resolution (Å)	50.00-3.2 (3.26-3.2)	50.0-3.6 (3.66-3.6)	50-3.85 (9.92-3.85)
R_{pim}(%) R_{merge}(%) $cc_{1/2}$	0.072 (0.408) 0.134 (0.794) 0.982 (0.757)	0.052 (0.554) 0.172 (1.829) 1.006 (0.763)	0.100 (0.479) 0.255 (1.286) 0.881 (0.763)
$I/\sigma(I)$	17.4 (3.6)	16.94(1.57)	1.6 (1.6)
Completeness (%)	96.53 (93.34)	99.15 (94.44)	98.60 (97.54)
Redundancy	3.5 (3.8)	6.1 (5.6)	7.8 (6.6)
Refinement			
Resolution (Å)	50.0-3.2 (3.26-3.2)	48.8-3.63 (3.76 - 3.63)	40.81-3.86 (3.998 - 3.86)
No. reflections	11970 (1136)	16935 (1579)	13870 (1346)
R_{work}(%)/ R_{free}(%)	0.2685/0.3042	0.28/0.31	0.31/0.34
No. atoms			
Protein	3560	4916	4805
Ligand/ion	66	75	103
Water	6	0	0
B-factors			
Protein	112.27	191	256
Ligand/ion	145.18	211	258
Water	72.97		0
R.m.s deviations			
Bond lengths (Å)	0.004	.006	.006
Bond angles (º)	0.82	1.2	1.13

*Highest resolution shell is shown in parenthesis.

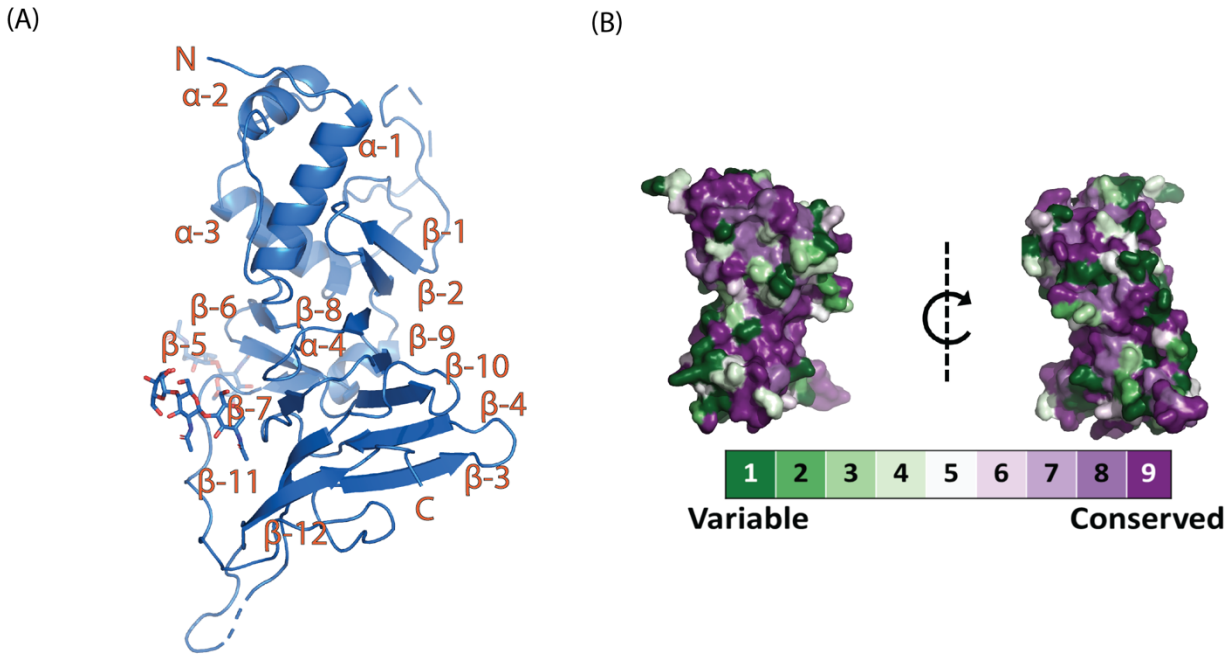

Figure S3.2 GP38 Diversity: **(A)** Secondary Structure labeling of GP38 Hoti **(B)** Consurf Analysis of GP38

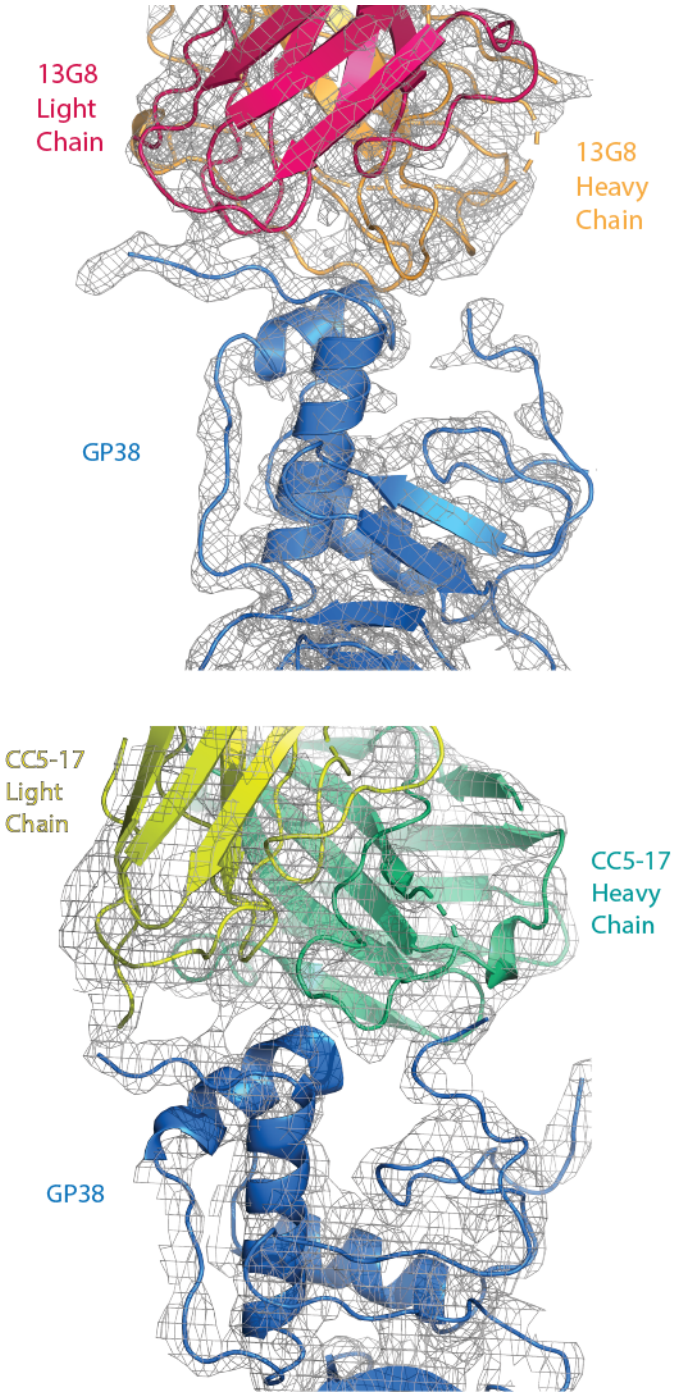

Figure S3.3 Electron Density of GP38 Epitopes: **(A)** 13G8 paratope and electron density **(B)** CC5-17 paratope and electron density

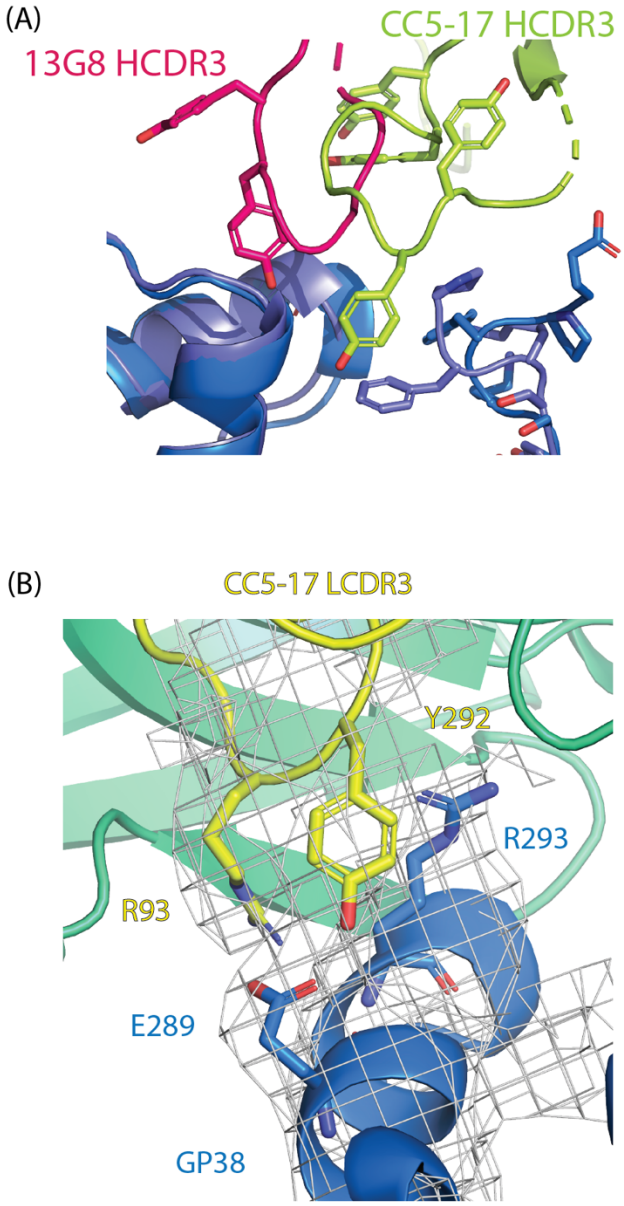

Figure S3.4 Comparison of how 13G8 or CC5-17 interact with Site I on GP38. **(A)** Overlay of the two structures and dominance of their HCDR3 **(B)** Interaction of the LCDR3 on helix 2 of GP38 Hoti

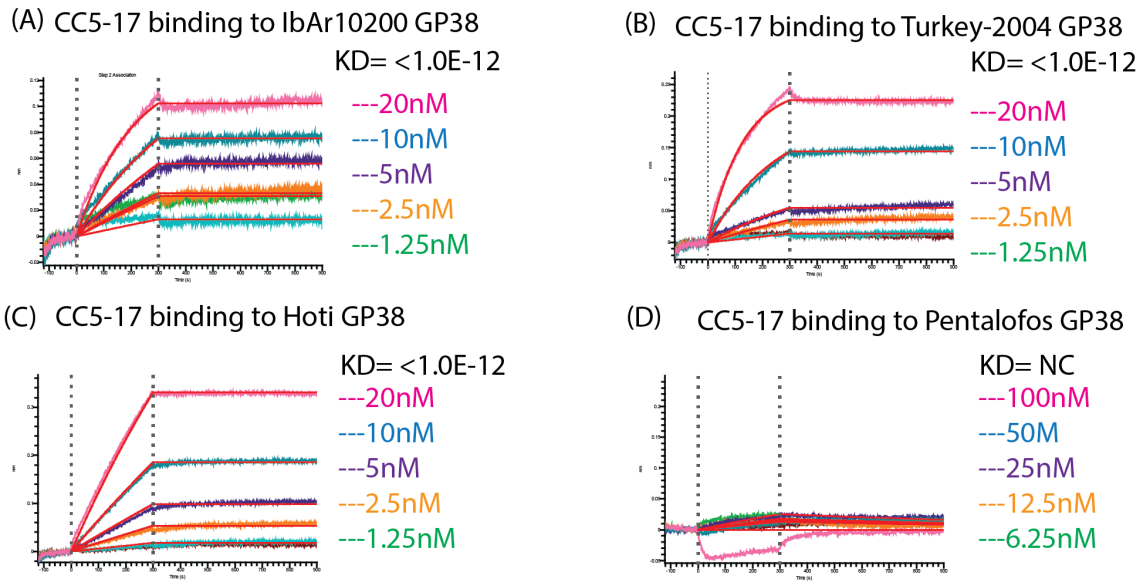

Figure S3.5 CC5-17 interactions across Nairovirus GP38 (**A** to **D**) BLI binding of CC5-17 mAb with GP38 from (**A**) CCHFV IbAr10200 (**B**) CCHFV Turkey-2004 (**C**) CCHFV Hoti (**D**) Aigai Virus Pentalofos

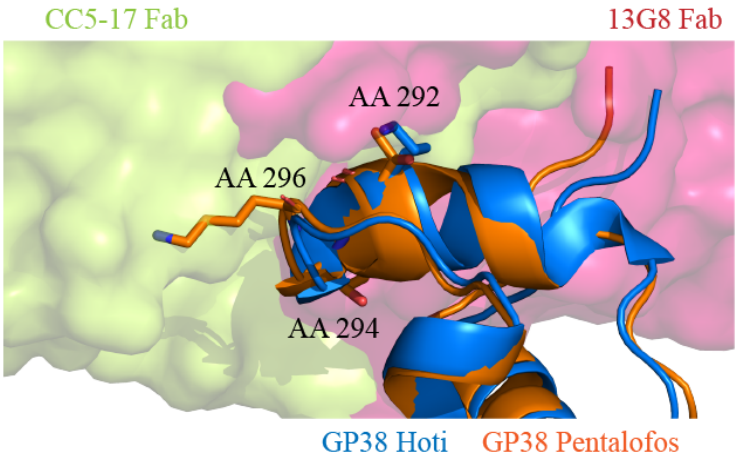

Figure S3.6 GP38 Pentalofos Overlay on Complex Structures from Aigai virus was overlayed over GP38 Hoti from our 13G8 and CC5-17 complex structures to understand the role of sites 292, 294, and 296 in binding Kinetics

CHAPTER 4

DISCUSSION

High-risk pathogens like coronaviruses and CCHFV both seek to interfere with innate immunity through de-ubiquitinase enzymes like the PLP or vOTU, which contributes to prolonged infection and even death. When innate immunity has been superseded, the adaptive immunity can come into play and use B and T cells to clear viruses through several functions. Because innate and adaptive immunity are vital to our survival, they can also be leveraged to prevent infection. Several methods can be used to prevent severe infection and in doing so serve as countermeasures against pathogens. This ranges from the most traditional involving the use of small molecules to interfere with enzymatic processes like genome replication and viral evasion, while more recently the use of larger scale antibodies has become popular to clear infections through neutralizing and non-neutralizing functions.

Following a focused exploration of these two high-risk pathogens and our immune system in chapter 1, in chapter 2, the *Alphacoronavirus* PEDV PLP was structural and biochemically evaluated to understand its ability to interact with Ub and ISG-15. In Chapter 3, the CCHFV glycoprotein GP38 was characterized as an antigen structurally and biochemically towards the therapeutically relevant mouse mAb 13G8, in addition to a new human derived mAb CC5-17. These two antibodies target a wide swath of CCHFV clades, in addition to biochemically characterizing how these two mAbs bind to GP38 from different CCHFV clades. Further studies show that although these two mAbs target the same site. Interestingly, their efficacy is inverse to their affinity highlighting that there is more to consider than just binding affinity when using

non-neutralizing antibodies to prevent and treat disease. Our immune system is highly complex and by better understanding how viruses hijack it, we can prevent severe infections.

Alpha **and** ***Beta*** **Coronavirus PLP Substrate Specificity**

Papain-like proteases (PLP) process Ubiquitin and ISG-15, but their substrate specificity can be wide ranging across *Alpha* and *Beta* genra. In particular, the substrate specificity of the Alphacoronavirus PEDV is significantly different than those within the *Betacoronavirus* genra. For instance, PEDV is primarily a de-ubiquitinase but has a lower turnover than that of SARS-CoV-2 and MERS-CoV. Even though PEDV does not readily deubiquitinate, it has a strong preference of di-Ub molecules (K6, K11, K48, and K63), while *Betacoronaviruses* PLP from SARS-CoV-2 and BtsCoV-Rf1.2004 only interact with that of K48(*1, 2*).

This gives rise to the question of the evolutionary benefit for *Alphacoronavirus* PLPs to process mono-Ub, and di-Ub substrates differently than their *Betacoronavirus* counterparts. Di-Ub linkages are associated with different and overlapping functions i.e. K11/K48/K63 are associated with leading to proteasomal degradation or protein stability (*3, 4*). We know that *Alphacoronaviruses* cause disease in animals like PEDV in swine, while *Betacoronaviruses* are known to cross over from animals and cause disease in humans(*5*). Interestingly the way in which the symptoms of these two coronaviruses differ, as the Alphacoronaviruses attack epithelial cells in the lower digestive system while Beta causing an upper-respiratory infections(*5, 6*). Recent work has highlighted that alphacoronaviruses have crossed over but do not appear to cause debilitating symptoms like those of *Betacoronaviruses*(*7*). The other main difference between these viral PLPs is through its de-ISGylase activity in which *Betacoronaviruses* have significantly higher enzymatic rates towards ISG-15(*1, 2*). The

disruption of this immune regulatory pathway could be a main indicator as to why *Betacoronaviruses* have increased pathogenicity within humans when spillover events due occur.

Alpha and _Beta_ Coronavirus PLP Therapeutic Target Potential

Because of the PLP's functional activity and antagonization of the immune system, it has been tested as a possible therapeutic target. As seen with recent publications *Betacoronavirus* PLP's are highly conserved in their enzymatic functions and have a highly conserved active site. Because of conservation surrounding the active site, small molecules with a naphthalene functional group can be used to inhibit the PLP's function as seen with the PLP's of SARS-CoV-1, SARS-CoV-2, and a closely related *Betacoronavirus* BtSCoV-Rf1.2004 (*2, 8, 9*). As seen through PEDV, its PLP interacts similarly in its mono-Ub and K48 di-Ub activity, even though it does not readily turnover ISG-15 in comparison to its Betacoronavirus counterparts. As seen with our complex PEDV-Ub structure, when the Ub tail rests in the active site, the BL2 loop shifts indicating a closed conformation. The structural commonalities between these two genra of coronaviruses with how the BL2 loop shifts give confidence in PEDV's ability to accommodate these small molecules in their active site. Crossover events with *Alphacoronaviruses* have already been detected in humans, and thus this class of inhibitors could be further explored as a cross genra approach to battling Coronaviruses.

Functional Roles of CCHFV Glycoproteins in Infection

The CCHFV GPC in inherently unique in comparison to that of other nairoviruses. GP38 is not unique to just CCHFV, but is also encoded through several nairoviruses, which include Hazara virus, Tofla virus, Ganjam virus, and Dugbe virus(*10*). Unlike CCHFV, Hazara is not known to infect and cause disease in humans while the other viruses have been listed as possible to spread to humans. It appears that GP38 in CCHFV is crucial to its replication and maturation of mature

viral particles. Further questions stem from the fact that the structural proteins of CCHFV have different abilities to enter primary human cells(*11*). Structural proteins need to have conservation as to properly engage receptors to enter cells. In comparison GP38 has a much lower conservation between strains and this could influence the ability of CCHFV to enter and spread. Alongside GP38, Nairoviruses, encode a Mucin-Like Domain (MLD), a highly O-glycosylated protein which is of unknown function. MLD are common throughout viruses which include Ebola, Human Immunodeficiency Virus (HIV), and Herpes-Simplex. MLD's in these viruses have been attributed to increase in pathogenesis(*12-15*). Because of the use of mucins in other viruses, the CCHFV MLD may play a similar role in evasion. Further evidence points towards CCHFV MLD and GP38 assisting in trafficking of the glycoproteins G_n and G_c and the knocking out the MLD reduces glycoprotein density on the outside of viral-like particles(*16*). This is not apparently the case in other nairoviruses as this MLD and GP38 complex are not defined in those genomes and characterized as hypervariable regions with minimal function(*17*). Furthermore the cleavage site is inherently different than that of other nairoviruses, instead of a furin cleavage site between the MLD and GP38 for CCHFV, a SK1 site is instead predicted within that region(*18*). Furin cleavage has been observed in coronaviruses and influenza and are necessary for their proliferation(*19, 20*). This inclusion of furin cleavage in the CCHFV genome could influence how the overall GPC is processed and the spread of CCHFV.

Characterization of Non-Neutralizing Antibodies Towards CCHFV

The foray into non-neutralizing antibodies has wide reaching impacts. Subunit and other vaccines that focus on expressing envelope proteins are developed to elicit a neutralizing response, and furthermore neutralizing antibodies are used as treatments and prophylactics, as seen with the most recent COVID-19 mAb, Regeneron(*21*). The straightforward connection

between blocking a virion from binding to the host and efficacy has largely driven interest in obtaining neutralizing responses. This has led non-neutralizing functions to be largely ignored and not taken advantage of regarding clearance of infection. However, an increasing number of viruses do not illicit strong neutralizing responses highlighting a needed shift in mAb development practices. This includes several high-risk pathogens like Lassa, and Nipah, where non-neutralizing antibodies are necessary to combat infection(*22, 23*). In the case of CCHFV, it has been shown that human survivors have poorly neutralizing antibodies, and most likely protection against CCHFV was facilitated through another mechanism(*24*). This is still under investigation but through our work we have further characterized the therapeutic potential of non-neutralizing antibodies targeting CCHFV GP38.

To advance not only development, but characterization of these CCHFV mAbs, non-neutralizing assays that can be linked to *in vivo* efficacy are necessary to explore the mechanistic approach. Experimental designs can be used and adapted to find out specifically what type of function these antibodies work through, especially regarding CCHFV. Of note is that even neutralizing antibodies function through their Fc and as a secondary function they can elicit non-neutralizing functions. Several methods have been utilized to study these non-neutralizing mechanisms; Erica Sapphire's group laid out a scoring system to determine the influence of Fc functions of several neutralizing Ebola antibodies(*25, 26*). Non-neutralizing functions rely on complement proteins, phagocytes, and natural killer cells and these assays can be engineered easily to determine what anti-GP38 mAbs rely on to clear infection (*25-28*).

Ideally to categorize the ability of non-neutralizing functions the first set of experiments should examine if they mediate cellular phagocytosis. This can easily be done with incubation of conjugated beads with their respective antigen (GP38), anti-GP38 mAbs, and monocytotic cells

from humans and mice. This can then be analyzed via flow cytometry to detect if a cellular/antibody complex has formed. A variation of this can be performed to determine if these antibodies can mediate neutrophil phagocytosis. The final cell-mediated experiment would need to examine if antibody-mediated NK cell degranulation and activation occurs.

To further characterize protective CCHFV antibodies, the complement system needs to be further explored. Originally when testing 13G8, $C3^{-/-}$ mice were tested to see if 13G8 relies on this form of the complement system. They observed mortality through our the $C3^{-/-}$, but this needs to be followed up with $C4^{-/-}$ mice (*29, 30*). To make matters more complicated through previous Fc receptor engineering on 13G8, protection was observed when Fc function was abolished through LALA mutations, while when the Fc function is abolished in the mice protection is observed(*10*). This leads to the possibility that Fc function is only one part in how 13G8 protects against CCHFV, and even the Fc can be further optimized, i.e. neonatal Fc receptor, to provide additional benefit(*31, 32*). A further characterization and animal study could also look to see if the FAB by itself provide protection. Through these experiments we will be able to see if synergy is needed between the various non-neutralizing functions or if there is one dominant pathway for protection.

To explore the role of GP38, we can adopt a similar approach as to what was performed with the BSL-3 pathogen Rift Valley Fever Virus (RVFV), a distantly related virus of Bunyaviridae. A CRISPR based screen was used to identify necessary host factors that influence infectivity of RVF and the role of RVF G_n. After identification they were able to produce knock-down cell lines to probe the impact of LRP1 on Rift Valley Fever Virus infectivity (*33*). Additionally, a pull-down or immunoprecipitation approach can be used to reconfirm the CRISPR knockdown method to identify the pathological functions of CCHFV GP38, and that of the mechanistic way

in which anti-GP38 mAbs provide protection. Because of the lack of knowledge surrounding GP38, these proteins need to be investigated to further understand not only viral pathology but as leverage for therapies.

Advancing Antibody Treatment Towards CCHFV

Several questions remain about the correlates of protection for CCHFV, and furthermore several questions remain as to what antigen is best used towards not only vaccines but to develop antibodies against. Through our work and a competing groups work, there are two candidates (anti-Gc and anti-GP38) that need to be tested together to see if they afford synergistic potential. The anti-Gc mAbs that have been developed have potent neutralizing ability but only towards IbAr10200, while seem to have diminished neutralizing potential against other major strains like Turkey-2004 and Hoti(*34*). In comparison our site I anti-GP38 antibodies target across strains to a highly conserved epitope. With the recent development and use of CCHFV Hoti in non-human primate models, this would be the next step to test how these antibodies function in a closely related system instead of the genetically altered immunodeficient mice used for challenge studies(*24, 35-38*). Previous combination challenge experiments used mouse derived anti-G_c mAbs in combination with 13G8, and appeared to have decreased the efficacy of 13G8(*29*). Current new anti-G_c candidates which provide protection in vivo may work better if given with 13G8. By using an antibody cocktail of anti-Gc and site I anti-GP38, we can possibly create a therapeutic option that targets most if not all the major CCHFV strains.

Through our work, only site I has been fully characterized, with other antigenic sites still at play. Our work disclosed two new antigenic sites of interest on GP38, to make a total of 4 antigenic sites that are unknown in their efficacy. Future work needs to fully characterize the antigenic sites on GP38 and if they have a difference in protection. Further characterization of these

antibodies would need to test the localization of GP38 on the outside of not only the virus but on infected cells with various cellular assays. Previously only 13G8 was used to detect GP38 on the outside of VLP's and infected cells(*39*). The orientation of how GP38 localizes could have an overall effect on how these mabs bind and thus how they provide protection.

Curiously anti-Gn mAbs are elusive in isolation, and issues were observed when isolating and constructing anti-G_n mAbs. As seen with the Mclellan Group, during their foray into isolating neutralizing antibodies they tried to get G_c and G_n candidates but were only successful in obtaining G_c mAbs. Their G_n construct was engineered to have an additional furin cleavage site between GP38 and G_n instead of the natural SK1/S1P-like cleavage site. Through mass spectrometry they observed that not all of GP38 was cleaved off their antigenic bait and thus they obtained several new anti-GP38 mAb candidates that were not explored. This gives rise to the question of the fidelity of the furin cleavage and between MLD and GP38, which could explain why GP85/GP160 is observed. Additionally, the fidelity of SK1/S1P site between GP38 and Gn could encounter a similar issue and thus we would observe uncleaved $PreG_n$. This would lead to GP38 being on the outside of the viral envelope and thus make it a target of anti-GP38 mAbs.

GP38's Use as an Antigen for Vaccination

GP38 as an antigen of interest has only been characterized in two studies(*40*). The first study surrounded whether a GP38 DNA vaccine could induce protection(*41*). The second, evaluated a VSV vector platform to generate GPC and inadvertently used 13G8 to measure expression of G_n, which at the time they were unaware that 13G8 targeted GP38(*40*). Because of the lack of testing of anti-GP38 titers in these studies, it is imperative to investigate the connection of anti-GP38 titers to efficacy in past vaccinations studies, future vaccinations studies, and CCHFV survivors.

With our own results from isolating anti-GP38 mAbs, patients' plasma contained variable reactivity to GP38, and one isolated antibody CC5-17 provided partial protection when administered at 1mg in IFNAR$^{-/-}$ mice against CCHFV Turkey-2004. Although only partial protection was observed at the higher dose, CC5's immune response to GP38, confirms the role of these mAbs in providing protection.

Of interest is the optimization of a GP38 based vaccine, which showed that surviving mice had two log higher anti-GP38 titers. This would indicate that survival may be achieved if the immune system mounts a large enough antibody response to GP38. When looking at the GP38 DNA vaccine construct, we noticed that they only encoded GP38. From our work, trying to produce only GP38, there was significant delays in production as we had to try several constructs and methods. Ultimately by trying to only produce GP38 from a plasmid it can cause it to be mis-localized and in return have low protein yields. Yields could be optimized by encoding not only GP38 but the MLD (GP85). By encoding GP85 and co-transfecting with furin, we were able to get optimal yields for our studies. A similar methodology would be needed to improve the GP38 vaccine. Most likely by reworking the DNA vector to GP85, a robust immune response would be induced. Another option would be to use of another viral vector like the vesicular stomatitis virus (VSV) or through an mRNA base(*42, 43*). Additional methods could see improved GP38 by conjugating C3d with GP38 in a new DNA vaccine. This combination could assist in B-cell activation to induce a robust immune and antibody response to GP38 (*41, 44*).

Additionally with our characterization of GP38's site I, this can be explored for future vaccination efforts using an epitope focused scaffold(*45, 46*). Because of 13G8's and CC5-17 heavy dominance with α-helix 2, this helix could be expressed by itself or the first 40-50 amino acids that GP38 is comprised of. The site I epitope is highly conserved where only three sites

within the GP38 α-helix 2 have influence on binding. Interestingly when mutational studies were carried out, single mutations did not have a dramatic effect on the binding of 13G8 and CC5-17. This is promising as the site I epitope GP38 which consists of clades III-V can be used to target most clinically relevant strains. To further bolster a site I vaccine approach, this epitope can be designed to target clades I-V in addition to the Aigai Virus Pentalofos(*47*).

References

1. B. T. Freitas *et al.*, Exploring Noncovalent Protease Inhibitors for the Treatment of Severe Acute Respiratory Syndrome and Severe Acute Respiratory Syndrome-Like Coronaviruses. *ACS Infectious Diseases* **8**, 596-611 (2022).

2. B. T. Freitas *et al.*, Characterization and Noncovalent Inhibition of the Deubiquitinase and deISGylase Activity of SARS-CoV-2 Papain-Like Protease. *ACS Infectious Diseases* **6**, 2099-2109 (2020).

3. K. Rajalingam, I. Dikic, SnapShot: Expanding the Ubiquitin Code. *Cell* **164**, 1074-1074.e1071 (2016).

4. K. N. Swatek, D. Komander, Ubiquitin modifications. *Cell Research* **26**, 399-422 (2016).

5. K. Jung, L. J. Saif, Q. Wang, Porcine epidemic diarrhea virus (PEDV): An update on etiology, transmission, pathogenesis, and prevention and control. *Virus Research* **286**, 198045 (2020).

5. R. Weiss Susan, S. Navas-Martin, Coronavirus Pathogenesis and the Emerging Pathogen Severe Acute Respiratory Syndrome Coronavirus. *Microbiology and Molecular Biology Reviews* **69**, 635-664 (2005).

6. A. N. Vlasova *et al.*, Animal alphacoronaviruses found in human patients with acute respiratory illness in different countries. *Emerging Microbes & Infections* **11**, 699-702 (2022).

8. B. T. Freitas *et al.*, Exploring Noncovalent Protease Inhibitors for the Treatment of Severe Acute Respiratory Syndrome and Severe Acute Respiratory Syndrome-Like Coronaviruses. *ACS infectious diseases* **8**, 596-611 (2022).

9. Y. Zhao *et al.*, High-throughput screening identifies established drugs as SARS-CoV-2 PLpro inhibitors. *Protein Cell* **12**, 877-888 (2021).

10. A. K. Mishra *et al.*, Structure and Characterization of Crimean-Congo Hemorrhagic Fever Virus GP38. *J Virol* **94**, (2020).

11. M. Zivcec *et al.*, Assessment of Inhibitors of Pathogenic Crimean-Congo Hemorrhagic Fever Virus Strains Using Virus-Like Particles. *PLoS Negl Trop Dis* **9**, e0004259 (2015).

12. M. Delguste *et al.*, Regulatory Mechanisms of the Mucin-Like Region on Herpes Simplex Virus during Cellular Attachment. *ACS Chemical Biology* **14**, 534-542 (2019).

13. S. Pinzón Martín, P. H. Seeberger, D. Varón Silva, Mucins and Pathogenic Mucin-Like Molecules Are Immunomodulators During Infection and Targets for Diagnostics and Vaccines. *Frontiers in Chemistry* **7**, (2019).

14. X. Zhang *et al.*, T-Cell Immunoglobulin and Mucin Domain 1 (TIM-1) Is a Functional Entry Factor for Tick-Borne Encephalitis Virus. *mBio* **13**, e02860-02821.

15. J. Mayor, G. Torriani, S. Rothenberger, O. Engler, T-cell immunoglobulin and mucin (TIM) contributes to the infection of human airway epithelial cells by pseudotype viruses containing Hantaan virus glycoproteins. *Virology* **543**, 54-62 (2020).

16. N. Freitas *et al.*, The interplays between Crimean-Congo hemorrhagic fever virus (CCHFV) M segment-encoded accessory proteins and structural proteins promote virus assembly and infectivity. *PLOS Pathogens* **16**, e1008850 (2020).

17. P. J. Walker *et al.*, A Global Genomic Characterization of Nairoviruses Identifies Nine Discrete Genogroups with Distinctive Structural Characteristics and Host-Vector Associations. *The American journal of tropical medicine and hygiene* **94**, 1107-1122 (2016).

18. P. J. Walker *et al.*, A Global Genomic Characterization of Nairoviruses Identifies Nine Discrete Genogroups with Distinctive Structural Characteristics and Host-Vector Associations. *Am J Trop Med Hyg* **94**, 1107-1122 (2016).

19. T. P. Peacock *et al.*, The furin cleavage site in the SARS-CoV-2 spike protein is required for transmission in ferrets. *Nature Microbiology* **6**, 899-909 (2021).

20. A. Stieneke-Gröber *et al.*, Influenza virus hemagglutinin with multibasic cleavage site is activated by furin, a subtilisin-like endoprotease. *The EMBO Journal* **11**, 2407-2414 (1992).

21. P. C. Taylor *et al.*, Neutralizing monoclonal antibodies for treatment of COVID-19. *Nature Reviews Immunology* **21**, 382-393 (2021).

22. T. Abreu-Mota *et al.*, Non-neutralizing antibodies elicited by recombinant Lassa–Rabies vaccine are critical for protection against Lassa fever. *Nature Communications* **9**, 4223 (2018).

23. L. Foster Stephanie *et al.*, A recombinant VSV-vectored vaccine rapidly protects nonhuman primates against lethal Nipah virus disease. *Proceedings of the National Academy of Sciences* **119**, e2200065119 (2022).

24. S. E. Rodriguez *et al.*, Immunobiology of Crimean-Congo hemorrhagic fever. *Antiviral Research* **199**, 105244 (2022).

25. E. O. Saphire *et al.*, Systematic Analysis of Monoclonal Antibodies against Ebola Virus GP Defines Features that Contribute to Protection. *Cell* **174**, 938-952.e913 (2018).

26. H. R. Wagstaffe *et al.*, Antibody-Dependent Natural Killer Cell Activation After Ebola Vaccination. *The Journal of Infectious Diseases* **223**, 1171-1182 (2021).

27. J. Pollara *et al.*, High-throughput quantitative analysis of HIV-1 and SIV-specific ADCC-mediating antibody responses. *Cytometry Part A* **79A**, 603-612 (2011).

28. M. E. Ackerman *et al.*, Polyfunctional HIV-Specific Antibody Responses Are Associated with Spontaneous HIV Control. *PLOS Pathogens* **12**, e1005315 (2016).

29. J. W. Golden *et al.*, GP38-targeting monoclonal antibodies protect adult mice against lethal Crimean-Congo hemorrhagic fever virus infection. *Science Advances* **5**, eaaw9535 (2019).

30. A. Rattan *et al.*, Synergy between the classical and alternative pathways of complement is essential for conferring effective protection against the pandemic influenza A(H1N1) 2009 virus infection. *PLOS Pathogens* **13**, e1006248 (2017).

31. B. C. Mackness *et al.*, Antibody Fc engineering for enhanced neonatal Fc receptor binding and prolonged circulation half-life. *mAbs* **11**, 1276-1288 (2019).

32. D. D. Patel, J. B. Bussel, Neonatal Fc receptor in human immunity: Function and role in therapeutic intervention. *Journal of Allergy and Clinical Immunology* **146**, 467-478 (2020).

33. S. S. Ganaie *et al.*, Lrp1 is a host entry factor for Rift Valley fever virus. *Cell* **184**, 5163-5178.e5124 (2021).

34. J. M. Fels *et al.*, Protective neutralizing antibodies from human survivors of Crimean-Congo hemorrhagic fever. *Cell* **184**, 3486-3501.e3421 (2021).

35. E. Haddock *et al.*, A cynomolgus macaque model for Crimean-Congo haemorrhagic fever. *Nat Microbiol* **3**, 556-562 (2018).

36. D. W. Hawman *et al.*, A DNA-based vaccine protects against Crimean-Congo haemorrhagic fever virus disease in a Cynomolgus macaque model. *Nature Microbiology* **6**, 187-195 (2021).

37. D. W. Hawman *et al.*, Efficacy of favipiravir (T-705) against Crimean-Congo hemorrhagic fever virus infection in cynomolgus macaques. *Antiviral Res* **181**, 104858 (2020).

38. D. Smith *et al.*, The pathogenesis of genetically diverse strains of Crimean-Congo hemorrhagic fever virus in the cynomolgus macaque model. *International Journal of Infectious Diseases* **79**, 16 (2019).

39. A. R. Garrison *et al.*, A DNA vaccine for Crimean-Congo hemorrhagic fever protects against disease and death in two lethal mouse models. *PLOS Neglected Tropical Diseases* **11**, e0005908 (2017).

40. S. E. Rodriguez *et al.*, Vesicular Stomatitis Virus-Based Vaccine Protects Mice against Crimean-Congo Hemorrhagic Fever. *Sci Rep* **9**, 7755 (2019).

41. J. J. Suschak *et al.*, A CCHFV DNA vaccine protects against heterologous challenge and establishes GP38 as immunorelevant in mice. *npj Vaccines* **6**, 31 (2021).

42. J. A. Regules *et al.*, A Recombinant Vesicular Stomatitis Virus Ebola Vaccine. *New England Journal of Medicine* **376**, 330-341 (2015).

43. T. Aligholipour Farzani *et al.*, Immunological Analysis of a CCHFV mRNA Vaccine Candidate in Mouse Models. *Vaccines (Basel)* **7**, 115 (2019).

44. T. M. Ross, Y. Xu, R. A. Bright, H. L. Robinson, C3d enhancement of antibodies to hemagglutinin accelerates protection against influenza virus challenge. *Nat Immunol* **1**, 127-131 (2000).

45. B. E. Correia *et al.*, Proof of principle for epitope-focused vaccine design. *Nature* **507**, 201-206 (2014).

46. Y. N. Lee *et al.*, Protection against respiratory syncytial virus by inactivated influenza virus carrying a fusion protein neutralizing epitope in a chimeric hemagglutinin. *Nanomedicine* **12**, 759-770 (2016).

47. F. Sesterhenn *et al.*, Boosting subdominant neutralizing antibody responses with a computationally designed epitope-focused immunogen. *PLoS Biol* **17**, e3000164 (2019).